STUDIES ON SOUND PROPAGATION MODELLING IN COASTAL SEAS -A RAY THEORETICAL APPROACH

THESIS SUBMITTED
IN PARTIAL FULFILMENT OF THE REQUIREMENTS
FOR THE DEGREE OF

DOCTOR OF PHILOSOPHY

IN

PHYSICAL OCEANOGRAPHY

M. P. AJAIKUMAR

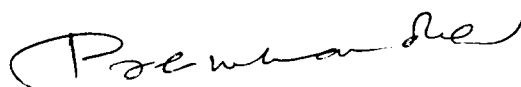NAVAL PHYSICAL AND OCEANOGRAPHIC LABORATORY, KOCHI - 682 021

COCHIN UNIVERSITY OF SCIENCE AND TECHNOLOGY
KOCHI - 682 022

JULY 1992

CERTIFICATE

This is to certify that this thesis on "Studies on sound propagation modelling in coastal seas - A ray theoretical approach" is an authentic record of research work carried out by Mr. M.P. Ajaikumar, M.Sc. under my supervision and guidance at the Naval Physical and Oceanographic Laboratory, Kochi-682 021 for the Ph.D degree of the Cochin University of Science and Technology and no part of it has previously formed the basis for the award of any other degree in any other University.

Dr. Kolli Premchand
(Research Guide)
Scientist,
Centre for Earth Science Studies,
Kochi-682 018.
Kerala.

Kochi-682 018,
July 1992

PREFACE

The oceans, covering about seventy one percent of the surface of the earth, present an extremely complex environment for man to understand and probe into. The complexities arise from a variety of factors like the sea bottom relief, interactions with the overlying atmosphere involving exchange of matter and energy, and processes taking place within the volume of the oceans. In the terrestrial environment, man uses electromagnetic radiation for long distance communication and in a wide range of environmental monitoring applications. Sea water, being an electrical conductor, strongly attenuates electromagnetic radiation except at very low frequencies. For example, even in the well-illuminated tropical oceans, no useful light is left behind at depths greater than a few tens of metres. Hence applications of electromagnetic radiation in the sea is extremely limited. Sound is the only form of energy that propagates in sea water over long ranges comparable to the dimensions of the oceans. With the realization of this fact a variety of exploratory techniques and equipments were developed, making use of sound as a tool. With increasing demands and requirement of efficient system designs, more attention became necessary in understanding the behaviour of sound energy in the oceanic environment. This led to the development of underwater acoustics as an area of extensive research, involving both theoretical and experimental studies.

There are a number of practical applications for ocean acoustics in the fields of science, commerce, and defence. A few examples are echo sounding, sub-bottom profiling, ocean acoustic tomography, deployment and remote control of underwater instrumentation, underwater communication, navigation, fish-finding, exploration for oil and minerals, underwater search and recovery operations, various types of sonars, acoustic mines, and homing weapons.

Ocean acoustics, which deals with the acoustical characteristics of the oceans and, in turn, their exploitation for extracting further information about the environment, has drawn heavily on extensive at-sea experiments and theoretical studies during its development to its present stage. The experiments require expensive infrastructure and involve specialized engineering, instrumentation, and data processing skills. Though the status of knowledge on the subject is much advanced and multi-disciplinary in the international scenario, within the country there have not been much studies reported in this field.

Propagation of sound in the sea is, to a large extent, controlled by the sound speed structure of the water column. The presence of geometrical boundaries of the oceans along with characteristics of the sound speed profiles form certain distinctive features of propagation like the existence of sound channels, convergence zones, and shadow zones. The main controlling factor of the deep water sound field is the inhomogeneous water column itself. Sound propagation in shallow waters is characterized by strong interaction of the energy with the sea bottom and is more complex.

Acoustics of shallow waters is of immense interest as the shallow coastal seas encompass the exclusive economic zone of the country and also on account of strategic reasons. A working model of sound propagation is an extremely useful research tool in both experimental and theoretical studies on ocean acoustics. It can also be useful in remote sensing of important geo-acoustic parameters, which are difficult to obtain by direct methods. In this thesis a ray theoretical model of sound propagation is developed, implemented, and its performance is evaluated. It is then applied to practical shallow water transmission loss modelling problems.

The first chapter of the thesis serves as an introduction, giving an outline of the oceanic sound field

characteristics and concepts in sound propagation modelling. Modelling studies based on normal mode and ray theory, and related work that has been carried out in India are reviewed. Then objectives and scope of this study are presented.

The second chapter contains the theoretical background on which the propagation model is developed. Basic ray theory equations and the methods of computing sound intensity and received time-series of a transmitted signal are presented. The third chapter discusses important sound attenuation mechanisms in the sea, viz., absorption in sea water, scattering at the sea surface, and reflection at the sea bottom and also methods for their estimation. These are then incorporated into the propagation model in order to obtain realistic outputs.

The ray theoretical model of sound propagation is developed and presented in the fourth chapter. The environment is assumed to be range-independent. Sound speed in the water column is allowed to vary arbitrarily with depth. An efficient algorithm for eigen-ray finding is developed, based on which the propagation model is implemented on a computer. The model outputs include transmission loss and received time-series of a monochromatic pulse transmission. Quality of the model is assessed by comparing the model outputs with results from a normal mode model and those available in published literature.

The fifth chapter contains an outline of the experimental methods for at-sea measurements of transmission loss. Then broad-band experimental transmission loss data collected at two coastal stations on the western continental shelf of India are compared with model computations. The results are discussed. The sixth, and the last, chapter summarises the work done and presents the conclusions drawn from this study.

CONTENTS

Chapter 1

INTRODUCTION

1.1. SOUND IN THE SEA

The science of production, transmission, reception, and utilization of sound in the sea is called *ocean acoustics*. Research and exploratory activities on underwater life and other resources, communication, sea bottom mapping, and remote control of equipment etc. utilize sound energy. It is essential in military and rescue operations and a number of commercial activities like exploration for minerals and oil, dredging, fisheries, and navigation. Except for a small number of special short-range applications, frequencies of interest in ocean acoustics are less than a few tens of kilohertz. This is because sound absorption by sea water increases so much with frequency that propagation ranges achieved at higher frequencies are very small.

1.1.1. Speed of sound in sea water

Sound speed in sea water is a fundamental acoustic parameter of the oceans. Accurate sound speeds are required whenever sound travel times are to be converted to corresponding distances. Examples are bathymetry, position keeping (navigation), and target ranging using sonars. But sound speed gradients, rather than the sound speeds as such, determine refraction of sound and related features of propagation.

Sound speed in sea water increases with temperature, salinity and pressure. Variation of the sound speed with temperature is more non-linear than that with salinity. The rate of change of sound speed with temperature is nearly 4.1 and 2.4 m s^{-1} per degree at 5 and 25°C respectively. With

1

salinity it is about 1.2 m s^{-1} per ppt (parts per thousand). Sound speed increases almost linearly with depth (pressure) at an approximate rate of 0.016 m s^{-1} per metre.

The phenomenon of sound propagation is associated with changes in the acoustic pressure and density of the medium. These changes are adiabatic. Sound speed C is related to physical properties of the medium through the relation $C = \sqrt{\varkappa/\rho}$ where $\varkappa$ is the adiabatic bulk modulus of the medium and ρ is the density. In the case of sea water, $\varkappa$ and ρ are functions of temperature, salinity, and pressure. It is possible to calculate sound speeds using the equation of state of sea water (Fofonoff and Millard, 1984). But the relations involved are cumbersome and computations are time consuming. Hence empirical relations are used for the calculation of sound speeds in sea water.

Empirical relations for sound speed are derived from the analysis of controlled laboratory measurements on water samples. Wilson (1960) published empirical equations of sound speed in sea water as a function of temperature, salinity, and pressure. Later improved results were published by Del Grosso and Mader (1972), Del Grosso (1974), and Chen and Millero (1977). The latter two of these differ significantly only for depths greater than about a kilometre. The Chen and Millero expression is the international standard for sound speed computations (Fofonoff and Millard, 1984). However, recent travel time measurements in the Pacific Ocean are reported to be inconsistent with travel times predicted from the international standard, but consistent with those predicted from Del Grosso's algorithm (Spiesberger and Metzger, 1991). The above-mentioned equations involve higher order terms of the variables and many number of terms. Also, in practical applications where hydrographic data are involved, there is an additional requirement of pressure-to-depth conversion using a suitable formula (e.g., Leroy, 1968; Fofonoff and Millard, 1984).

2

Leroy (1969) and Medwin (1975) published equations for sound speed as a function of temperature, salinity, and depth rather than pressure. A more general nine-term equation valid for depths of upto 8000 m was published by Mackenzie (1981). This equation, which takes the Del Grosso and Mader equation as the "truth" has a standard error estimate of 0.07 m s^{-1} and is accurate enough for practical computations of sound speed in sea water. Sound speed is given by (Mackenzie, 1981)

$$C = 1448.96 + 4.591T - 5.304 \times 10^{-2} T^2 + 2.374 \times 10^{-4} T^3 +$$
$$1.340(S-35) + 1.630 \times 10^{-2} D + 1.675 \times 10^{-7} D^2 - \tag{1.1}$$
$$1.025 \times 10^{-2} T(S-35) - 7.139 \times 10^{-13} TD^3$$

where C is the sound speed (m s^{-1}), T is the temperature ($^{\circ}$C), S is the salinity (ppt), and D is the depth (m). In this study we follow Mackenzie's equation for sound speed computations.

Direct measurements of sound speed can be done using sound velocimeters which are now commercially available. They give accurate sound speed profiles at sea. These velocimeters work on the sing-around principle (Greenspan and Tschiegg, 1957) and are factory-calibrated against an empirical relation of sound speed. Velocimeters are available with accuracies of the order of ∓ 0.1 m s^{-1}, very near to accuracies achievable from the use of empirical relations.

1.2. AN OVERVIEW OF THE OCEANIC SOUND PROPAGATION SCENARIO

It is the spatial distribution of temperature and salinity that define water mass structures of the world ocean. Because temperature and salinity are two controlling factors of sound speed, oceanic sound speed structures are closely related to the prevailing water mass structures. The oceans show maximum variability in near-surface layers due to diurnal and seasonal changes in temperature and salinity. So also are

the sound speed structures. In the first few hundred metres of the water column, a sound speed profile closely resembles the vertical profile of temperature. At higher depths the changes in temperature are more gradual and pressure is the dominant controlling factor.

Propagation of sound in the sea over long ranges is always by some form of ducted or guided propagation in which maximum energy is confined within the boundaries of the duct. These ducts are called *sound channels*, or *wave guides* in general. The deep sound channel, the surface duct, and the shallow water channel are the important types of wave guides that exist in the oceans.

The competing effects of temperature and pressure on sound speed results in a characteristic feature of deep water sound speed profiles. A typical deep water profile has a sound speed minimum below the thermocline. If a sound source is located at or near this minimum, part of the radiated energy gets confined to a water column of limited thickness. Being refracted continuously back to the depth of the sound speed minimum where the vertical sound speed gradient reverses its direction, this energy interacts with neither the sea surface nor the sea bottom. The only attenuation mechanisms acting on this energy are absorption and scattering by the medium. Consequently, sound at low frequencies (where absorption and scattering losses are small) travel over long ranges of global dimensions. This natural duct of sound propagation, with its axis located at the sound speed minimum, is known as the *deep sound channel* (DSC). The channel was given the name SOFAR channel by its discoverers Ewing and Worzel (1948). SOFAR is the acronym for SOund Fixing And Ranging, implying the usefulness of the channel in long-range underwater navigation and communication applications. The channel axis may be as deep as 2000 m in tropics and rises to the sea surface at high latitudes.

4

Phenomena associated with long range sound propagation in deep waters are discussed by many authors (Urick, 1975, 1982; Brekhovskikh and Lysanov, 1982). Lens-like action of the water column causes the formation of zonal patterns of energy distribution with high and low intensity areas. These are associated with the existence of convergence zones (CZ) and shadow zones. Typical propagation characteristics associated with a DSC were first described by Ewing and Worzel (1948). Though signals sent through a DSC can be heard at very long ranges, distortion due to multipath effects is severe. Other than for applications in communication and navigation, the fact that the multiple arrivals pass through different "slices" of the water column has found its application in Ocean Acoustic Tomography (Munk and Wunsch, 1979). Hale (1961) discusses characteristics of CZ propagation along with experimental evidence. Urick (1965) investigated the existence and characteristics of the convergence zones using ray diagrams and by field measurements. Several experiments related to DSC and CZ propagation have been reported (Bryan et al., 1963; Urick, 1963, 1966; Baxter et al., 1964; Thorp, 1965; Kibblewhite and Denham, 1967).

The *surface ducts* or *surface sound channels* are characterised by a surface layer of the water column within which sound speed increases with depth. Typical thicknesses of the layer vary from a few metres to a few tens of metres. Below this layer there is a negative sound speed gradient. A common reason for their occurrence is the presence of a well-mixed, near-isothermal surface layer (usually referred to as the mixed layer). Such layers may form due to turbulent mixing caused by the effects of strong winds or currents. Another causative factor is the sea surface cooling due to a lower air temperature or strong evaporation which sets up convective mixing in the near-surface layers. Surface ducts form even in the absence of a mixed layer when there is a positive gradient of temperature and/or salinity.

The presence of a surface duct has important consequences in the distribution of energy from an in-duct sound source (Kinsler and Frey, 1962; Urick, 1975). Sound from the source is trapped in the duct by the positive sound speed gradient and propagates to long ranges and a shadow zone forms beneath the duct. This shadow zone is not perfect- it may get insonified by energy scattered from the sea surface, reflected from the bottom, and partially "leaking" out of the duct due to diffraction effects. This leakage depends on the frequency of sound, duct thickness, and the gradient below the layer.

A surface duct is characterised by a cut-off frequency, below which energy is trapped less effectively (Kibblewhite and Denham, 1965). Effective channeling occurs only at frequencies higher than this cut-off. Main losses encountered by energy propagating in the duct are absorption by sea water and scattering at the sea surface. Presence of air bubbles near the sea surface and internal waves at the lower boundary of the duct are other factors which affect the propagation by scattering, absorption, and diffraction (Urick, 1982). Propagation in surface ducts have been studied theoretically and experimentally by several researchers (Pedersen, 1962; Kibblewhite and Denham, 1965; Bucker and Morris, 1967; Bucker, 1970, 1980; Barnard and Deavenport, 1978), and the behaviour of these channels are relatively well understood and predictable.

The above two types of sound channels arise from characteristics of the sound speed profiles. In both the cases, lower boundaries of the channels are well within the water column. Hence for an in-duct source, there is limited interaction of the energy with the sea bottom. Another type of oceanic wave guide is the *shallow water channel* in which energy propagates by alternate reflections at the sea surface and sea bottom. This is typical of low frequency propagation where sound speed gradients in the water column are insufficient to contain the energy. Important features of

6

shallow water wave guides in relation to sound propagation are discussed separately in Section 1.4.

One of the prominent features of the oceanic sound field is its variability, both in space and time. Interference due to multiple propagation paths are characteristic of the field. Properties of the medium may change laterally due to many reasons, in turn causing range dependence of the field. Examples are proximity to river influxes, presence of relatively permanent or quasi-permanent oceanographic features like fronts, eddies, and currents. Other factors which contribute to the range dependence are sea bottom topography, sediment variability, and sub-bottom structure. However, effects of the sea bottom are more pronounced in shallow water propagation (Section 1.3). Temporal variability of the acoustic field is caused by time-varying characteristics of the medium along the propagation path, apart from possible fluctuations at the source itself. In addition to seasonal and diurnal variations, currents, internal waves, and turbulence also cause temporal fluctuations in sound speeds and hence on the acoustic field. Another factor is the unstable sea surface geometry. The amount of scattering from the sea surface depends, among other factors, on the surface wave height.

There have been several studies on the effects of environmental range-dependence on sound propagation. Propagation in the presence of a sea mount or a rise and the shadowing caused by the obstacle has been of interest to many workers (Northrop, 1970; Bannister et al., 1974, 1977; Nutile and Guthrie, 1979; Medwin and Spaulding, 1980; Ebbeson and Turner, 1983; Dosso and Chapman, 1987). Effects of oceanographic features like fronts, eddies, and internal waves have been studied by experimental and theoretical investigations (Levenson and Doblar, 1976; Emery et al., 1979; Baxter and Orr, 1982; Henrick and Burkom, 1983; Mellberg et al., 1991).

7

Reverberation and ambient noise are two other important acoustical characteristics of the oceans. Inhomogeneities within the volume of the ocean (thermal microstructure, gas bubbles, biological population etc.) and the boundaries (sea surface and sea bottom) scatter part of the energy incident upon them (Urick, 1975:p-211). The sum total of the scattering contributions from all the scatterers is called *reverberation*. Based on causative factors, reverberation may be classified into sea surface, sea bottom and volume reverberation. Surface and bottom reverberations are much stronger than the volume reverberation. An estimate of the reverberation level expected under operating conditions is a necessary part of the design process of certain underwater systems. For example, active sonars detect their targets by transmitting powerful signals and then listening for the echoes from the targets. Strong reverberation interferes with the detection of targets by an active sonar if the target echoes happen to arrive during the reverberation period. This makes system performance a function of the reverberation characteristics of the environment.

The ocean by itself is not a quiet environment. It can be extremely noisy depending on the location and proximity to geological and man-made disturbances. The ambient noise background of the ocean is the noise background that is "left over", after all identifiable noise sources (including those of "self-noise") in the noise recorded by a non-directional receiver are accounted for (Urick, 1975:p-181). Sea surface and marine organisms are potential sources of locally generated ambient noise in the sea. The noise background interferes with extraction of desired acoustic signals from the environment. Obviously, the spectral characteristics, directionality, and variability (temporal and spatial) of the ambient noise are of relevance in the performance of acoustic sensors which listen to signals from a distant sound source.

8

1.3. SHALLOW AND DEEP WATER ACOUSTICS

Based on broad propagation characteristics and controlling factors, ocean acoustics can be divided into deep water acoustics and shallow water acoustics. The "shallowness" depends on the relative depth of the water column compared to the acoustic wavelength, i.e., on the dimensionless parameter kh where h is the water depth and k is the horizontal wave number. In shallow water acoustics one mostly deals with propagation conditions with small to moderate kh values (Tolstoy and Clay, 1966:p-97). At sufficiently low frequencies even the deepest areas of the ocean become acoustically shallow. Sound propagation in coastal waters of depths < 200 m and at frequencies of less than about a kilohertz can be considered as cases of shallow water propagation.

In general, deep water propagation can be explained using geometrical acoustics whereas more complete wave theory is required for describing propagation in shallow waters. Regarding the applicability of geometrical acoustics in propagation modelling in relation to sound speed variations in a waveguide and the acoustic wavelength, Lurton (1992) points out that according to common experience in underwater acoustic modelling, a lower limit of 200 Hz is convenient in deep water (depth > 1000 m) for most configurations, while a value of 1000 Hz should be more adequate in shallow water (depth < 200 m) where very high sound speed gradients may be found.

Shallow water propagation is characterized by strong interaction of sound energy with sea bottom. This interaction is a function of frequency and typically extends to a depth of a few wavelengths beneath the bottom, depending on the strength of the signal. In contrast, the main controlling factor of the deep water acoustic field is the water column itself.

9

1.4. SOUND PROPAGATION IN SHALLOW WATERS

Shallow water acts as a sound channel through which the energy propagates by successive reflections at the upper and lower boundaries of the medium. There are reflection and scattering losses associated with the boundary interactions. Hence propagation ranges achieved in shallow waters are in general small compared to those in deep waters. Sound propagation in shallow waters is complex due to inherent variability of the environment and interaction of the energy with sea bottom. It is a case of propagation in multi-layered wave guides, with strong frequency dependence and high attenuation rates compared to deep water propagation.

The shallow water-column over the continental shelves is characterized by small- to medium-scale processes. Large changes in salinity may occur near fresh water inlets depending on the season and tidal phase and amplitude. Near-shore circulation and internal waves induce cyclic changes in the structure of the water column. Presence of abundant biological population increases the volume scattering of sound. Noise generated by various organisms contribute to the ambient noise background of the sea. Human activities on nearby land and in coastal waters add another dimension to this noise background.

Sediment type, and hence the bottom acoustic parameters may vary considerably across continental shelves (e.g., Murty et al., 1986; Murty and Pradeepkumar, 1987; Murty and Muni, 1987). Small-scale bottom topography and the extent of layering may also show significant variations from region to region (Siddiquie and Almeida, 1985; Murty and Pradeepkumar, 1986; Murty and Muni, 1988). High frequency interaction of sound is limited to surficial layers of the sea bottom. But lower frequencies penetrate deeper into the bottom. Then the bottom layering, if any, and properties of deeper sediment

10

layers assume importance in determining the sound field in the overlying water column. As a result, sea bottom is an important factor determining range-dependence of shallow water sound propagation.

Another characteristic of shallow water propagation is the existence of an optimum frequency band in which propagation loss is the minimum. High frequencies suffer high loss due to absorption and scattering, and low frequencies penetrate more into the bottom. This leaves an optimum frequency band for long-range propagation in the water column (Akal, 1980). The optimum frequency is a function of the water depth, nature of the sea bottom, sound speed profile, and the source/receiver geometry (Jensen and Kuperman, 1983; Gershfeld and Eller, 1985).

Two other phenomena associated with shallow water propagation are dispersion and signal distortion (Clay and Medwin, 1977:p-311). Dispersion occurs due to the propagation geometry involving the water column and the sea bottom and is dependent on the channel parameters. Multi-path propagation from a source to a receiver results in numerous arrivals of a transmitted signal. The interference among them cause time-stretching and distortion of the received signals.

1.5. SOUND PROPAGATION STUDIES

Acoustics of shallow water is more complex than that of deep water. It is also clear that there are many interesting phenomena associated with sound propagation in these natural ducts. Analysis of field experimental data can help in revealing propagation features under various environmental conditions. Theoretical studies and mathematical modelling give a better picture of various physical processes controlling the propagation.

11

1.5.1. Experimental studies

Experimental studies on sound propagation may be carried out either by measurements at sea or by using scale model studies in the laboratory. Laboratory studies are useful in testing theoretical models of propagation in relatively simple environments and allow some control over many of the important parameters. Though expensive and difficult to carry out, at-sea experiments provide more realistic data than the laboratory methods. Model-studies in a laboratory cannot replace field measurements in some cases; for example, in studies related to low frequency and long range propagation. Field studies also help in the development of sub-models of certain phenomena related to propagation, e.g., like signal coherence, scattering, and reverberation. Experimental studies are presented in Chapter 5.

1.5.2. Sound propagation modelling

Mathematical models of sound propagation help us in interpreting and predicting propagation features observed in an environment. A range of mathematical methods exist for propagation modelling- and there are simple analytical models and complex numerical models of propagation. Predictions of the expected propagation conditions are useful in the planning of many underwater and related activities. They are used in purely research oriented work, in commercial applications, and in military requirements.

A realistic propagation model may be thought of as an integral model consisting of a wave propagation model and a number of environmental sub-models. The sub-models account for different phenomena which influence propagation. These include models of sound speed, absorption coefficients, scattering, and sea bottom interaction and may be based on theoretical, empirical or semi-empirical formulae. This means that the

performance of a propagation model depends on the capabilities and limitations of the constituent sub-models.

1.6. REVIEW OF PROPAGATION MODELLING STUDIES

Fundamentally, sound propagation modelling involves a solution of the wave equation (Chapter 2, Section 2.1). Based on the assumed geometry of the environment and the type of solution chosen for, different techniques exist for propagation modelling. Two widely used approaches have been based on normal mode theory and ray theory. The concepts of normal modes and rays are discussed in Chapter 2.

Normal mode theory has been very successful in explaining many shallow water propagation phenomena. Major work on propagation modelling started with the work of Pekeris (1948), who developed and applied the normal mode theory of ducted propagation in layered media to shallow oceanic environments. The model could explain many experimental observations like modal structure of the field and geometric dispersion. The environmental model is based on a number of simplifying assumptions and is known as the *Pekeris channel*. In this model, an isospeed water column of constant thickness overlies a homogeneous, semi-infinite half-space of fluid bottom having a higher sound speed. Both the media are assumed to be non-absorbing. In this case solutions of the wave equation are obtained analytically.

The Pekeris model was modified and extended by various workers so as to accommodate the realistic environment in a better way. Vertical sound speed profiles were introduced by dividing the wave guide into a number of homogeneous layers, by the use of simple analytical curves, and allowing for arbitrary variation of sound speed with depth (Tolstoy, 1958; Bucker and Morris, 1965; Tolstoy and Clay, 1966:p-85,97; Newman and Ingenito, 1972; Ryder and Williams, 1973; Jensen

13

and Ferla, 1979). A further extension of the normal mode approach was the inclusion of a visco-elastic solid bottom in place of a fluid bottom (Brekhovskikh, 1960; Tolstoy, 1960; Bucker and Morris, 1965; Ingenito and Wolf, 1976; Ellis and Chapman, 1985; Beebe and Holland, 1986).

Acoustic field in a sound channel may be represented in terms of transmission loss or propagation loss (in intensity) relative to the intensity at the source. Kornhauser and Raney (1955) discussed the effects of bottom losses on the attenuation of normal modes in a two-layered wave guide. Other attenuation mechanisms were later introduced in terms of the modal attenuation coefficients to obtain realistic estimates of transmission loss (Ingenito, 1973; Kuperman and Ingenito, 1977; Ingenito *et al.*, 1978; Jensen and Ferla, 1979; Gershfeld and Eller, 1985)

Description of the sound field in terms of normal modes is only exact when the physical situation is independent of range. The simplest extension of normal mode theory to a sloping bottom situation (wedge shaped ocean) is to make the "adiabatic approximation" (Eby *et al.*, 1960; Pierce, 1965; Denham, 1966; Milder, 1969). Here it is assumed that there is no coupling of energy from one mode to another. The validity of such an assumption holds for slopes of upto about $1°$ (Eby *et al.*, 1960). However, the approximation fails for upslope propagation where modes get "cut-off" as the depth decreases. A solution to the problem in terms of coupled modes was given by Evans (1983). Here the environment is divided into a number of range-independent segments, each of which may have arbitrary variation of the parameters with depth. Solutions based on this approach has been applied to benchmark propagation problems to yield excellent agreement with analytical solutions (Jensen, 1988; Jensen and Ferla, 1990).

As compared to the mode theory which is valid at all frequencies, ray theory is a high frequency approximation of

14

the wave theory (comparison between the normal mode and ray theoretical approaches are given in Chapter 2). Initially, the method of intensity calculations using ray theory involved a sound speed profile approximation consisting of layers of constant velocity gradient. This method was in widespread use prior to 1960's. Some of the difficulties in applying ray theory to propagation problems were addressed by Pedersen (1961). He showed that in the calculation of ray theory intensities in underwater sound field the use of constant gradient layers can introduce spurious caustics and in some cases can omit real caustics. Polynomial curve approximations of the sound speed profiles and related ray theory involving various polynomial functions were developed to overcome such problems to some extent (Stewart, 1965; Pedersen and Gordon, 1967; Pedersen 1968; Cohen and Einstein, 1970; Moler and Solomon, 1970; Weinberg, 1971,1973; Krol, 1973).

As simple ray theory fails in the vicinity of caustics and shadow zones, there were efforts to apply corrections to ray theory at such regions (Brekhovskikh, 1960; Ludwig, 1966; Blatstein, 1971,1972; Sachs and Silbiger, 1971; Weinberg, 1975,1981a). Mackenzie (1961) and Urick (1969) used ray method to compute transmission loss in shallow water propagation. But the ray method remained as the deep water, high frequency, short range option as compared to the normal mode theory due to its failure in predicting many of the propagation phenomena in shallow waters (Weston, 1963; Urick, 1965; Kibblewhite and Denham, 1967; Cohen and Cole, 1977).

As a major breakthrough in successful application of ray theory to shallow water propagation problems, Tindle and Bold (1981) and Tindle (1983) published experimental data and theoretical results based on an improved ray theory which agreed very well with mode theory calculations for a Pekeris channel. This modified ray theory included a lateral displacement called beam displacement (Brekhovskikh, 1960) for bottom reflected rays and an associated time displacement.

Early work on the role of beam displacement in modified ray theory was done by Murphy and Davis (1974) and Murphy (1974, 1977). Further studies revealed the connection between modal attenuation rates and the attenuation in a ray cycle distance. It was shown that the attenuation rates of normal modes and their equivalent rays are equal provided that the ray cycle distance is modified to include beam displacement at the bottom (Weston and Tindle, 1979; Tindle, 1979; Tindle and Weston, 1980; Tindle et al., 1980).

Tindle (1983) showed that modified ray theory is as good as normal mode theory for practical calculations in shallow water acoustics. Tindle and Deane (1985) extended this method to a uniformly sloping bottom. Westwood and Tindle (1987) used modified ray theory for shallow water time series simulation which showed very close agreement with measured signal time series in an indoor tank.

The inclusion of beam displacement generates ray theory caustics, for which correction formulas are to be applied. Also, behaviour of the rays near the critical angle is not modelled accurately. Westwood (1989a) develops accurate complex ray methods based on the saddle point method outlined by Brekhovskikh (1980) for finding the reflected and transmitted fields due to a point source in the presence of a plane, penetrable interface. Westwood (1989b) applies this model to both flat and sloping waveguides. Concurrent work by Tindle and Plumpton (Tindle and Plumpton, 1988; Plumpton and Tindle, 1989) on similar lines formulate an identical complex saddle point criterion and develop improved procedures for evaluating the field in the caustic region. Westwood (1990) applies his complex ray model to the benchmark penetrable wedge problems which show excellent agreement with two-way coupled mode solutions (Evans, 1983, 1986) which are accurate numerical solutions of the posed mathematical problems (Jensen, 1988; Jensen and Ferla, 1990).

16

Jensen and Kuperman (1982) and Jensen (1988) present overview of the most commonly used wave theory models for propagation modelling in complex ocean environments. It was the availability of powerful computers in the early 1970's that stimulated development of a number of accurate numerical solutions of the wave equation, encompassing normal mode, fast field (FFP) and parabolic equation (PE) techniques.

In the fast field solution, the environment is range-independent which allows Fourier decomposition of the acoustic field into an infinite set of horizontal waves. Advantages of the fast field program are that it includes the "near field" (which is ignored in normal mode theory) and it can include shear propagation effects with no restrictions on the shear velocity relative to the compressional wave (sound) velocity in water. Its disadvantages are that the procedure is not easily automated, only one source/receiver depth configuration can be done for each numerical solution and the sampling of the field in range is restricted (Jensen and Kuperman, 1982).

If the environment varies both in range and depth, the wave equation is to be solved numerically. For this an approximate wave equation that lends itself to practical numerical solution is derived. The parabolic equation method is such an approximation. There are different implementations of numerical schemes for solutions of the parabolic equation.

Reviews on operational underwater acoustic propagation models (Urick, 1982; Jensen, 1988) indicate that important classes are based on

a) normal mode theory (e.g., Newman and Ingenito, 1972; Miller and Ingenito, 1975; Jensen and Ferla, 1979; Miller and Wolf, 1980)

b) ray theory (e.g., Cornyn, 1973a, 1973b; Weinberg, 1973; Spofford, 1974; Yarger, 1976; Bartberger, 1978)

c) fast field theory (e.g., DiNapoli, 1971; Kutschale, 1973; Schmidt, 1988)

d) coupled modes (e.g., Evans, 1986) and

e) parabolic equation methods (e.g., Tappert, 1977; Lee and Botseas, 1982; Jensen and Martinelli, 1985).

The review on propagation modelling as presented above, though not complete, gives an idea about the status of modelling methods and sophisticated models currently in use for practical applications. When viewed with this background, work on similar lines that has been done in India is extremely limited, more so if one considers the broad field of ocean acoustics as such.

The first and comprehensive study related to acoustical aspects of the North Indian Ocean was by Fenner and Bucca of the U.S. Naval Oceanographic Office (Fenner and Bucca, 1972a, 1972b). They analysed all the data for north of 10° S latitude then available from the National Oceanographic Data Centre (NODC), to present the sound velocity structure of the North Indian Ocean. Rao and Sundararamam (1974) analysed temperature, salinity, and depth data collected on board *INS Kistna* during the International Indian Ocean Expedition (IIOE) and presented the sound velocity structure in the upper 500 m of Arabian Sea during September-December 1962. A similar work based on STD data collected on board *INS Darshak* during February-May 1974 in the Arabian Sea was presented by Somayajulu *et al.* (1980). Pradeepkumar and Mathew (1988) studied the geographical variation of the deep sound channel in the Indian Ocean in terms of the prevailing temperature and salinity structures derived from NODC data for the period after 1956.

Murty *et al.*, (1984,1986), Murty and Muni (1987), and Murty and Pradeepkumar (1986,1987,1988,1989,1990) presented studies on acoustical aspects of the sediments overlying the

continental shelves of India. The shelf sediments are mostly sandy in nature and rich in carbonate content. Murty *et al.*, (1984) and Murty and Muni (1987) presented empirical relations applicable to the shelf sediments. In the analysis of sediment samples collected off Cochin, Murty *et al.*, (1984) note that sound speeds for coarser sediments show higher values compared to Hamilton (1980), but agree reasonably well with Sutton *et al.*, (1957). Supported by the observations of Sutton *et al.*, the higher sound speeds were attributed to a higher percentage of carbonate present in these calcareous sediments. In a study on the applicability of sound speed models to marine sediments, Murty and Pradeepkumar (1989,1990) compared measured sound speeds for two environments off Cochin with sound speeds calculated using various sound speed models. They found that compared to other models, the Biot-Stoll model (Stoll, 1977) and Nobes's model (Nobes, 1989) fit the experimental data well, with the latter showing better results. This was attributed to the inadequacy of Hamilton's relation of bulk modulus used in their Biot-Stoll model computations, which do not model the carbonate-rich sediments satisfactorily.

In the field of propagation modelling, Karthikeyan (1981) developed a normal mode computer program for transmission loss computations in a Pekeris channel. Another normal mode program for an ocean with one or two layers, and under upward refracting conditions was reported by Karthikeyan (1986a). Anand and Balasubramanian (1983) applied modified ray theory to downslope propagation in an isovelocity ocean. Karthikeyan (1985,1986b) describes a model of sound propagation in shallow sea with a bilinear sound speed profile. This modified ray theory model was also used for time series simulation. Using conventional ray theory, Murthy and Murthy (1986) examined the influence of internal waves in the ocean on sound transmission.

Past few years have shown more significant efforts in the

19

field of propagation modelling. Anand and Avudainayagam (1989) described a modified ray theory model applicable to three dimensional propagation in a wedge shaped ocean with isospeed water column. They compared results from the model with normal mode theory (in the case of a Pekeris channel) which showed good agreement. Vijayakumar (1989) presented a detailed account of experimental procedures for at-sea sound propagation studies and discussed the results of a few such experiments conducted off the west coast of India. He also described a normal mode propagation model of a lossy Pekeris channel including shear wave effects, and compared model simulations with the experimental results. In this model, shear wave effects were incorporated using an approximate modal shear attenuation coefficient (Ingenito and Wolf, 1976; Eller and Gershfeld, 1985)

Balasubramanian (1989) presented a ray theoretical sound propagation model for a range-independent ocean with an arbitrary sound speed profile. Here the rays are classified into seventeen unique types to enable the specification of search conditions for each type of rays. Balasubramanian and Muni (1990a,b) described a transmission loss model based on the exact effective depth of a Pekeris wave guide, including shear wave effects. As a part of investigations aimed at developing techniques for acoustic tomography, Murty *et al.* (1990) reported results of computations of some acoustic ray parameters in the Bay of Bengal.

Vijayakumar and Ajaikumar (1990a) presented experimental data from two shallow water locations on the western continental shelf of India showing the existence of optimum frequency bands of propagation. They showed that the optimum frequency bands could be predicted with fair degree of accuracy using normal mode theory of a Pekeris channel (Vijayakumar, 1989; Vijayakumar and Ajaikumar, 1989). Following Wakeley (1978), Vijayakumar and Ajaikumar (1990b) described a computer model for estimation of the source levels

20

of shallow underwater explosions which are essential in experimental measurements of propagation loss. Balasubramanian and Radhakrishnan (1990) published results of comparisons of measured propagation loss off Cochin with corresponding simulations using an implementation of a propagation model based on the parabolic equation method (Balasubramanian and Radhakrishnan, 1989) and found good agreement for frequencies below 2000 Hz.

1.7. OBJECTIVES AND SCOPE OF THE PRESENT STUDY

The review on propagation modelling indicates that within the country, there have not been much studies on various aspects of propagation modelling. Realistic estimates of transmission loss requires proper selection of environmental sub-models for quantifying various sound attenuation mechanisms in the sea. In assessing model predictions of propagation characteristics and comparing these with field measurements, one should be cautious about capabilities and limitations of these sub-models in representing the actual phenomena taking place during propagation. It was also noted that propagation models contain solutions to the wave equation and that one or more simplifying assumptions may be involved depending on the geometry of the environment and the type of solution. Hence for proper application of a model to a realistic situation, it is essential to know the conditions under which a particular type of solution is valid.

Acoustics of coastal seas is of considerable interest as the coastal waters encompass the exclusive economic zone of the country where various exploratory and research activities are being carried out. Shallow water acoustics is also important from a strategic point of view, as it is essential for effective operation of the maritime defence forces of the country. It is also clear that shallow water acoustics is very much complex compared to that of deep waters. A working model

21

of sound propagation could be an extremely useful tool for the study and interpretation of the propagation characteristics of sound in the sea. It can also be used, along with suitable data analysis techniques, for remote sensing of various environmental parameters, especially of the sea bottom, which are otherwise difficult or virtually impossible to obtain.

With this background, a realistic model for practical applications in sound propagation studies is proposed and presented. Review of literature on propagation modelling show that normal mode theory and the more recent modified ray theory have been successful in practical modelling of shallow water propagation. In the present study, a ray theoretical model of sound propagation in a range-independent environment with an arbitrary sound speed profile is developed and implemented.

The next chapter (Chapter 2) contains the essential theoretical background based on which the model is developed. Basic ray theoretical equations and concepts in modified ray theory are presented. Important sound attenuation mechanisms in the sea, viz., absorption in sea water, sea surface scattering, and bottom reflection are discussed in Chapter 3. Methods and expressions for their estimation are presented. These attenuation mechanisms are incorporated into the ray theoretical propagation model presented in Chapter 4.

The propagation model is developed and presented in Chapter 4. An efficient algorithm for eigen-ray finding is developed, based on which the propagation model is implemented on a computer. The model outputs include propagation loss and the received time series of a transmitted single-frequency pulse. Quality of the model is assessed by comparing model outputs with those from a normal mode propagation model and also with published results in the literature.

Chapter 5 contains an outline of the experimental methods

for the estimation of transmission loss at sea. Details of two shallow water transmission loss experiments conducted on the western continental shelf of India are presented. The transmission loss estimates are compared with computations using the propagation model. The results are discussed. The last chapter (Chapter 6) summarises the results and conclusions drawn from the study.

Chapter 2

THEORETICAL BACKGROUND

2.1. THE WAVE EQUATION

Propagation of elastic waves in a medium can be described
by solutions of the governing *wave equation*. The simplest form
of the wave equation is derived under certain physical
assumptions and making use of three basic physical laws. We
assume a non-viscous, isotropic, perfectly elastic fluid with
no physical or chemical attenuation mechanisms present. The
mathematical treatment of sound propagation is much simplified
if it is assumed that the pressure fluctuations due to the
acoustic waves are small compared to the ambient static
pressure (the small amplitude assumption). This is true even
for signals generated by powerful explosions, provided that
the reference point is sufficiently away from the source. One
important and useful consequence of this assumption is that
the stress-strain relationship in the medium is then linear.
The effect of gravity is neglected so that density ρ_0 and
pressure P_0 are uniform throughout the medium. The three basic
laws are

a) The law of conservation of mass
   (The equation of continuity)
b) The law of conservation of momentum
   (Newton's second law of motion)
c) The law of existence of an equation of state
   (A thermodynamic relation between sets of variables such as
   pressure and density)

Derivation of the wave equation from these laws is dealt with
in detail in many text books (Officer, 1958; Kinsler and Frey,
1962; Clay and Medwin, 1977). It can be shown that the form of
the equations which satisfy the three physical laws is the

same for pressure p, particle velocity u, and density fluctuations $d\rho$ provided that

a) only linear terms are kept,
b) condensation s is small ($s=d\rho/\rho_0 \ll 1$),
c) only irrotational motion is considered, and
d) the ratio $dp/d\rho$ is constant (the equation of state for an acoustic disturbance, the small amplitude assumption).

The wave equations obtained under these conditions are

$$\nabla^2 \begin{Bmatrix} p \\ u \\ s \end{Bmatrix} = \left(\frac{1}{c^2}\right) \frac{\partial^2}{\partial t^2} \begin{Bmatrix} p \\ u \\ s \end{Bmatrix} \qquad (2.1)$$

where c is the sound speed, t is the time, and ∇^2 is the Laplacian operator. Many fluid flows, in acoustics as well as in fluid mechanics, may be treated as irrotational. Whenever the curl of a vector $\underline{A}$ is zero, it is possible to define that vector quantity in terms of the gradient of a scalar potential ϕ as $\underline{A}=\pm\nabla\phi$. Thus the existence of a scalar potential implies irrotationality. Potentials are used frequently, since they allow irrotational vector fields to be treated in terms of scalar fields, thereby essentially replacing the three equations for the three vector components by a single equation.

Because of the assumption of irrotationality used in deriving the wave equation, it is possible to define a scalar velocity potential by

$$u= -\nabla\phi= -(\partial\phi/\partial x + \partial\phi/\partial y + \partial\phi/\partial z) \qquad (2.2)$$

and to relate density and pressure fluctuations to this potential. The acoustic pressure and the velocity potential are related by $p= \rho_0\, \partial\phi/\partial t$ and the condensation is related to ϕ through the relation $s= (1/c^2)\, \partial\phi/\partial t$.

The acoustic potential also satisfies the wave equation. Hence, a single equation with a scalar parameter is possible from which all acoustic variables are derivable:

$$\nabla^2 \phi = (1/c^2) \; \partial^2 \phi / \partial t^2 \tag{2.3}$$

where ϕ is related to u, p, and s as already defined above. This is the linear, undamped, scalar wave equation for propagation of sound in a fluid. The equation states that apart from boundary effects, the propagation is dependent only on c.

The assumption of linearity of the medium makes it possible to treat any arbitrary acoustic disturbance as the sum of sinusoidal components, each of the form

$$\phi = \Phi \; \exp(i\omega t) \tag{2.4}$$

where $i = \sqrt{-1}$ and $\omega = 2\pi f$ is the angular frequency of the sound. $\Phi = \Phi(x, y, z, f)$ is a complex amplitude. Substituting this into the wave equation (Eq. 2.3) and re-arranging terms,

$$\nabla^2 \phi + k^2 \phi = 0 \tag{2.5}$$

where $k = \omega/c$ is the wave number. This is the *Helmholtz equation* for the propagation of monochromatic sound in a fluid.

2.1.1. Solution of the wave equation

The wave equation can be solved in a number of ways. The solutions describe the characteristics of propagation. For a particular problem of interest, the equation is solved by applying suitable boundary and initial conditions. For example, the boundary conditions in ocean acoustics are the known pressures and particle velocities at the boundaries of the medium (the sea surface and the sea bottom) and the initial conditions pertain to the sound source. The plane wave

26

and spherical wave solutions are two most useful and simple solutions of the wave equation.

Exact solutions of the wave equation exist only for a few simple models of the oceanic environment. The classic example of such a model is the *Pekeris channel* (Pekeris, 1948). This is a two layer model of the shallow water environment where a homogeneous, loss-less fluid layer of constant thickness overlies a non-absorbing fluid bottom which is a semi-infinite, homogeneous half-space having higher sound speed. A large amount of theoretical work on shallow water acoustics has been centered around this model and its simple extensions.

When the environmental model is such that exact solutions are difficult to obtain, one resorts to approximate solutions of the wave equation. Solutions of the general wave equation without any simplifications are usually limited to iterative finite difference techniques (Urick, 1982:p-3-2). Solutions of practical interest frequently use simplified models of the environment and numerical methods of solution. Such solutions give insight into the physical processes controlling the propagation besides having the advantage of less involved mathematical procedures.

2.1.2. Normal modes and rays

Normal mode theory and ray theory are two widely used approaches in sound propagation modelling. Mathematically normal modes are solutions of the wave equation. Physically they correspond to interference patterns, in the form of standing waves, generated by plane waves travelling in opposite directions but at different angles. Normal modes represent possible states of vibration of a medium. A source may excite a number of such modes of vibration having different amplitude and phase relationships so as to produce a travelling wave. These *discrete propagating modes*, as they are called, are formed by energy interacting with the bottom at

angles less than a critical grazing angle. Energy incident at steeper angles get rapidly attenuated and they constitute the modes with continuous spectrum. These modes are important only at ranges close to the source.

In addition to the loss in amplitude due to geometrical spreading, each propagating mode suffers a steady attenuation due to various mechanisms. Higher order modes which correspond to higher-angle equivalent rays attenuate at faster rates. At long distances from the source only a few of the modes are significant, the rest being of negligible amplitude. At sufficiently large ranges there is a single propagating mode (the lowest order mode) which suffers the least attenuation. Acoustic pressure field at any point in the medium is obtained as a summation over the significant propagating modes.

Basically, ray theory is a high frequency approximation of wave theory. Rays are normals to the wave fronts and undergo reflection and refraction obeying Snell's laws. The basic conditions under which ray theory is applicable are a) the properties of the medium do not change appreciably over a distance of one wave length and b) the water depth is much larger than the acoustic wave length. Conventional ray theory with appropriate modifications yield results comparable with the normal mode theory and offers an alternative method of shallow water sound propagation modelling.

The description of propagation in terms of rays is more appealing and intuitive than a normal mode interpretation. But wave theory has the advantage that it is rigorous and applicable under certain circumstances where ray theory fails. Normal mode theory can give formal and complete solutions of the wave equation for propagation in simple environments. When the frequencies are high and the water is deep, the number of propagating modes increases drastically so that normal mode computations become prohibitive. Ray theory can be effectively used under such conditions.

In addition to advantages of simple interpretation of results, ray theory has other plus points compared to mode theory. Ray theory is more suited to model strongly range dependent environments than the mode theory. Directionality of the acoustic source can be easily incorporated into ray theory by suitable source weighting functions. Another advantage is that the time series of signal at the receiver can be generated by simple in-phase addition of arrivals along multi paths of propagation. To obtain the same result by the mode theory, Fourier transform techniques have to be employed.

A good account on the basic concepts normal modes and rays and the connection between them is available from various references other than text books (e.g., Tolstoy, 1959; Weston, 1960a; Bucker, 1964; Guthrie, 1974; Tindle and Guthrie, 1974; Guthrie and Tindle, 1976; Chapman and Ward, 1990).

2.2. RAY THEORY OF SOUND PROPAGATION

Ray theory gives an easy visualization of certain propagation characteristics in an inhomogeneous ocean, like the formation of sound channels and shadow zones. In ray theory it is assumed that energy propagates along rays which, by definition, are normals to the wave fronts. Each ray is a "tube" of infinitesimal cross section through which the energy "flows". There is no flow of energy across a ray tube. Hence the sound intensity along a ray path is related to the cross sectional area of the ray tube. The energy may reach a given receiver along different ray paths. Acoustic intensity at the receiver is the sum of contributions due to all these rays (called the *eigen-rays*).

For ray theory to be applicable, the sound speed c and the acoustic impedance of the medium should not change appreciably over a distance comparable to an acoustic wave

length λ. In the case of a stratified environment $c=c(z)$, and assuming a uniform density for the medium, this condition can be written as $(\lambda/c)|dc/dz|\ll 1$ (Brekhovskikh and Lysanov, 1982). Conventional ray theory does not consider diffraction effects. Hence the receiver should not be located at or near caustics or shadow zones. But the accuracy of ray theory can be improved in the vicinity of caustics by using asymptotic corrections (references are given in Section 1.6). Another condition necessary for the validity of classical ray theory is that the water depth be much larger than the acoustic wavelength.

The process of ray tracing is of basic importance in ray theory. This involves computation of the range and depth coordinates of a ray along its path. A *ray diagram* consists of the paths of selected rays in a sound beam. The rays are specified by their respective projection angles at the source. The path of a ray is governed by Snell's laws. In the coming sections we present the classical ray path equations and the method we shall use in ray tracing in a range-independent environment with an arbitrary sound speed profile. The concept of beam displacement in modified ray theory and the associated characteristics are described. Equations for individual ray amplitudes and phases, and the methods of transmission loss computation and signal structure simulation are presented.

2.2.1. Snell's law and the equations for ray paths

This section contains the equations used for ray tracing in stratified media. It is assumed that the impedance (product of density and sound speed) variations in the medium are small so that partial reflections at the layer boundaries can be neglected. Thus the equations are applicable to ray refraction within the water column where the above assumption holds.

2.2.1.1. Stratified medium with homogeneous layers

In a stratified medium consisting of homogeneous layers with sound speeds c_1, c_2,... (Fig. 2.1), Snell's law gives

$$\frac{c_1}{\cos \theta_1} = \frac{c_2}{\cos \theta_2} = \cdots = \frac{c_i}{\cos \theta_i} = \cdots = \Re \qquad (2.6)$$

Here $\Re$ is called the *ray parameter* and is a constant for a ray. This is a basic equation used in tracing the path of a
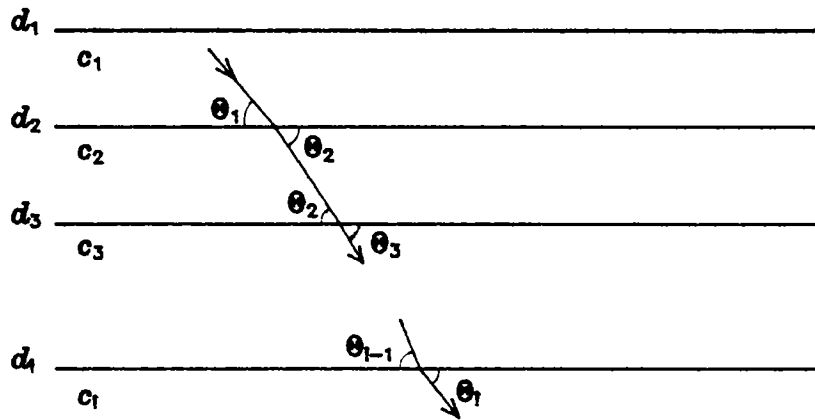

Fig. 2.1. Ray path in a medium with homogeneous layers.

ray. For convenience, ray angles θ are expressed with reference to the horizontal (*grazing angles*). In Fig. 2.1., let d_1, d_2, ..., d_i be the depths of the layer boundaries such that $d_1 < d_2 < ... < d_i$. The subscripts refer to the corresponding layer numbers. Ray path in each layer is a straight line segment and refraction takes place only at the layer boundaries. The horizontal range increment r_i of a ray in layer i is given by

$$r_i = (d_{i+1} - d_i)/\tan \theta_i \qquad (2.7)$$

where the angle of refraction θ_i is obtained from Snell's law (Eq. 2.6) as

31

$$\theta_i = \cos^{-1}\left[(c_i/c_{i-1})\cos\theta_{i-1}\right] \qquad (2.8)$$

The distance $(r_a)_i$ covered by the ray (distance along the ray path) in the layer and the corresponding travel time t_i are given by

$$(r_a)_i = r_i/\cos\theta_i$$

and

$$t_i = (r_a)_i/c_i \qquad (2.9)$$

2.2.1.2. Continuously stratified medium with layers of constant sound speed gradient

Snell's law of refraction applies to continuously stratified media as well. In Fig. 2.2, a ray enters layer i of constant sound speed gradient $g_i = (c_{i+1}-c_i)/(d_{i+1}-d_i)$. Let c_{i+1} be greater than c_i. The angle θ_{i+1} at which the ray leaves the layer is given by Snell's law. Unlike in the previous case, sound speeds here are continuous at layer boundaries. Therefore ray angles immediately on either side of a boundary are equal. The path of the ray within the layer is an arc of a circle whose radius of curvature R_i is given by (Kinsler and Frey, 1962)

$$R_i = \frac{c_i}{g_i \cos\theta_i} = \frac{c_{i+1}}{g_i \cos\theta_{i+1}} = \frac{\Re}{g_i} \qquad (2.10)$$

The ray turns towards the region of lower sound speed. In the figure, let O be the centre of curvature. Then the horizontal range increment r_i of the ray in travelling through the layer is

$$r_i = R_i (\sin\theta_i - \sin\theta_{i+1}) \qquad (2.11)$$

The distance along the ray path is given by

$$(r_a)_i = \int_{\theta_i}^{\theta_{i+1}} R_i \, d\theta \qquad (2.12)$$
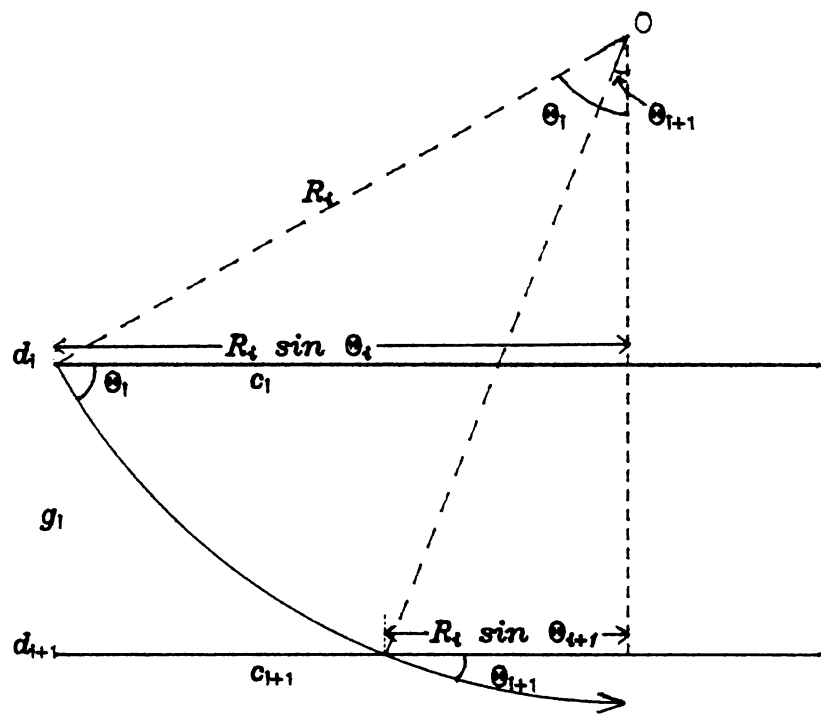
Fig. 2.2. Ray path in a medium with constant gradient of sound speed.

Travel time t_i of the ray is obtained from

$$t_i = \int_{\theta_i}^{\theta_{i+1}} (1/c)\, R_i\, d\theta$$

where c is the sound speed. From Snell's law, $c = \Re \cos \theta$, so that

$$t_i = (R_i/\Re) \int_{\theta_i}^{\theta_{i+1}} \frac{d\theta}{\cos \theta}$$

Substituting for R_i from Eq. 2.10, we get (Ewing and Worzel, 1948)

$$t_i = \frac{1}{g_i} \int_{\theta_i}^{\theta_{i+1}} \frac{d\theta}{\cos \theta} = \frac{1}{2g_i} \left[\log \frac{1+\sin \theta}{1-\sin \theta} \right]_{\theta_i}^{\theta_{i+1}} \tag{2.13}$$

Referring to Fig. 2.2, θ_i is such that $c_{i+1} < \Re$, and the ray passes across the layer. From Snell's law, the ray angle θ becomes zero at points where the sound speed is equal to the ray parameter. This means that if θ_i is such that $c_{i+1} >= \Re$, the ray undergoes total internal reflection within the layer (Fig. 2.3). The turning point depth d_t of the ray is given by
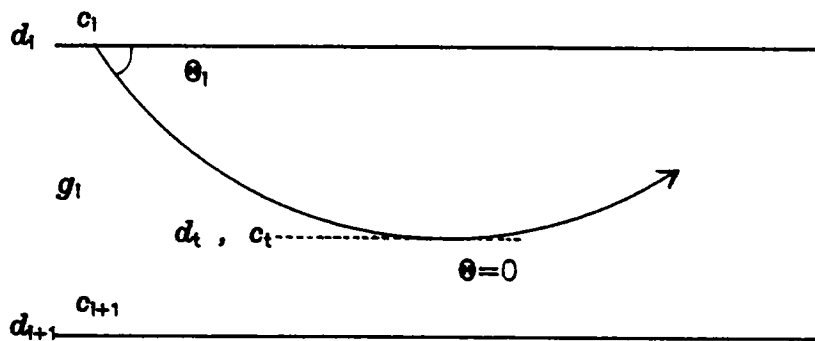

Fig. 2.3. Total reflection of the ray in a layer of constant sound speed gradient.

$$d_t = d_i + \frac{c_t - c_i}{g_i} \qquad\qquad (2.14)$$

such that $d_i < d_t <= d_{i+1}$. Here c_t is the sound speed at the turning point depth d_t and is equal to $\mathfrak{R}$. Substituting $\theta_{i+1} = 0$ in Eqs 2.11 to 2.13, we get the horizontal range increment, distance along the path, and the travel time respectively of the ray upto the turning point. The lower turning point in the path of a ray is named a *nadir* and an upper one, an *apex*.

Because conventional ray theory is valid only in the high frequency limit (the deep water case), till the beginning of 1980's shallow water propagation problems were, in general, described using normal mode theory. Next we discuss the beam displacement and related phenomena, inclusion of which enhances the performance of ray theory in shallow waters and at low frequencies.

2.2.2. Modified ray theory of shallow water sound propagation- Beam displacement at the sea bottom

The process of reflection of sound from the water-sediment interface is often represented by the plane wave reflection coefficient. Most often, sound sources of interest in the ocean are point sources located at finite distances from the boundaries. At such distances, the spherical sound waves from these sources can not really be approximated by plane waves. The reflection and refraction of spherical waves at a plane boundary is a more difficult problem due to the difference between the symmetry of the wave and that of the boundary (Brekhovskikh and Lysanov, 1982). Hence the spherical wave is represented as an integral over plane waves propagating in all directions. The reflected and transmitted waves are integrated over all directions to get the corresponding fields due to the point source. An analysis of the reflected wave shows certain interesting phenomena.

An acoustic beam incident at the sea bottom is generally displaced laterally on reflection (Brekhovskikh, 1960). This is called the *beam displacement*. Thus the incident energy
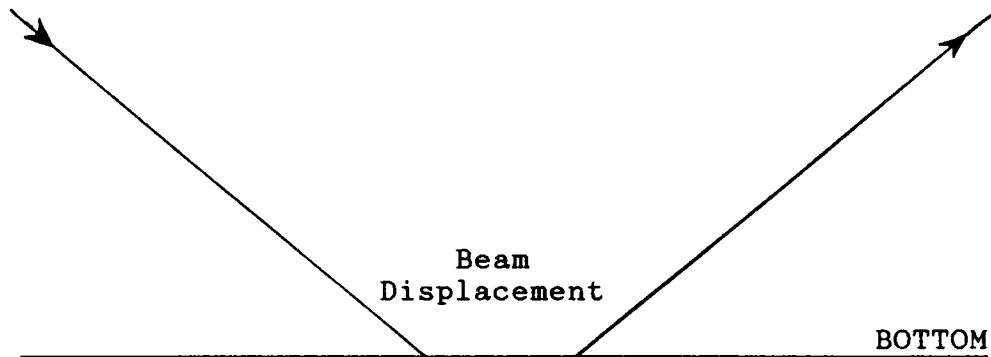

Fig. 2.4. Beam displacement on reflection at the sea bottom

travels near the bottom interface for a while before returning to the water as a reflected wave. Brekhovskikh suggested that this idea of beam displacement is still meaningful for a ray of fixed angle as opposed to a beam so that the path of a bottom reflected ray is modified as shown in Fig. 2.4.

Beam displacement is the effective lateral displacement of a spherical or bounded plane wave (like a ray) on reflection at the bottom. It is given by $-\partial\phi_b/\partial k$ where ϕ_b is the phase of the reflection coefficient and k is the horizontal component of the wave number (Brekhovskikh, 1960). There is no beam displacement at the sea surface because the phase shift is a constant. Beam displacement is a function of the acoustic characteristics of the media, the frequency, and the angle of incidence at the bottom.

2.2.2.1. Beam displacement at a perfect fluid bottom

Reflection of plane waves at a perfect fluid bottom (as in the case of a Pekeris channel) is described by the *Rayleigh reflection coefficient*. The reflection coefficient is a function of the acoustic impedances of the media and the angle

35

of incidence. Following Tindle (1983), the reflection coefficient R_b and phase ϕ_b of reflection are given by

$$R_b = (\rho_2 \gamma_1 - i\rho_1 \gamma_2)/(\rho_2 \gamma_1 + i\rho_1 \gamma_2)$$

$$\phi_b = -2 \tan^{-1}(\rho_1 \gamma_2/\rho_2 \gamma_1)$$

(2.15)

Here ρ and γ stand for the density and vertical component of the wave number for the two fluid media. The subscripts 1 and 2 refer to the upper (water) and the lower (sediment) medium respectively. Representing sound speed by C and assuming an angular frequency of $\omega = 2\pi f$ for the sound wave, $\gamma_1 = (\omega/C_1) \sin \theta$ and $\gamma_2 = (\omega/C_1)(\cos^2 \theta - C_1^2/C_2^2)^{1/2}$.

The beam displacement Δ_h for a ray incident at a grazing angle θ is given by

$$\Delta_h = -\partial\phi_b/\partial k = 2k\rho_1\rho_2\left[\gamma_1^2 + \gamma_2^2\right]/\left[\gamma_1\gamma_2\left(\rho_1^2\gamma_2^2 + \rho_2^2\gamma_1^2\right)\right]$$

(2.16)

where the horizontal wave number $k = (\omega/C_1) \cos \theta$.

There is a time displacement τ associated with the beam displacement. This is given by $\partial\phi_b/\partial\omega$ and is related to Δ_h through the relation (Tindle and Bold, 1981)

$$\Delta_h/\tau = C_1/\cos \theta$$

(2.17)

This is the apparent speed of propagation of energy along the beam displacement path.

Beam displacement is zero for grazing angles greater than the critical, that is, for partially reflected rays. Δ_h increases asymptotically to infinity as θ tends to 0 or to the critical angle. This behaviour of the Δ_h versus θ curve results in the formation of *beam displacement caustics* (Tindle, 1983). Calculation of the field in the vicinity of these caustics requires corrections to the ray theory involving the Airy function and its derivative (Brekhovskikh

and Lysanov, 1982; Tindle, 1983; Lawrence, 1985; Tindle and Deane, 1985).

2.2.2.2. Beam displacement at a lossy bottom

Formulation of the beam displacement concept as above is applicable to a perfect fluid bottom with no attenuation. Siegmann *et al.* (1987) investigates the influence of realistic amounts of compressional wave attenuation in the bottom when modified ray theory is used for shallow water propagation modelling. One of the consequences of attenuation is that Δ_h is nonzero for any incident ray angle. In general, Δ_h decreases monotonically as θ increases. An important result is that the asymptotic increase in the beam displacement towards infinity as θ tends to the critical angle is now absent. This eliminates the source of beam displacement caustics in most cases of realistic sea bottoms. The study also showed that the presence of even a small amount of attenuation can significantly influence the ray geometry, amplitudes, phases and hence the total field intensity. Further discussion on beam displacement at a lossy bottom is presented in Chapter 3, which deals with sound attenuation mechanisms in the sea.

2.2.3. Ray tracing in an environment with arbitrary, range-independent sound speed profile

To a first approximation, the oceans may be regarded as a stratified medium. In general, vertical gradients of sound speed are about 1000 times the horizontal gradients except in, for example, frontal zones. Ignoring horizontal gradients we assume that the sound speed $c(z)$ is an arbitrary function of depth z and also that the sea surface and the sea bottom form two plane parallel boundaries. Now, for a sound source located within the medium, the environment is cylindrically symmetrical and ray refraction is limited to a vertical plane. The requirement is to trace the ray paths in the vertical plane and in a radial direction away from the source.

The fact that ray paths in a layer of constant sound speed gradient are arcs of circles is widely used in ray tracing with arbitrary sound speed profiles. For this, the profile is divided into a number of segments, each having a constant sound speed gradient. For convenience in practical computations, additional layer boundaries are introduced at depths corresponding to the source and the receiver. In effect, the water column is assumed to be composed of layers of constant sound speed gradient separated by horizontal boundaries. These layers need not be of a constant thickness. In practice this division is often done by a visual observation of the gradients in the profile. A layer boundary is introduced at each depth where there is a significant change in the gradient such that the resulting profile satisfactorily represents the actual profile. In the new profile obtained by this approximation, sound speed is continuous throughout the depth but its gradients are discontinuous at layer boundaries. This approximation of the profile works well with ray theory, provided the gradient discontinuities are not too large.

2.2.4. Eigen-ray finding and computation of transmission loss

A common and convenient way of representing the field of a sound source is in the form of a graph where transmission loss is plotted against distance from the source. For this, acoustic pressures are converted to corresponding transmission loss values so that the numerical values become independent of the actual level of the source. Another method of presentation is by means of transmission loss contours in the vertical plane which gives a more comprehensive picture of the field. In any case, transmission loss is to be computed for a number of points in the range-depth plane. The first step towards the computation of the field is the determination of eigen-ray structures. Ray tracing procedure outlined in the previous section along with a suitable algorithm is used in obtaining

38

the eigen-ray structure. Amplitudes and phases of these rays
are used for computing the field at the receiver.

2.2.4.1. Amplitude and phase of a ray

The amplitude of an eigen-ray is determined by the
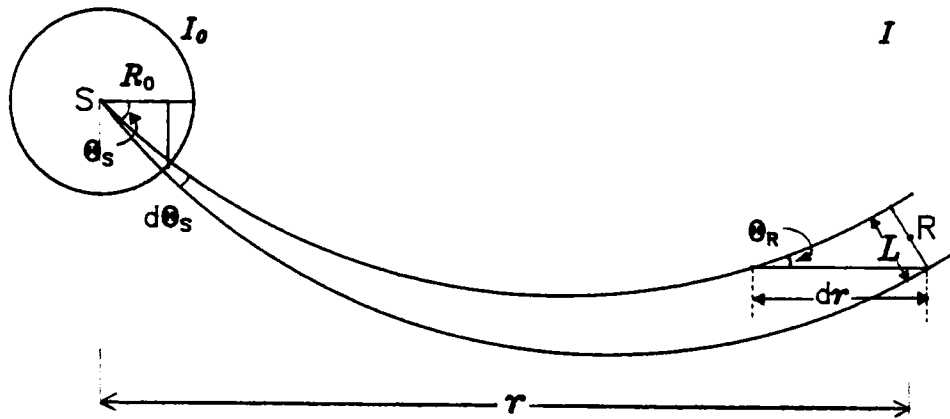geometrical spreading undergone by the ray (spreading loss)

Fig. 2.5. Spreading of a ray tube of angular width $d\theta_S$

and attenuation encountered along its path. Spreading loss can
be estimated from the geometrical spreading of a ray tube.
Referring to Fig. 2.5, S is an omnidirectional point source
and R is a receiver at a distance of r from the source. Ray
refraction in the vertical plane alone is considered. The ray
tube shown has an angular width of $d\theta_S$ in the vertical plane
and is projected at a grazing angle of θ_S. Let I be the sound
intensity at R and I_0 that at a reference distance R_0 from the
source. The power P_0 contained within a ring of width $d\theta_S$ is

$$P_0 = I_0 \cdot 2\pi R_0 \cos \theta_S \cdot R_0 d\theta_S \qquad (2.18)$$

As there is no energy flow across a ray tube, the energy
contained in a ray tube remains constant provided that
attenuation is not present. Hence from Fig. 2.5,

$P_0 = I \cdot 2\pi r \cdot L = I \cdot 2\pi r \cdot dr \sin \theta_R$

where θ_R is the arrival angle of the ray at the receiver R. If the reference distance R_0 is taken to be 1 m, we get

$$I/I_0 = \cos \theta_S / \left[r \frac{dr}{d\theta_S} \sin \theta_R \right] \qquad (2.19)$$

The quantities θ_S, θ_R and r are known from ray tracing computations and $dr/d\theta_S$ is estimated numerically. The spreading loss in decibels is given by $-20 \log (A/A_0)$ where A and A_0 are the pressure amplitudes corresponding to the intensities of I and I_0. For $A_0 = 1$, the pressure amplitude at the receiver (in the absence of attenuation) is given by

$$A = \left[\cos \theta_S / \left(r \frac{dr}{d\theta_S} \sin \theta_R \right) \right]^{1/2} \qquad (2.20)$$

The quantity on the right hand side of Eq. 2.20 is called the *spreading factor S*. This is the amplitude reduction factor arising from geometrical spreading.

This equation for spreading factor is not valid at and near caustics. Spreading factor increases enormously near caustics and it goes to infinity on the caustic envelopes as $dr/d\theta_S$ tends to zero. Here the geometrical ray theory needs correction, as mentioned at the beginning of Section 2.2. Also, the equation is not valid at ray turning points where θ_R becomes zero.

Important mechanisms of sound attenuation and their estimation are discussed in Chapter 3. These are volume absorption by sea water and reflection loss at the boundaries. If α_w is the sound absorption coefficient in sea water, the corresponding attenuation is $\exp(-\alpha_w r_a)$ where r_a is the distance along the ray path. Now, if R_s and R_b are the sea surface and bottom reflection coefficients, the amplitude A of an eigen-ray is given by

40

$$A = R_s{}^{N_s} \; R_b{}^{N_b} \; S \; \exp(-\alpha_w r_a) \qquad\qquad (2.21)$$

where N_s and N_b are the number of surface and bottom reflections respectively and S is the spreading factor. Note that we have assumed unit pressure amplitude at the source.

Other than by differences in travel times, phases of the individual eigen-rays are determined by reflection at the boundaries and refractive turning within the medium. Reflection at the sea surface introduces a phase change of $-\pi$ independent of the angle of incidence (Tolstoy and Clay, 1966:p-26). Reflection at the sea bottom causes a phase change of ϕ_b which is a function of the angle of incidence and nature of the sea bottom (Section 2.2.2 and Section 3.3.4). Total internal reflection of plane waves within a stratified medium is characterised by a phase change of $-\pi/2$ (Tolstoy, 1968).

Thus, if T is the travel time of an eigen-ray with N_s surface reflections, N_b bottom reflections and N_t turning points (apex and nadir), then a general expression for phase ψ of the corresponding arrival can be written as

$$\psi = \omega T - N_s \pi - N_b \phi_b - N_t (\pi/2) \qquad\qquad (2.22)$$

2.2.4.2. Computation of transmission loss

Equations 2.21 and 2.22 give the amplitudes and phases of individual arrivals along the eigen-ray paths. These are then added coherently (taking into consideration the phases of the individual arrivals) to get the resultant acoustic pressure at the receiver. If there are n eigen-rays, the coherent transmission loss TL (in dB) from the source to the receiver (assuming unit pressure amplitude at the source) is given by

$$TL = -20 \; \log\left(\left| \sum_{j=1}^{n} A_j \; \exp(i\psi_j) \right| \right)$$

41

$$= -10 \log \left[\left(\sum_{n} A_j \cos \psi_j \right)^2 + \left(\sum_{n} A_j \sin \psi_j \right)^2 \right] \qquad (2.23)$$

where A_j and ψ_j are the amplitude and phase of the jth arrival.

2.2.5. Time series simulation

The use of time series analysis techniques is a recent advent in low frequency ocean acoustics (Jensen, 1988). Low frequency propagation is more stable and predictable so that powerful time series analysis techniques might be valuable for studying complex propagation situations encountered in the oceans. The ability to simulate signals reflected from the sea floor would be valuable in the interpretive analysis of experimental data used to determine sea floor structure, important geo-acoustic parameters, and major acoustical mechanisms (Westwood and Vidamar, 1987). Jensen (1988) presents results of wave theory modelling of pulse transmission in shallow and deep waters using mode theory and shows that pulse modelling permits a detailed analysis of ocean acoustic propagation not achievable from continuous wave results. Modified ray theory has been successfully used in narrow band (Tindle, 1981) and broad band (Westwood and Tindle, 1987) shallow water time series simulations.

Compared to other approaches, the ray based approach is well suited for the simulation of time series. Individual arrivals can be added with reference to the arrival time to generate the time series. Compared to most other numerical models, the ray approach is more efficient at higher frequencies. Its computer memory requirements are independent of frequency. For example, pulse modelling in deep water using wave theory is practical only for frequencies below 50 Hz (Jensen, 1988). Ray theory is more attractive for broad band

time series simulation as the characteristics of eigen-rays with beam displacement turn out to be smooth functions of frequency (Westwood and Tindle, 1987).

The transmitted signal we use in the simulations is a narrow band pulse centered at a frequency of ω and having unit amplitude. This is represented by

$$p_0(t) = g(t) \exp(i\omega t) \qquad (2.24)$$

where $g(t)$ is the envelope of the pulse and t is the time. This pulse arrives at the receiver along multiple eigen-ray paths. Each of the arrivals is characterised by its own amplitude and phase. Out of all the arrivals, the first one is taken as a reference to which the remaining arrivals are added in phase to get the resultant pulse $p(t)$. If there are n arrivals,

$$p(t) = \sum_{j=1}^{n} g(t - T_j) \, A_j \, \exp(i(\omega t - \psi_j)) \qquad (2.25)$$

2.3. SUMMARY

We started this chapter reviewing the fundamental assumptions involved in the derivation of the wave equation and then outlined various approaches for its solution. Then the concepts of normal modes and rays, useful in describing the propagation characteristics of sound were outlined. The rest of the chapter was devoted to the ray theory of sound propagation. The ray path equations for homogeneous and stratified media were presented and the concept of beam displacement and related phenomena were discussed. Finally, the procedure for ray tracing with an arbitrary sound speed profile was described and the methods and expressions for the computation of transmission loss and time series simulation were presented.

In order to obtain realistic transmission loss values and signal structures from simulations using a propagation model, the effects various sound attenuation mechanisms are to be accounted for. In the next chapter we review three important sound attenuation mechanisms and present expressions for their estimation. These are then incorporated into the propagation model presented in Chapter 4.

Chapter 3

ATTENUATION OF SOUND IN THE SEA

Transmission loss or *propagation loss* is an important propagation characteristic used in describing the oceanic acoustic field. Broadly, transmission loss in the sea can be attributed to two factors- *spreading loss* and *attenuation*. Spreading loss accounts for the changes in intensity due to geometrical focussing and de-focussing effects. The method of spreading loss estimation was discussed in the previous chapter (Section 2.2.4.1).

Processes leading to attenuation can be considered under two categories- processes taking place within the medium and those associated with the boundaries of the medium. The processes of absorption in sea water, scattering and absorption by inhomogeneities, and diffraction and leakage out of ducts belong to the first category. Absorption involves the conversion of elastic energy into heat and represents a true loss of the energy to the medium. The remaining processes basically re-distribute the energy in space and consequently make it unavailable at the receiver. Attenuation related to boundary interactions arises from scattering losses at the sea surface and the sea bottom and also absorption in the sea bottom. In this chapter we discuss sound attenuation due to absorption by sea water, interaction with a rough sea surface, and reflection at a homogeneous sea bottom.

3.1. ABSORPTION OF SOUND IN SEA WATER
3.1.1. The Absorption coefficient

Absorption in sea water is quantitatively expressed in terms of an absorption coefficient which gives attenuation of

the energy per unit distance travelled in the medium. Attenuation in the amplitudes of particle displacement, acoustic pressure etc. are frequently expressed in units of *neper*, a natural logarithmic unit corresponding to a reduction in amplitude to 1/e of the reference value where e is the base of the natural logarithm. If the pressure variation with distance r from a source is given by

$$P = P_0 \exp(-kr) \qquad\qquad (3.1)$$

the attenuation coefficient k will have units of neper m^{-1}. In Eq. 3.1, P_0 is the reference pressure at the source. In terms of the corresponding acoustic intensities this can be re-written as

$$I = I_0 \exp(-2kr). \qquad\qquad (3.2)$$

For a plane wave, the rate of decrease in intensity with range $-dI/dr$ is proportional to the intensity I at the point of measurement so that

$$dI/I = -n\, dr, \qquad\qquad (3.3)$$

where n is a constant of proportionality. If I_1 and I_2 are the intensities at distances r_1 and r_2 from the source, then integrating Eq. 3.3 between these limits,

$$I_2/I_1 = \exp(-n(r_2 - r_1)) \qquad\qquad (3.4)$$

In this equation $n = 2k$, where k is the amplitude attenuation coefficient in neper m^{-1}. Now, the attenuation in decibels is given by

$$10 \log(I_2/I_1) = -10n(r_2 - r_1) \log e$$
$$= -8.686k(r_2 - r_1)$$
$$= -\alpha_w(r_2 - r_1) \qquad\qquad (3.5)$$

where the attenuation coefficient α_w is in units of dB m^{-1}. Thus, one neper corresponds to an attenuation of 8.686 dB. Because magnitudes of sound absorption in sea water are numerically small, it is usual to express the absorption coefficient in dB km^{-1} rather than in dB m^{-1}.

3.1.2. Sound absorption processes in sea water and estimation of the absorption coefficient

From a phenomenological viewpoint, absorption of energy from sound waves in fluids is associated with a time lag of the condensation relative to the varying acoustic pressure (Kinsler and Frey, 1962:p-218). During each cycle of pressure variation, a net amount of work is done by the passing sound wave on the medium. The phase lags, expressed in terms of characteristic *relaxation times*, are associated with a) conduction of heat from high pressure regions (condensations) to low pressure regions (rarefactions) b) equalization of fluid particle velocities in the presence of viscous stresses and c) changes in molecular energy in the presence of the acoustic pressure fluctuations. In water, sound absorption due to heat conduction is negligibly small because of poor thermal conductivity of the medium.

Absorption in pure water is due to the presence of *shear viscosity* and *volume viscosity*. The latter was introduced in order to take into account the theory of molecular structural relaxation put forth to explain the excess absorption in pure water over that due to shear viscosity alone. The coefficient of volume viscosity for water is 2.81 times the shear viscosity coefficient (Urick, 1975:p-99).

Measurements of sound absorption coefficients for frequencies between 5 and 100 kHz in sea water during World War II showed that the attenuation was about 30 times its value in fresh water at the same frequency (Urick, 1982:p-5-2). This was later discovered to be due to a chemical relaxation involving dissolved magnesium sulphate ($MgSO_4$) in sea water. $MgSO_4$ molecules dissociate and re-associate under the pressure of the passing sound wave which loses energy to the medium.

47

Based on at-sea measurements of attenuation between 2 and 25 kHz, Schulkin and Marsh (1962) presented an equation for the absorption coefficient including the effects of $MgSO_4$ relaxation. However, a compilation of field data at low frequencies indicated the presence of an additional source of absorption at frequencies below 1 kHz (Thorp, 1965). Origin of this low frequency absorption was later traced down to the presence of boric acid (Yeager et al., 1973). Boric acid $(B(OH)_3)$ has a relaxation frequency near to 1 kHz and its effect is significant at frequencies below 5 kHz. Based on laboratory measurements, Fisher and Simmons (1977) presented an equation for absorption coefficient in sea water for a constant salinity of 35 ppt and a pH of 8. Based on a review of work on low frequency absorption in the ocean and laboratory, Schulkin and Marsh (1978) found an exponential dependence of absorption on pH and published an equation for the boric acid contribution to the absorption.

More accurate equations for pure water and $MgSO_4$ components of absorption were presented by Francois and Garrison (1982a). They used these equations to obtain better estimates of low frequency absorption from field measurements. Combining these results, Francois and Garrison (1982b) published an equation to predict absorption in natural sea water in the frequency range of 200 Hz to 1 MHz and to depths of 5000 m. Their equations "represent an improvement of 10-20% in absorption prediction over most ocean conditions and over the acoustic frequencies of interest". The Francois-Garrison (FG) equation is given in Appendix 1.

Sound absorption in sea water is a function of frequency, temperature, salinity, pH, and pressure. Fig. 3.1 shows the variation of the absorption coefficient α_w with frequency as computed using the FG equation and upto a frequency of 100 kHz. Relative contributions of the component mechanisms to the low frequency absorption coefficient are presented in Fig. 3.2. At frequencies above 3-4 kHz, more than 50% of the
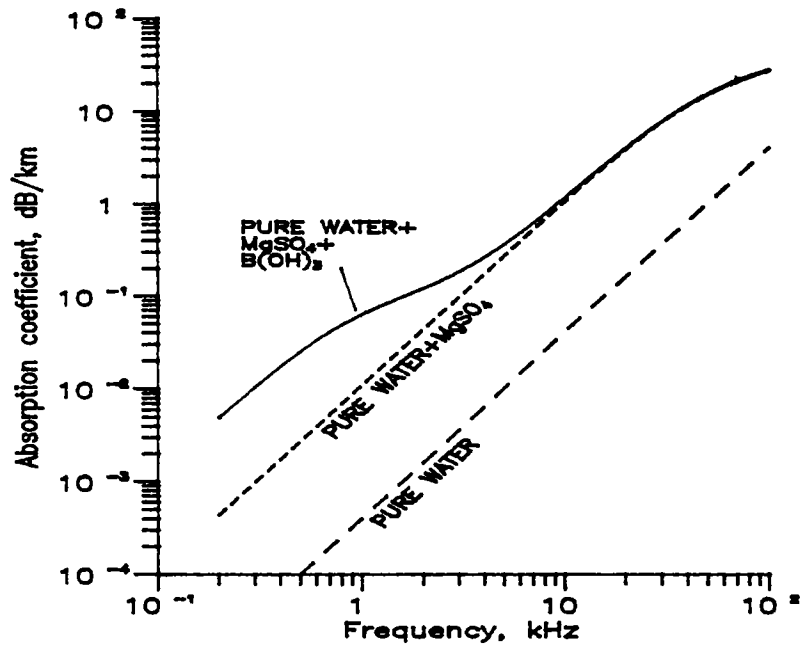
48

Fig. 3.1. Sound absorption coefficient in sea water computed using Francois—Garrison (FG) equation. D=0m, T=4°C, S=35ppt, pH=8.
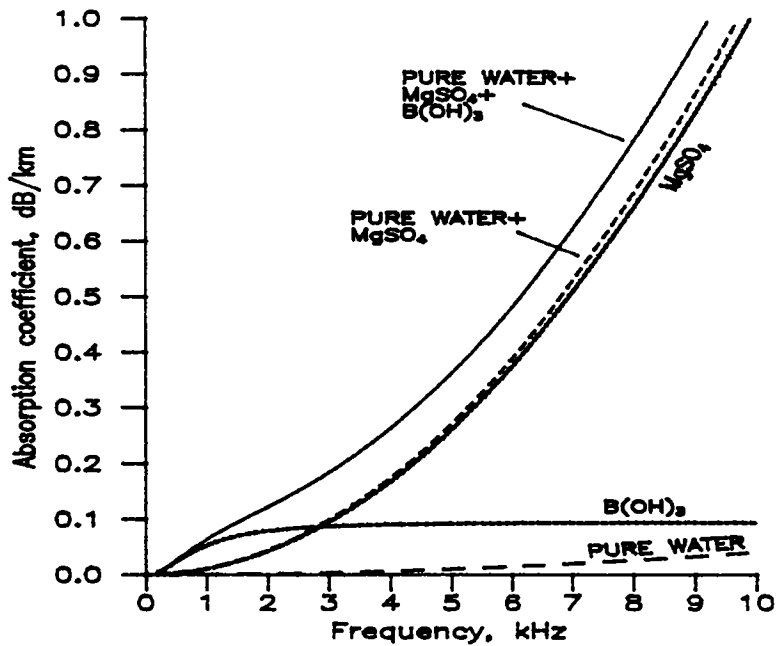

Fig. 3.2. Contribution of component mechanisms to the absorption coefficient at low frequencies. D=0m, T=4°C, S=35ppt, pH=8.
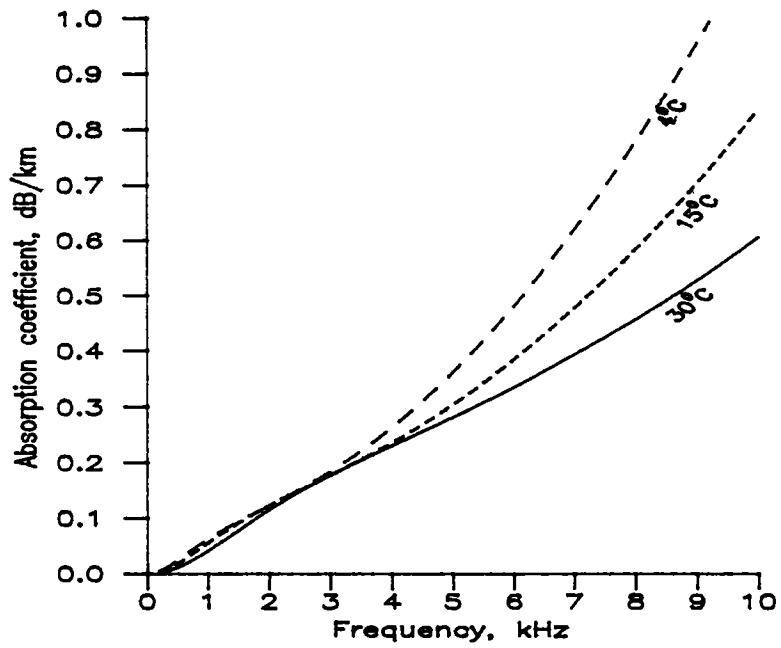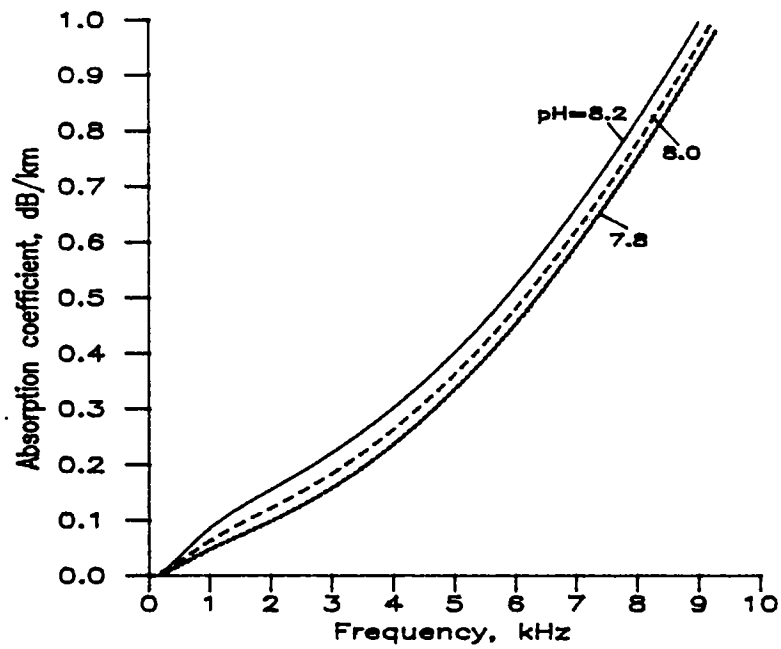
Fig. 3.3. Variation of the absorption coefficient with temperature. D=0m, S=35ppt, pH=8.

Fig. 3.4. Variation of the absorption coefficient with pH of sea water. D=0m, T=4°C, S=35ppt.

absorption arises due to the presence of $MgSO_4$. At lower frequencies, major contribution is from $B(OH)_3$.

Absorption decreases with temperature and it increases with frequency, salinity, and pH. Figs 3.3 and 3.4 show the variation of α_w with temperature and pH respectively. At high frequencies, the dependence of α_w on temperature is much stronger than that on the remaining parameters. At low frequencies where the effect of boric acid is significant, absorption coefficient shows considerable variation with the pH of sea water.

3.2. SEA SURFACE COUPLED LOSSES

Sea surface coupled losses in sound propagation include the losses encountered by the energy on reflection and scattering at the sea surface and in travelling through an inhomogeneous layer that may be present near the sea surface. In rough seas, the surface layer of the water column upto a depth of a few metres is characterized by the presence of air bubbles. Inhomogeneities in density and sound speed caused by the bubble layers affect sound propagation considerably. Air bubbles may be generated by breaking waves, atmospheric pressure changes or biological activity. Bubbles generated near sea surface are carried further down and maintained by turbulence. A dense bubble layer is a good reflector of sound, acting as a screen and masking the sea surface from the incident sound energy. It also scatters the energy depending on the bubble distribution and absorbs part of the energy that passes through. Bubble layers are also known to significantly affect the near-surface sound velocity profile (Novarini and Bruno, 1982). Another reason for inhomogeneity is the presence of biological population. It is not practical to separate out the effects of such near-surface inhomogeneities from those of sea surface scattering. Hence the terminology *surface-coupled*

49

loss (often referred to as the *surface loss*) has come into existence in studies related to transmission loss.

Surface loss is a major factor determining transmission loss in surface duct propagation. It is also important in shallow water propagation and long-range propagation in deep waters. Theoretical models of surface loss are limited to the prediction of loss due to the surface scattering alone. This section outlines various theoretical and empirical models for the estimation of surface loss. These models are then compared in terms of the variables involved and also based on their predictions of surface loss.

3.2.1. Scattering at a rough sea surface

The water-air boundary is a free surface (considering the very small density of air) for which the reflection coefficient can be shown to be -1 (Tolstoy and Clay, 1966:p-26). This means that a relatively smooth sea surface acts as an almost perfect reflector of sound but introduces a phase change of $-\pi$ on reflection. With increasing roughness, the specular component of the reflected energy decreases because the energy gets scattered in other directions also.

Roughness of the sea surface is a relative term and can be determined approximately by using the Rayleigh criterion for sea surface roughness (Urick, 1982:p-10-1). For this, a parameter $\mathcal{R}$ (called the *Rayleigh parameter*) is defined as $\mathcal{R}=2kh_{rms}$ sin θ, where $k=2\pi/\lambda$ is the incident wave number. Here λ is the incident wave length, θ is grazing angle of incidence, and h_{rms} is the rms roughness height of the sea surface (characterization of the sea surface roughness in terms of surface wave height or wind speed observations and some useful interrelations among different wave height parameters are given in Appendix 2). Empirically, it has been shown that for values of $\mathcal{R}<<1$, the sea surface acts as a reflector, and for $\mathcal{R}>>1$ the sea surface is a scatterer of

sound. It can be seen that a rough sea surface is effectively
smooth when λ is large enough or θ is small enough.

Scattering from a rough sea surface is a random process,
both in space and time. In the theory of surface scattering,
the sea surface is postulated to act as a diffraction grating.
Scattering is produced by only those waves or wavelets of the
sea surface roughness that "match" the incident sound. The
fraction of incident energy propagating in the specular
direction can be defined in terms of a *mean specular
reflection coefficient*. Factors that determine this reflection
coefficient are a) sea surface wave spectrum b) frequency of
the incident acoustic wave and c) grazing angle of incidence
at the sea surface.

Fortuin (1970) published a detailed survey of literature
on sea surface scattering. The survey contains a review of the
chronological development of theory on rough surface
scattering, from the pioneering work of Lord Rayleigh on
scattering from a periodic (sinusoidal) surface to various
theories on scattering from random boundaries. Eller (1985)
discusses inconsistencies in the implementation of sea surface
losses in sonar performance models. A recent paper by Kuo
(Kuo, 1988) reviews sea surface scattering loss estimates
based on perturbation methods, known to be quite accurate for
estimating low frequency scattering loss. He also presents a
new method of scattering loss prediction involving numerical
integration of the specular component equation for the
scattered field.

3.2.2. Theoretical models of sea surface scattering
3.2.2.1. Sinusoidal surfaces

The first theoretical attempt to study scattering from a
periodically corrugated surface was by Lord Rayleigh. He
showed that the diffracted acoustic field propagates in
certain discrete modes determined by the grating formula

51

(Fortuin, 1970). Correcting a mathematical defect which
limited the validity of Rayleigh's approach to small roughness
values, Uretsky (1963, 1965) presented a rigorous solution of
the problem thus extending the applicability of the approach
to even more rough surfaces. However, the actual sea surface
is never perfectly sinusoidal and stationary.

3.2.2.2. Random boundaries
A. Eckart's theory

Based on a Gaussian distribution of surface vertical
displacements and the assumption of small surface slopes,
Eckart (1953) developed a scattering theory for random
boundaries. Eller (1985) gives two models based on Eckart's
theory for the prediction of sea surface loss- the Eckart
model (E) and the Modified Eckart model (ME). However it is
known that Eckart's models under-predict the scattering loss
at low grazing angles typical in surface duct propagation
(Eller, 1985; Kuo, 1988).

B. Marsh, Schulkin, and Kneale (MSK) theory

The method of Rayleigh was generalized for a random
surface by Marsh (1961) and was worked out in more detail by
Marsh, Schulkin, and Kneale (MSK) employing the Neumann-
Pierson (NP) model for the ocean surface wave spectrum (Marsh
et al., 1961). They were able to integrate the specular
components of the scattered field under two simplifying
assumptions to obtain a closed form solution for the
scattering loss. These assumptions are the small scattering
loss assumption and the assumption of large horizontal
roughness scales. The mean reflection coefficient is given by

$$R_s = \left[1 - 1.516 \times 10^{-4} \ f^{3/2} \ h_{rms}^{8/5} \ \sin \theta \right]^{1/2} \tag{3.6}$$

where f is the frequency (Hz), h_{rms} is the rms wave height

52

(m), and θ is the grazing angle of incidence (degrees). This is the corrected version of the original MSK expression where algebraic errors made by MSK have been corrected (Kuo, 1988). The scattering loss (dB) is then given by $-20 \log R_s$.

MSK theory is valid only upto a scattering loss of about 3 dB beyond which the first order approximation to the scattering process is not accurate (Marsh et al., 1961).

C. Brekhovskikh and Lysanov (BL) method

Following a method different from that of Marsh, Brekhovskikh and Lysanov (1982) obtained an expression for the mean specular reflection coefficient. Retaining only the first two terms in a binomial expansion involved in the expression for mean reflection coefficient (small scattering loss assumption) and adopting the assumptions of MSK (small θ and large horizontal roughness scales) a closed form solution is obtained. The mean specular reflection coefficient is given by (Kuo, 1988)

$$R_s = 1 - 7.682 \times 10^{-5} f^{3/2} h_{rms}^{8/5} \sin \theta. \qquad (3.7)$$

A binomial expansion of the MSK equation (Eq. 3.6) gives

$$R_s \approx 1 - 7.580 \times 10^{-5} f^{3/2} h_{rms}^{8/5} \sin \theta,$$

which is very much similar to Eq. 3.7.

D. Kuo's method

The approach of Marsh (1961) was generalized by Kuo (1964) for a transmitting rough boundary such as an ocean bottom. For the special case of a pressure release boundary (sea surface), Kuo's expression for the reflected field reduces to that of Marsh. Without resorting to simplifying assumptions to obtain a closed form solution, Kuo used direct

numerical integration of the specular component equation for the estimation of scattering loss (Kuo, 1988). For the integration, the sea surface wave spectrum (Neumann-Pierson or Pierson-Moskowitz (PM)) could be used.

3.2.3. Empirical models of surface loss

Empirical models of surface loss are derived from experimental measurements of surface duct propagation loss. Experimental data from deep surface ducts have long been used for estimating the absorption loss in sea water because there are fewer contacts of the acoustic energy with the sea surface. Effect of the sea surface on propagation loss is more predominant with shallow ducts because there are more number of surface contacts per channel length. Hence data sets from experiments in such ducts are used in arriving at empirical relations for surface loss.

3.2.3.1. Schulkin's model

An extensive set of high frequency (2.2-25 kHz) propagation data was collected during the AMOS program (Marsh and Schulkin, 1967). When the effects of spreading and absorption are accounted for, the transmission anomaly in the surface duct can be designated as a *residual attenuation*. Based on AMOS data for shallow surface ducts, Schulkin (1968) fitted an expression for the residual attenuation as

$$\alpha_L = 1.64 \ (fH_{av})^{1/2} \ \text{dB per limiting ray cycle} \qquad (3.8)$$

where f is frequency (kHz) and H_{av} is the average wave height (ft). The surface ducts were of depths less than 90 m. A lower limit for the data occurred at fH_{av} product of about 3 to 4 kHz ft ($\approx$1 kHz m), corresponding to a loss of 3 dB per limiting ray cycle.

Limiting ray is the ray that grazes the lower boundary of

the duct. If C_0 is the sound speed at the sea surface and C_L that at the base of the layer, grazing angle θ_g of the limiting ray is given by $\cos^{-1}(C_0/C_L)$. Radius of curvature of the ray path is equal to $R_0 = C_0/(g \cos \theta_g)$ where g is the sound speed gradient in the layer. Then the limiting ray cycle is given by $2R_0 \sin \theta_g$ and is a constant for a given duct. Hence α_L may be considered as a *leakage coefficient* having units of dB per unit distance. The leakage coefficient accounts for all additional loss mechanisms in a surface duct which have not been taken into account while estimating the transmission anomaly. These mechanisms may include, other than surface scattering, processes of absorption and scattering like those due to bubbles and biological population. For example, Schulkin (1968) attributed the difference between predictions using MSK theory and his empirical relation to additional loss mechanisms like absorption and scattering by near surface bubbles.

3.2.3.2. Marsh-Schulkin model

This expression (Weinberg, 1973) gives the surface loss α_L in dB per limiting ray cycle as

$$
\begin{aligned}
&10 \, \log\left[1+(fH_{av}/4.14)^4\right] && fH_{av} < 4.2691 \\
&1.59 \ (fH_{av})^{1/2} && fH_{av} \geq 4.2691
\end{aligned}
\tag{3.9}
$$

where f is the frequency (Hz) and H_{av} is the average wave height (ft). No limits for frequency or sea state were specified. In addition to the AMOS data, the basic data set used was supplemented by additional data that extend to lower values of fH_{av} product.

3.2.3.3. Baker's formula

Baker's formula (Baker, 1975) is based on 438 measurements for frequencies in the range of 3.25-7.5 kHz. Sea

states varied from 2 to 5 and duct depths were 24 to 60 m. The leakage coefficient α_1 is given as

$$\alpha_1 = \frac{26.6 \ f}{\left[\left(1452 + 3.5t\right)H\right]^{0.5}} \times 1.4^{ss} \text{ dB per kiloyard}$$

where f the frequency (kHz), t is temperature (°C), H is the duct thickness (ft), and ss is the sea state so that

$$\alpha_L = (10/9) \ \alpha_1 \ R_{lim} \text{ dB per limiting ray cycle} \qquad (3.10)$$

where R_{lim} is the limiting ray cycle (km) and the factor (10/9) converts α_1 into dB km^{-1}.

3.2.4. Comparison among the prediction models

Validity of a theoretical or empirical prediction of surface loss depends on the prevailing environmental conditions for which the prediction is made. Important distinctions between these two types of models are given in Table 3.1. Now we compare both the types of models separately. Computations using Kuo's approach are not attempted in this study. Kuo's results shown in the figures to follow are transferred from those in his paper (Kuo, 1988).

3.2.4.1. Comparison among theoretical models

In Fig. 3.5, the theoretical models are compared for a frequency of 3.5 kHz and an average wave height of 0.734 m (15 knots wind speed). The results of MSK, BL, and Kuo show excellent agreement for grazing angles less than about 2°. The results of BL start to deviate from those of MSK from about 3° grazing angle. This is due to the additional assumption of small scattering loss used by BL. The figure shows that Eckart's results (E and ME) under-predict the loss at low grazing angles.

56

Theoretical Models	Empirical Models
These are models of rough surface scattering loss.	Represents total surface coupled losses, including the effects of inhomogeneities such as bubbles and biological population.
Loss is a function of the grazing angle θ.	Dependence of loss on grazing angle is not evident. The loss is an average over rays with $\theta \leq$ limiting ray angle.
Loss is expressed in dB per bounce of a ray.	Expressed in terms of a leakage coefficient with units of dB per unit distance or dB per bounce of the limiting ray.
When used in transmission loss models, sea surface coupled losses other than that due to scattering are to be taken into account additionally.	Gives an estimate of the total surface coupled losses associated with environmental parameters within the ranges of the basic data set from which the empirical relation was derived.
Scattering loss can be computed for a wide range of frequencies.	Expressions are limited to high frequencies, as they are derived from shallow surface duct propagation studies.

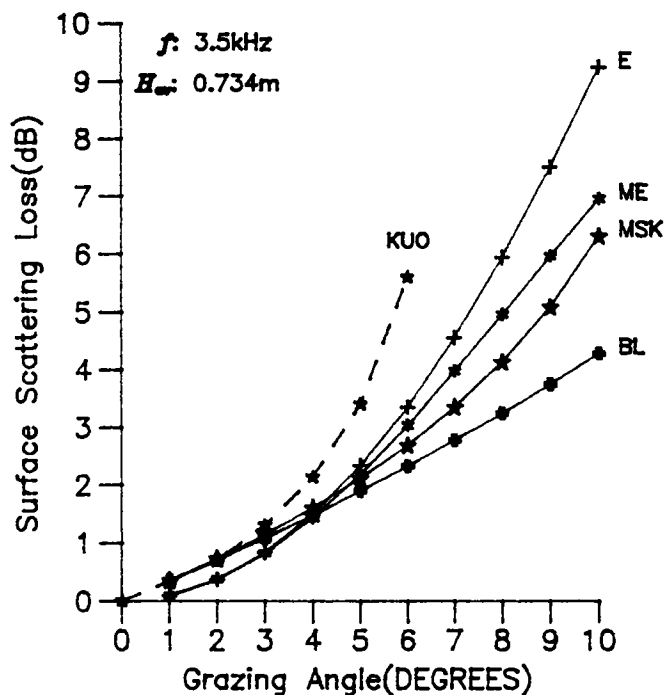Table 3.1. Distinctions between theoretical and empirical models of surface loss.

Fig. 3.5. Comparison of theoretical models
of sea surface scattering loss (see text
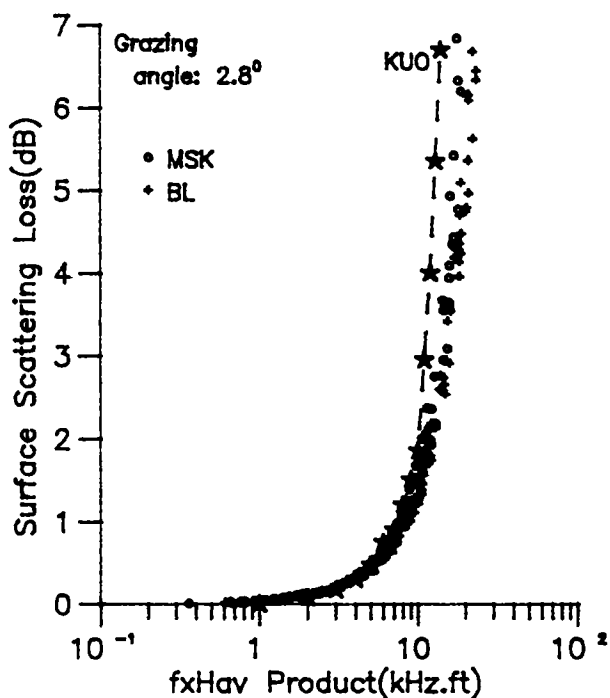for abbreviations).

Fig. 3.6. Comparison of MSK, BL and Kuo
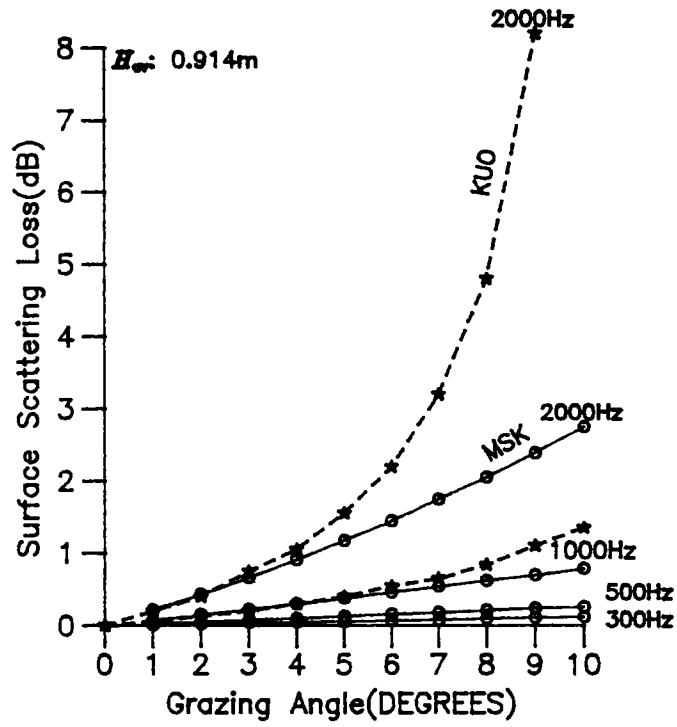predictions for a grazing angle of 2.8°.

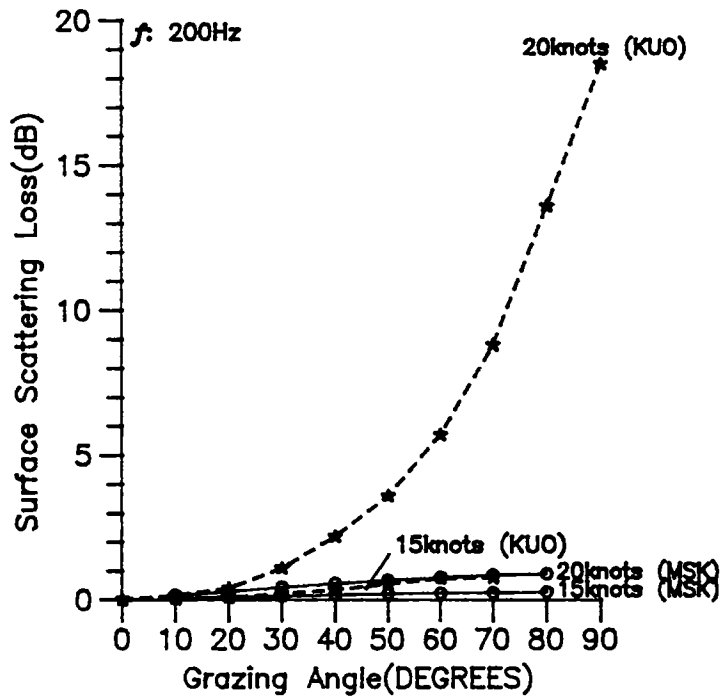Fig. 3.7. Variation of scattering loss with grazing angle for different frequencies.

Fig. 3.8. Variation of scattering loss with grazing angle for two wind speeds.

Marsh *et al.* (1961) reported a method of presenting scattering loss data by plotting the loss values against the product of frequency and wave height (the "*fh*" parameter). Following this method, Fig. 3.6 compares these models based on the scattering loss predictions for different fH_{av} products and for a grazing angle of 2.8°. Satisfactory agreement is seen upto an fH_{av} product of about 10 kHz ft (≈3 kHz m). For a typical duct of 60 m thickness, grazing angle of the limiting ray is about 2°. Thus, under typical surface duct propagation conditions, these three models agree in the predicted scattering loss.

Predicted loss increases with frequency and wind speed (Figs 3.7 and 3.8). Compared to MSK, Kuo's predictions at higher grazing angles are relatively large for high frequencies and wind speeds. The differences are due to the simplifying assumptions used in deriving the closed form solution for scattering loss. These assumptions restrict the applicability of the MSK model to low grazing angles and smaller fH_{av} products.

The theoretical models of MSK, BL, and Kuo utilized the NP spectrum for a fully developed sea (Eckart used a Gaussian distribution of surface displacements). Kuo (1988) compared scattering loss predictions based on Neumann-Pierson and Pierson-Moskowitz sea surface spectra for a wind speed of 20 knots and a frequency of 200 Hz. The predictions showed slight difference only beyond a grazing angle of 70°.

3.2.4.2. Comparison among empirical models

Comparisons among the empirical models are shown in Figs 3.9 and 3.10. The ordinates are loss in dB per limiting ray cycle in the case of empirical models. The loss per bounce of a 2° ray, as predicted by MSK theory, is also plotted in each figure to facilitate comparison with the corresponding theoretical prediction. It might be recalled that the
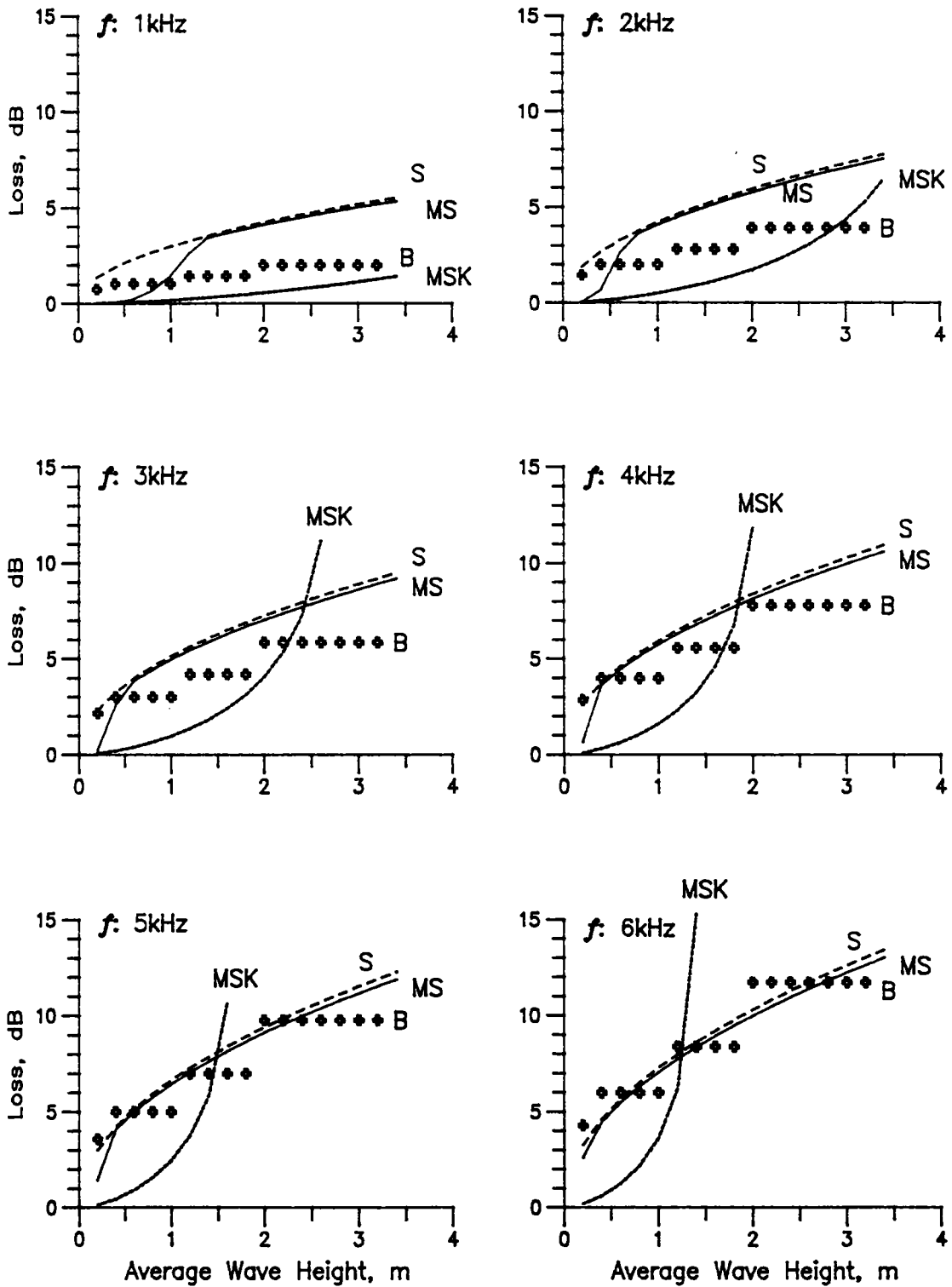
57

Fig. 3.9. Comparison of empirical models showing variation of surface loss with wave height for six frequencies.

theoretical prediction is also a function of the grazing angle θ. Fig. 3.9 shows how the surface loss varies with wave height for six frequencies. Variation of the loss with frequency for four average wave heights (corresponding to four sea states of 1,2,3, and 4) is shown in Fig. 3.10.
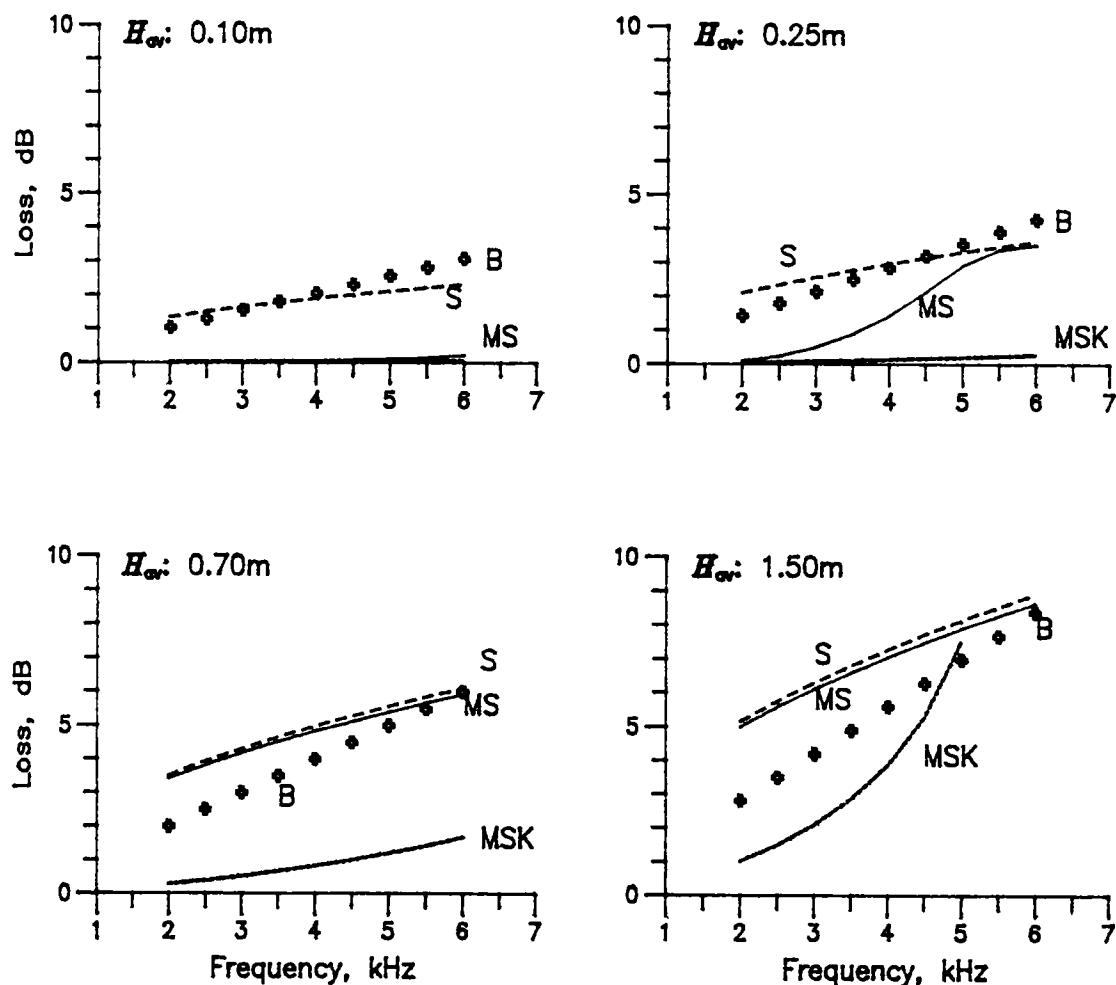

Fig. 3.10. Comparison of empirical models showing variation of surface loss with frequency for four sea states.

Schulkin (S) and Marsh-Schulkin (MS) relations (Eqs 3.8 and 3.9) are based on a common and major data set from the AMOS program and the model equations differ significantly only for small fH_{av} products. Hence, mostly their predictions follow each other closely.

In the case of Baker's formula (B), predicted loss shows step-like increase with wave height (Fig. 3.9). This is because sea state number is used to characterize the surface roughness. A sea state number corresponds to a range of wave heights. Hence uncertainty in the estimated sea state numbers at transition regions (of sea state) would affect the predicted loss. The spread in predictions using Baker's formula is illustrated further in Fig. 3.11. Here the loss is
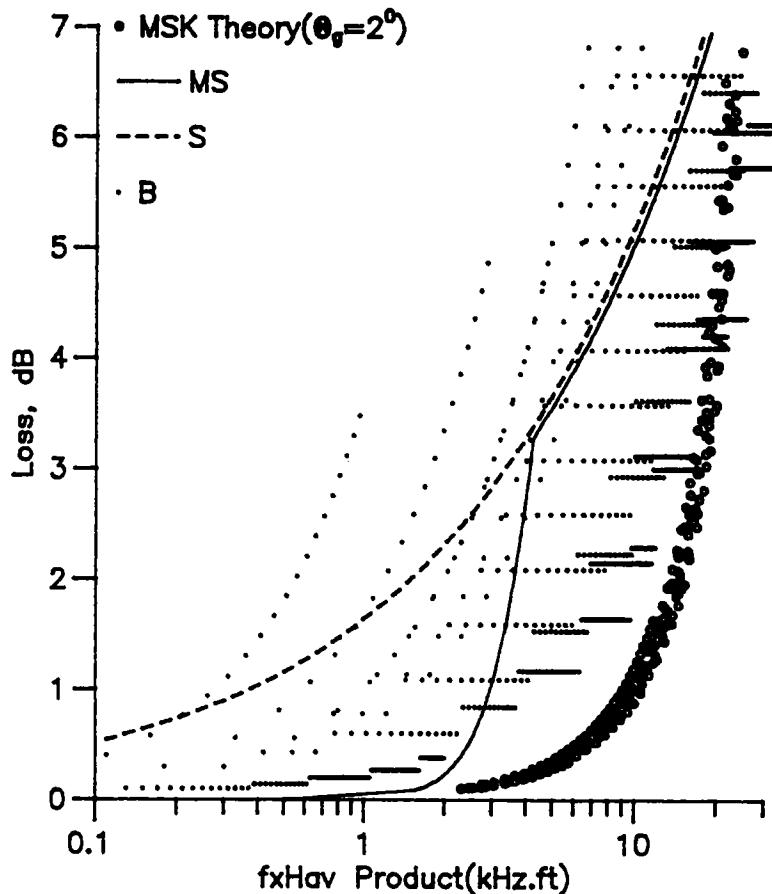
Fig. 3.11. Comparison of empirical model predictions of surface loss for a typical surface duct.

plotted against fH_{av} product. Calculations are done for a typical surface duct where the limiting ray angle is about $2°$. Sea state numbers corresponding to different wave heights ar from Wenz (Appendix 2, Table 1). It is clear that spread i the predicted loss would decrease if the ranges of wav heights corresponding to the sea state numbers were smaller

59

To summarize,

1. Under typical surface duct propagation conditions (with surface grazing angles less than $2\text{-}3^{\circ}$), MSK, BL, and Kuo models give practically the same results for the surface scattering loss. Applicability of MSK and BL models are restricted to low grazing angles and small fH_{av} products because of simplifying assumptions used in arriving at the closed form solutions.

2. For higher grazing angles of incidence, Kuo (1988) predicts relatively high values of scattering loss as compared to earlier theoretical models. These results are considered to be more accurate and applicable to a wider range of environmental conditions.

3. For most cases of practical interest, the selection of either NP or PM surface wave spectrum causes little difference in the predicted scattering loss.

4. Eckart's results under-predict the scattering loss at low grazing angles typical of surface duct propagation.

5. Use of sea state numbers for characterizing sea surface roughness introduces considerable uncertainty in the predicted surface loss.

6. The Marsh-Schulkin model is based on extensive data sets from various sources. The sea surface roughness is represented by average wave height rather than sea state. Hence this model is widely used for estimating surface loss in sea surface ducts.

3.3. REFLECTION AT THE SEA BOTTOM

Compared to the sea surface, the sea bottom is a highly complex boundary affecting sound propagation. Composition of the bottom and hence its acoustic properties are diverse. A multi layered bottom plays an important role in determining low frequency propagation characteristics. Both the sediment composition and bottom roughness vary spatially. In areas where active geological processes take place (for example, mid-ocean ridges) the sea bottom can be very rough. Also, there exist extensive and essentially plane areas covered with fine sediment (e.g., the abyssal plains).

The following mechanisms affect the energy incident at the sea bottom and hence the transmission loss. a) Scattering b) Compressional to shear wave conversion and c) Compressional and shear wave attenuation. Like the sea surface, a rough sea bottom scatters sound energy. Though highly stable in time unlike the sea surface geometry, sea bottom physiography is less easily observed. Surveys with bottom scanning sonars and underwater cameras are used in identifying small-scale features of topography (Clay and Medwin, 1977:p-352). But very few data exist on sea bottom roughness (Urick, 1983:p-279). A rough sea bottom can increase the propagation loss at high frequencies. However, the present study does not consider the bottom scattering effects.

3.3.1. Geo-acoustic modelling of the sea floor

A *geo-acoustic model* is defined as a model of the real sea floor with emphasis on measured, extrapolated, and predicted values of those properties important in underwater acoustics and those aspects of geophysics involving sound transmission (Hamilton, 1980). The model details the true thicknesses and properties of the sediment and rock layers in the sea floor. A complete model includes water-mass data, a detailed bathymetric chart, and profiles of the sea floor.

61

Only the first few or few tens of metres of the bottom need be modelled for high frequency propagation studies whereas information regarding the whole sediment column and the lower substrate is necessary at low frequencies.

The general philosophy behind geo-acoustic modelling of the sea floor is discussed by Hamilton (1980). Properties of the bottom that are important in sound transmission studies are the speeds and attenuation coefficients of compressional and shear waves, and the density. These can be determined by *in situ* measurements accompanied by coring, or from laboratory measurements on field samples, corrected to *in situ* values. In the absence of *in situ* measurements or cores from an area, these can be predicted from preliminary environmental information and the sediment type, using suitable empirical relations or tables as given in Hamilton (1980). The empirical relations (formulated based on existing knowledge on similar sediments) relate the physical properties of the sediment that can be determined in the laboratory to parameters relevant to acoustics.

Direct observation of sea bottom layering involves collection of samples using corers (usually a few metres long) or from bore holes and subsequent analysis of the samples in laboratory. Sub-bottom profilers provide the advantages of higher area coverage and deeper penetration. Such a survey along with core sample analysis can give a fairly good idea about the essential geo-acoustical properties of the surface layers of sea bottom.

In marine geo-acoustics, field studies involving direct access to the sea bottom are difficult and expensive. Hence there have been efforts to make use of inverse techniques for remote sensing of the bottom properties and their depth variation, especially in the low- and middle-frequency ranges, in horizontally stratified environments (e.g., Stoll and Houtz, 1983; Frisk *et al.*, 1986; Zhou *et al.*, 1987b) and in

weakly range-dependent environments (Frisk *et al.*, 1989).

3.3.2. Frequency dependence of compressional wave attenuation

Attenuation of sound in sediments occurs due to a number of mechanisms. These include the friction between mineral grains, relative movement of the mineral frame and pore fluid, and scattering (due to gas bubbles, shells and other inhomogeneities). There are other processes like reflections from layers within the bottom, and the conversion of energy between compressional, shear, and interface waves. The attenuation arising from processes involving the pore fluid are believed to vary nonlinearly with frequency (Kibblewhite, 1989). Hamilton's compilation of results from many field studies on compressional wave attenuation at kilohertz frequencies in marine sediments (Hamilton, 1972,1974a,1974b, 1976; Bjorno, 1977) indicated an approximate linear dependence of the attenuation with frequency (Hamilton, 1980). The results are widely accepted and used in propagation modelling.

However, applying Biot's theory of wave propagation in fluid-saturated porous media to unconsolidated sediments, Stoll and others favoured a non-linear dependence of attenuation with frequency (Biot, 1956a;1956b; Stoll and Bryan, 1970; Stoll, 1974,1977,1978,1985). The Biot-Stoll model is an elaborate model requiring the input of a number of parameters pertaining to the sediment skeletal frame and the pore fluid. Some of these parameters are calculated from fundamental physical properties of the sediment sample while the others are determined experimentally or obtained from empirical relations. The outputs include the speeds and attenuations of compressional and shear waves. According to the Biot-Stoll model, the frequency dependence of attenuation approaches f^2 for coarser sediments and f^1 for the finer ones (Beebe *et al.*, 1982). In addition, the magnitude of absorption is considerably greater for coarser sediments.

Kibblewhite (1989) presents a review of sound attenuation in marine sediments and rocks with emphasis on new low frequency data, and concludes that, in spite of the sparsity of data for marine sediments at low frequencies, the widely held assumption that the relationship between attenuation and frequency is linear from seismic to ultrasonic frequencies does not appear justified. It is shown that in both sands and silts, the attenuation versus frequency relationship becomes nonlinear at low frequencies, and that, in response to the interaction of the pore fluid and sedimentary frame, the attenuation will approach the dry-state value. The frequency at which this occurs is less than 100 Hz for sands, 10 kHz for silts, and some intermediate frequency for sand-silt mixtures. At very low frequencies, the attenuation is similar to that in dry state. Thus, if a nonlinear dependence of attenuation on frequency exists, it appears around 10-100 Hz in the sands and 1-10 kHz in the silts. It is also noted that these characteristics are compatible with the Biot-Stoll formulation for the attenuation of acoustic waves in porous media.

3.3.3. Effect of shear waves

Majority of the bottom sediments cannot really be assumed to be fluids. Depending on the degree of consolidation (or rigidity) of the sediment, sea bottom can support shear waves also. Compressional to shear wave conversion at the sea bottom is a mechanism by which sound energy is carried away from the water column where it appears as an additional attenuation (Jensen and Kuperman, 1983).

It is essential to take into account the shear wave properties of the bottom in modelling propagation over a consolidated sea bottom (e.g., Ingenito and Wolf, 1976; Ellis and Chapman, 1985). Excitation of shear waves in a thin layer of sediment over a hard-rock basement has been shown to be associated with high transmission loss in shallow waters (e.g., Beebe and Holland, 1986; Hughes *et al.*, 1990). Chapman

et al., (1990) demonstrates the importance of including shear wave propagation in the substrate in modelling the bottom interaction in deep water environments.

3.3.4. Sea bottom as a homogeneous fluid half-space
3.3.4.1. The Rayleigh reflection coefficient

The simplest model of the sea bottom is a semi-infinite fluid half-space with no attenuation (as in the Pekeris channel). Reflection coefficient R_b in the case of such a bottom is given by the Rayleigh reflection coefficient (Eq. 2.15). Behaviour of R_b for different combinations of density and sound speed ratios between the media is given in various text books (e.g., Kinsler and Frey, 1962:p-142; Clay and Medwin, 1977:p-61; Brekhovskikh and Lysanov, 1982:p-47; Urick, 1983:p-137).

Here we consider only one case, where the sound speed and impedance (the product of density and sound speed) of the bottom are higher than those of the overlying water, which is a very common condition for natural sea bottoms. According to Rayleigh's theory, the reflection coefficient (or reflectivity) increases as the grazing angle of incidence θ decreases from near vertical ($90°$) to a *critical angle* θ_c given by $\theta_c = \cos^{-1}(C_1/C_2)$. Here C_1 and C_2 are the compressional wave (sound) speeds in water and the sediment respectively. At θ_c, there is a sharp change in the reflection coefficient. For incident angles less than θ_c the reflection coefficient is 1. The phase angle between reflected and incident waves decreases from π to 0 as the grazing angle increases from 0 to θ_c. For $\theta \geq \theta_c$ there is no phase change on reflection.

3.3.4.2. Reflection from a lossy, fluid sea bottom- The Mackenzie model

Real sea bottoms attenuate sound energy to some extent.

One of the effects of attenuation is to smooth out the sharp changes at the critical angle. Also the reflection coefficient is never unity even for grazing angles of incidence less than the critical. A model of the reflection process in the case of an attenuating fluid bottom was given by Mackenzie (1960) (Mackenzie indicates that the expression was originally derived by R.W. Morse and is contained in an unpublished memorandum).

The reflection coefficient R_b and phase change ϕ_b in the Mackenzie bottom model are given by (Siegmann et al., 1987)

$$R_b = \left\{ \left[(h-\sigma \sin \theta)^2 + g^2 \right] / \left[(h+\sigma \sin \theta)^2 + g^2 \right] \right\}^{1/2}$$

$$\phi_b = \tan^{-1} \left\{ 2\sigma g \sin \theta / \left[\sigma^2 \sin^2\theta - (h^2 + g^2) \right] \right\}$$

(3.11)

where

$$h^2 = \beta + (\alpha^2 + \beta^2)^{1/2},$$

$$g^2 = -\beta + (\alpha^2 + \beta^2)^{1/2},$$

$$\beta = \left[1 - (C_1/C_2)^{-2} \cos^2 \theta - \alpha^2 \right] / 2, \quad \text{and}$$

$$\sigma = (\rho_2 C_2) / (\rho_1 C_1).$$

Here α is the compressional wave attenuation expressed in neper rad^{-1}. If α_s is the attenuation coefficient (dB m^{-1} Hz^{-1}), then α is given by 0.1151 α_s $C_2/(2\pi)$ neper rad^{-1} for C_2 expressed in m s^{-1}. When attenuation is zero, Mackenzie's equation reduces to that of Rayleigh.

Using the Mackenzie model, Siegmann et al. also derive an expression for beam displacement. The beam displacement Δ_h is given by

$$\Delta_h/\lambda = \left(\frac{g\sigma \cos \theta}{2\pi c^2 (\alpha^2 + \beta^2)^{1/2} \sin \theta} \right) \times$$

$$\left[2c^2\sigma^2\sin^2\theta \ (\alpha^2 + \beta^2)^{1/2} + 4c^2(\alpha^2 + \beta^2) - 2 \sin^2\theta \ (\alpha^2 + \beta^2)^{1/2} + \right.$$

$$\sigma^2 \sin^4\theta - 4\beta \sin^2\theta \Big] / \Big[\sigma^4 \sin^4\theta + 4(\alpha^2 + \beta^2) - 4\beta\sigma^2 \sin^2\theta \Big] \quad (3.12)$$

where $c = C_1/C_2$. In the above equation λ is the acoustic wave length given by C_1/f where f is the frequency. Knowing Δ_h, the corresponding time displacement τ may be calculated using Eq. 2.17.

3.3.4.3. Reflection from a lossy bottom that can sustain shear

Through adaptation of an expression by Officer (1958), a more general equation for the plane wave reflection coefficient at the water/sediment interface when the bottom is lossy and can support shear is given by Eller and Gershfeld (1985). The complex reflection coefficient is given by

$$R_b \, \exp(i\phi_b) = \frac{P + i(1 - S)Q}{P - i(1 + S)Q} \quad (3.13)$$

where
$$P = \sin\theta \left[\frac{\rho_2}{\rho_1}\right] \left[1 - 2\left[\frac{\beta_2}{C_1}\right]^2 \cos^2\theta \right]^2$$

$$Q = \left[\cos^2\theta - \left[\frac{C_1}{C_2}\right]^2 \right]^{1/2}$$

and

$$S = 4\left[\frac{\rho_2}{\rho_1}\right] \left[\frac{\beta_2}{C_1}\right]^3 \sin\theta \, \cos^2\theta \left[1 - \left[\frac{\beta_2}{C_1}\right]^2 \cos^2\theta \right]^{1/2}$$

Here β_2 is the shear wave speed in the sediment. Compressional wave absorption is included by treating the wave number in the sediment to be complex as per the expression

$$\omega/C_2 \; \longrightarrow \; (\omega/C_2) - i\alpha \quad (3.14)$$

where $\omega = 2\pi f$ is the angular frequency of sound and α is the plane wave attenuation coefficient in neper m^{-1}. Equation 3.14 can be re-written as $1/C_2 \longrightarrow (1/C_2) - i(\alpha/2\pi f)$. Now, expressing

67

α in decibel units and assuming a linear frequency dependence for α,

$$1/C_2 \ \text{-->} \ (1/C_2)-i(0.1151/2\pi)\alpha_s \hspace{3cm} (3.15)$$

where α_s is in dB m^{-1} Hz^{-1}. With the substitution of Eq. 3.15 in Eq. 3.13, the quantity Q (and hence the reflection coefficient) becomes complex. When shear waves are not present, Eq. 3.13 and the Mackenzie model give identical results.

Analytical expressions for computing beam displacement in the presence of shear waves in a homogeneous bottom are now derived based on Eq. 3.13. The derivation and the final expressions are presented in Appendix 3. No attempt is made to simplify the expressions as these can be used conveniently for calculations on a computer.

3.3.4.4. Sample computations in the case of very fine sand

A sample calculation for reflection coefficient, phase shift, and beam displacement in the case of very fine sand appear in Figs 3.12 and 3.13. We use Equation 3.13 for calculating the reflection coefficient and the expressions given in Appendix 3 for beam displacement computations. The sediment parameters are taken from Table I of Eller and Gershfeld (1985) and are as follows:

$C_1 = 1520$ m s^{-1}, $C_2 = 1688.72$ m s^{-1}, $\beta_2 = 472$ m s^{-1},

$\rho_1 = 1022$ kg m^{-3}, $\rho_2 = 1866$ kg m^{-3}, and

$\alpha_s = 0.00068$ dB m^{-1} Hz^{-1}.

The critical angle θ_c in this case works out to be $25.83°$. The computation results shown in Fig. 3.12 are in good agreement with corresponding results published by Eller and Gershfeld (1985).
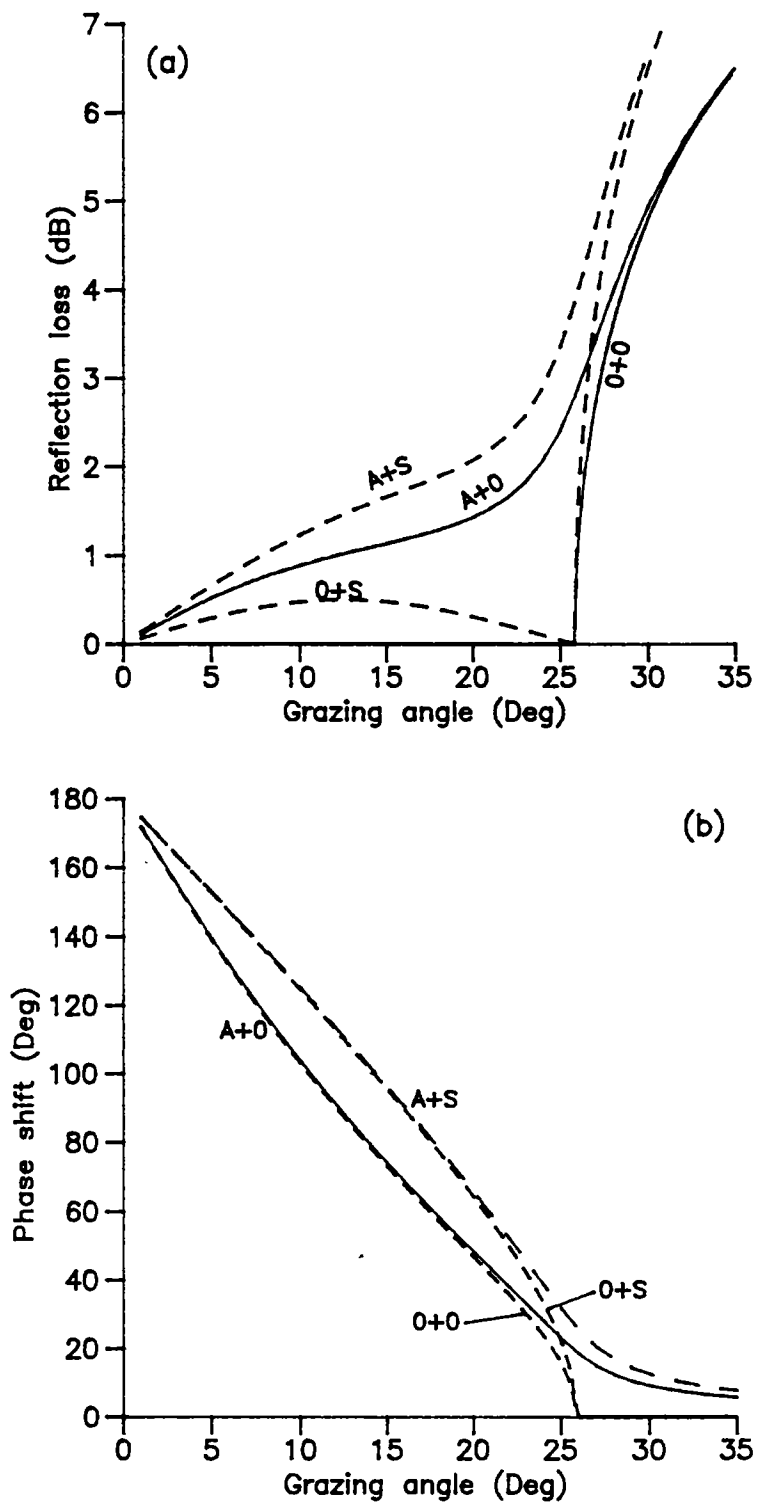
Fig. 3.12. (a) Reflection loss and (b) phase shift at the water/sediment interface for very fine sand as computed using Eq. 3.13.

There are four labelled curves each in Figs 3.12(a) and (b). A label includes the symbols A and S if the computation for that curve is done taking into account the effects of absorption coefficient and the shear wave speed respectively. An omission of either of these is indicated by a 0. For example, the curve labelled A+S means that both absorption and shear waves are present; in A+0, absorption is present whereas the shear wave effects are neglected.

Behaviour of the Rayleigh reflection coefficient (Section 3.3.4.1) is illustrated by curves labelled 0+0. There is no reflection loss for $\theta < \theta_c$ where θ is the grazing angle of incidence. It increases sharply beyond the critical angle. The phase shift decreases from 180° to 0° as θ increases from 0 to θ_c. There is no phase shift for $\theta > \theta_c$.

Curves labelled A+0 correspond to the Mackenzie bottom model (Section 3.3.4.2). It can be seen that sharp changes at the critical angle are now absent. Reflection loss is no longer zero for $\theta < \theta_c$ and is high enough to be considerable even at small values of θ. But noticeable changes in phase shift occur only near and beyond the critical angle θ_c (Fig. 3.12(b)).

As indicated by the curves labelled A+S, there is an increase in reflection loss in the presence of shear waves. This is more significant at higher grazing angles. A marked increase in the phase shift is also noticed.

Fig. 3.13 shows the beam displacement (Δ_h) per wave length for the four combinations of A and S as above. At small grazing angles the presence of absorption alone does not affect the beam displacement noticeably. This is consistent with the behaviour of the phase shift curves in Fig. 3.12(b) which show no significant change in the phase shift at small values of θ, irrespective of whether absorption is present or not.
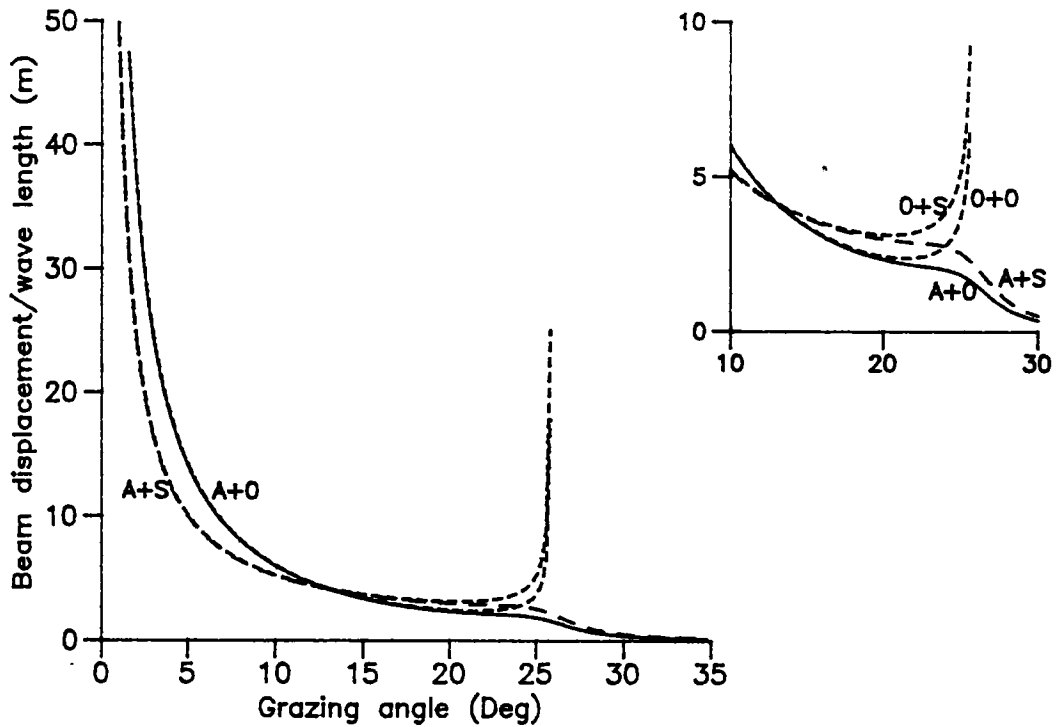
Fig. 3.13. Beam displacement per wavelength versus grazing angle for very fine sand as computed using equations in Appendix 3.

The behaviour of beam displacement is modified in the presence of absorption for grazing angles near to and beyond θ_c. An enlarged view of the curves for $10 < \theta < 30°$ is shown to the right of Fig. 3.13. From Figs 3.12(b) and 3.13 it is seen that in the absence of absorption Δ_h increases asymptotically, as bottom phase shift falls sharply near θ_c. When absorption is introduced, this sharp change in phase shift near θ_c and, consequently, the asymptotic increase in Δ_h also vanish. This transition occurs rather rapidly, even with very small increase in the attenuation coefficient (Siegmann et al., 1987).

Beam displacement is also modified in the presence of shear waves. There is noticeable reduction in Δ_h at small values of θ, wherefrom it gradually approaches the (A+O) curve (Fig. 3.13). For the particular sediment type considered, we note a crossover near to $13°$ grazing angle, beyond which Δ_h is

70

slightly higher. Another observation is that the presence of shear waves alone does not prevent the increase in Δ_h near θ_c. This again is consistent with the behaviour of the corresponding phase shift curves near critical angle.

3.4. SUMMARY

In this chapter, three important mechanisms of sound attenuation in the sea viz., absorption in sea water, scattering at the sea surface and reflection loss at the sea bottom were reviewed. Excess absorption of sound in sea water compared to pure water arises from the chemical relaxation processes involving dissolved magnesium sulphate and boric acid. A few calculations based on the Francois-Garrison equation for absorption were presented to highlight the relative importance of various factors controlling absorption (Section 3.1.2).

In Section 3.2 we reviewed the process of sound scattering from the sea surface and the models for estimating surface loss. Distinctions between theoretical and empirical models were brought out and their predictions of surface loss were compared (Section 3.2.4). Among the theoretical models, it was seen that scattering at small grazing angles is adequately described by the MSK, BL, and Kuo models. The MSK and BL equations, which are closed form solutions for scattering loss, under-predict the loss at higher grazing angles and fH_{av} products due to simplifying assumptions used in obtaining the solutions. Kuo's numerical integration method predicts relatively higher scattering loss at such grazing angles. Though no comparisons with field data are available, Kuo's results are considered to be more accurate and applicable to a wider range of environmental conditions. Another important point noted is that using sea state number for characterising sea surface roughness could cause considerable uncertainty in the predicted loss.

The last section of this chapter reviewed concepts in geo-acoustic modelling of the sea floor. We saw that this could be one of the complex areas in realistic propagation modelling. Formulation and validation of geo-acoustic models are often difficult due to non-availability of sufficient field data. Non-linear frequency dependence of compressional wave attenuation and compressional-to-shear wave conversion play significant roles in determining the propagation characteristics, especially, at low frequencies (Sections 3.3.2 and 3.3.3). Models of reflection from a homogeneous lossy sea bottom were presented in Section 3.3.4. Expressions were derived for computing the beam displacement in the presence of shear waves in the bottom (Appendix 3). And finally, behaviour of the reflection coefficient, phase shift, and beam displacement were examined based on sample computations for very fine sand (Section 3.3.4.4).

Chapter 4

A RAY THEORETICAL MODEL OF SHALLOW WATER SOUND PROPAGATION

A sound propagation model based on modified ray theory is presented in this chapter. The model is applicable to a range-independent environment where a water column with an arbitrary sound speed profile overlies a homogeneous, lossy sea bottom. An efficient algorithm for eigen-ray finding is developed, based on which a propagation model is implemented on a computer. The model outputs include transmission loss and received time series of a single frequency pulse transmission. In order to test the efficacy of the model, the outputs for an isospeed environment are compared with those from a normal mode model of the environment and corresponding results from published literature. The results are discussed.

4.1. THE ENVIRONMENT

The range-independent environment is schematically shown in Fig. 4.1. Water depth is D and the sound speed profile $c(z)$ is arbitrary. The sea bottom is assumed to be a homogeneous, lossy, semi-infinite half-space with compressional and shear
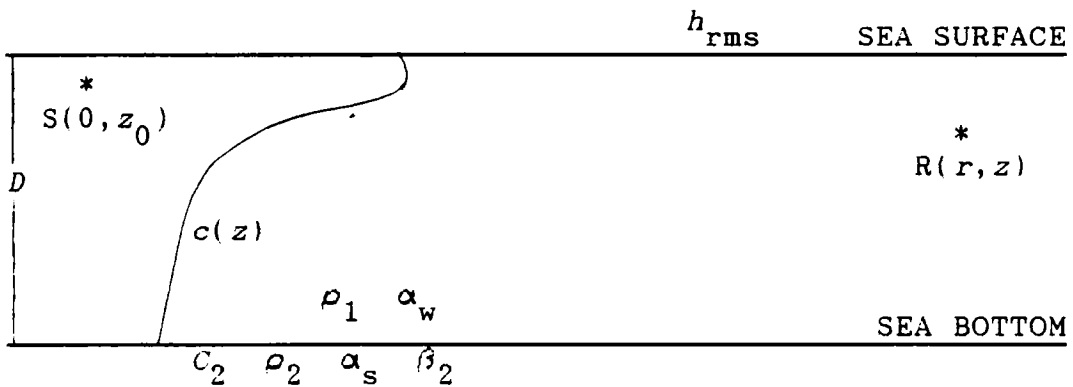

Fig. 4.1. Range independent shallow water environment with an arbitrary sound speed profile.

wave speeds of C_2 and β_2 respectively and forms a smooth, plane boundary. Sea surface roughness is characterized by an rms roughness height of h_{rms}. Densities of the sea water and the bottom are designated by ρ_1 and ρ_2. The corresponding compressional wave attenuation coefficients are α_w and α_s.

The point source $S(0,z_0)$, radiating at frequency f, is at a depth of z_0 from the sea surface. The receiver $R(r,z)$ is located a distance r from the source and is at a depth of z. Both the source and the receiver are omnidirectional. First it is required to determine the eigen-ray structure between the source S and the receiver R.

4.2. DETERMINATION OF EIGEN-RAY STRUCTURES
4.2.1. Ray path computations

The ray path computations use the linear segmentation approximation of the sound speed profile (Section 2.2.3). The profile is specified by N pairs of [depth, sound speed] values. If the source and receiver depths do not coincide with any of the profile point depths, additional boundaries are introduced at those depths. Sound speeds at these additional boundaries are calculated by linear interpolation between those at the immediate upper and lower boundaries.

A ray path in a range-independent environment consists of identical ray cycles. For purposes in this study, one *cycle distance* $L(\theta)$ is taken as the horizontal distance between two corresponding points on a ray path and at the depth of the source. The term *fractional ray path* refers to the ray segment towards the receiver end which is less than one complete cycle (Fig. 4.2). θ is the initial projection angle of a ray. Each ray cycle consists of an upper and a lower turning point. For bottom reflected rays, cycle distance includes the beam

displacement at the bottom (not shown in the figure). In this model, beam displacement is calculated using the equations derived in Appendix 3.

In Fig. 4.2, the ray path segments SA and AS_1 are symmetrical about the apex A. So also are the segments S_1N and NS_2. Once θ is specified, the basic quantities of horizontal
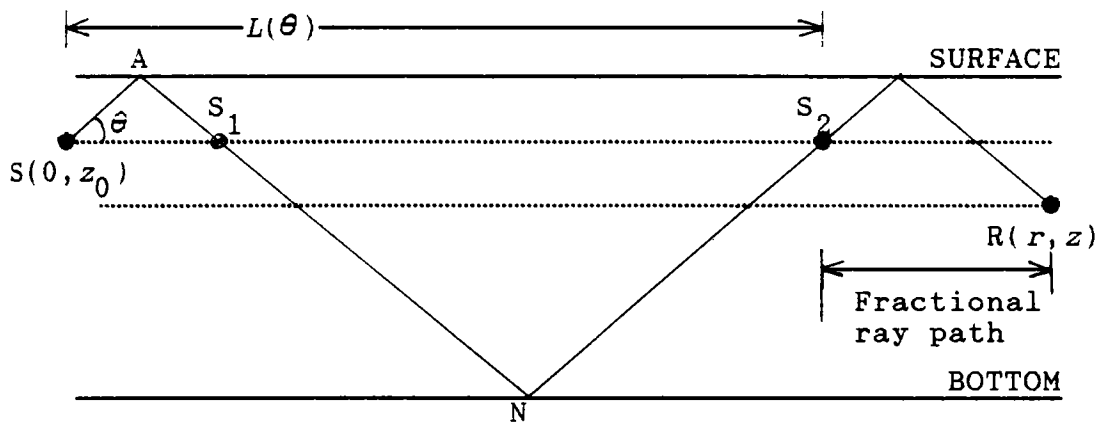

Fig. 4.2. Cycle distance $L(\theta)$ and fractional ray path

range increments, beam displacement, travel times, distances along the ray path, and ray angles in the layers through which the ray passes are calculated. These define the ray segments SA and S_1N, and hence a complete ray cycle.

From the point of view of ray amplitudes, not all the eigen-rays are significant beyond a sufficiently large distance from the source. Bottom reflected rays with grazing angles more than the critical suffer higher attenuation due to high reflection loss at the bottom. Hence their amplitudes become negligible after a few bottom reflections. The corresponding projection angle θ_{max} of the ray at the source is obtained from Snell's law. By default, the model computations are limited to rays within a source beam width defined by $\mp\theta_{max}$. But this can be over-ridden by explicitly specifying a larger beam width.

4.2.2. An identifier variable for describing ray paths

We designate a ray path by an identifier containing essential characteristics of a ray as required by the eigen-ray finding algorithm. The identifiers are used by the algorithm in monitoring changes in the ray type as the initial projection angle of the ray is varied.

The ray identifier is of the form $n^{\mp} t_1 t_2^{\mp} f_1 f_2$. Here n is a positive integer specifying the number of complete ray cycles between the source and the receiver. $t_1 t_2$ is an alphabetic character variable describing the turning points in a ray cycle. For example, $t_1 t_2 =$SR (or RS) means that the ray is a refracted surface reflected (RSR) ray; $t_1 t_2 =$SB (or BS) represents a surface-reflected bottom-reflected (SRBR) ray; and $t_1 t_2 =$RR is a ray with no boundary interaction. $f_1 f_2$ is a variable similar to $t_1 t_2$ and describes the turning points of the fractional ray path (Fig.4.2) upto the receiver range. The +/- sign preceding $t_1 t_2$ explicitly indicates the direction of the ray at the source. A ray projected upwards is designated +ve and one projected downwards is assigned a -ve sign. In a similar way, the +/- sign after $t_1 t_2$ indicates the direction of arrival of the ray at the receiver.
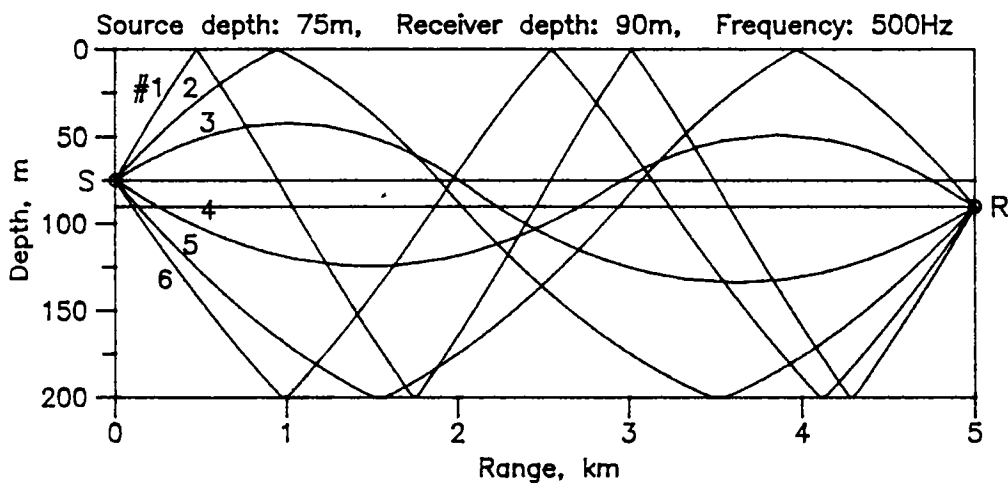

Fig. 4.3. Six eigen—rays connecting the source S and receiver R.

Ray	Ray angle (deg)	Ray identifier
1	+9.88083	1+SB+SB
2	+6.30292	0+SB+SB
3	+3.73965	0+RR+RR
4	-3.34817	1-RR- ·
5	-6.44805	1-BS-
6	-8.41367	1-BS+B

Table 4.1. Angles and identifiers of the eigen-rays in Fig. 4.3.

Fig. 4.3 and Table 4.1 illustrate the above scheme of ray type identification. In Fig. 4.3, the water column is 200 m deep, with a bilinear sound speed profile. Sound speed at the surface is 1540 m s^{-1} and the minimum in sound speed occurs at 80 m. The gradients above and below the minimum are taken arbitrarily as -0.1 and 0.07 s^{-1} respectively. The source S is at a depth of 75 m. The 90 m deep receiver R is at a range of 5 km from S. Six selected eigen-rays for a frequency of 500 Hz are shown in the figure. Eigen-ray angles and the corresponding ray identifiers are as in Table 4.1.

4.2.3. Finding the eigen rays

Briefly, the procedure used for eigen-ray finding is as follows. Let θ be the initial projection angle of a ray (Fig. 4.4). The corresponding fractional ray path crosses the receiver depth at ranges r_1 and r_{11}. Now the initial ray angle θ is decremented by a small amount $\Delta\theta$ and the computations are repeated to obtain a second set of ranges r_2 and r_{22}. The range value pairs (r_1 and r_2) and (r_{11} and r_{22}) are checked to determine whether either of them bracket the receiver range r. If so, an iteration procedure with a pre-defined error criterion determines the eigen-ray angle. If none of the pairs bracket the receiver range, the ray projection angle is decremented further and the procedure continues.
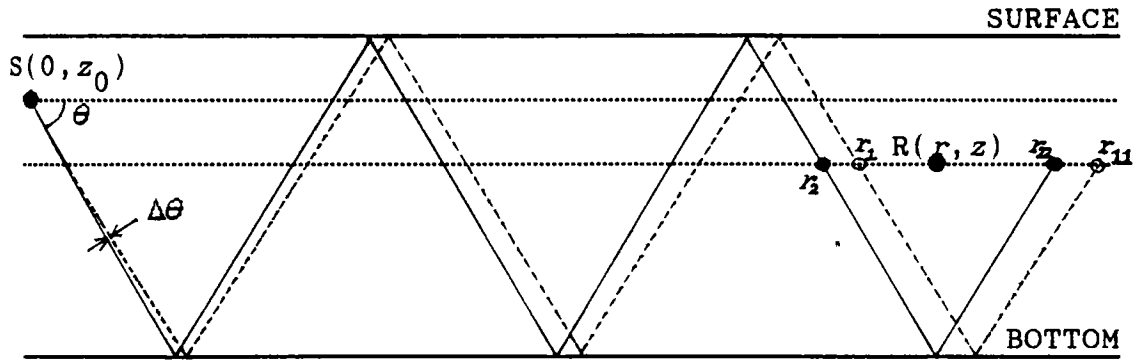
Fig. 4.4. A pair of adjacent rays with initial projection angles of θ and $\theta-\Delta\theta$. Following Section 4.2.2, θ is -ve here.

Search for the eigen-rays starts with an initial ray angle of θ_{max}. This initial angle is successively decremented by $\Delta\theta$ as computations proceed. Considerable reduction in computation time is achieved by allowing $\Delta\theta$ to be variable. A lower limit to the value of $\Delta\theta$ is fixed at $\Delta\theta_{min}$. A value of $0.0001°$ is found to be satisfactory for realistic shallow water environments. The upper limit of $\Delta\theta_{max}$ is arbitrarily set at 100 times the lower limit.

The magnitude of $\Delta\theta$ is gradually incremented during the computation until it reaches the upper limit of $\Delta\theta_{max}$ where it stabilizes. Though the increment steps are arbitrary they are so selected that a satisfactorily optimum performance is achieved. In the present algorithm, this is done as follows: The first five decrements in θ are of magnitude $\Delta\theta_{min}$. During the next 20 decrements, $\Delta\theta$ is incremented successively by an amount of $\Delta\theta_{min}$. That is, at the end of 25 decrements in θ, the value of $\Delta\theta$ would be 20 times $\Delta\theta_{min}$. With the 26th decrement onwards, $\Delta\theta$ is set to $\Delta\theta_{max}$.

Reduction in computation time by the use of a variable $\Delta\theta$ is achieved from SRBR type of rays which, in general, show a simple and smooth variation of range with ray angle. As the behaviour of other ray types are complex, $\Delta\theta$ is reset to $\Delta\theta_{min}$ when the ray identifier changes to that of another type. $\Delta\theta$ is

78

incremented or kept at its maximum until one or more of the following conditions are tested positive:

a) one (or both) of the two adjacent rays is not of SRBR type
b) ray identifiers of adjacent rays do not match. In the case of SRBR rays, this happens when the number of complete ray cycles are different for the rays
c) θ is -ve and $(\theta - \theta_{max})$ is less than or equal to $\Delta\theta_{max}$.

Then θ is brought back to its previous value by adding the current value of $\Delta\theta$. Before restarting the computations, $\Delta\theta$ is reset to its lower limit of $\Delta\theta_{min}$.

When two adjacent rays having the same identifier pass on either side of the receiver, an iteration procedure following the bisection method determines the eigen-ray angle. Iteration is terminated when the ray passes within a distance δ from the receiver such that δ is much less than the acoustic wave length λ. In the transmission loss computations to be presented here, δ is taken to be 1/100 of λ.

4.2.4. Computation of ray travel times, amplitudes, and phases

The eigen-ray structure determined as above is used in transmission loss computation and time series simulation. For this the travel times, amplitudes, and phases of individual eigen-rays are to be calculated. Depending upon the prevailing sound speed gradient, the travel times of the ray in individual layers of the water column are given by Eq. 2.9 or 2.13. The time displacement corresponding to lateral ray displacement at the sea bottom is given by Eq. 2.17. The total travel time for an eigen-ray is then the sum of travel times along the component ray path segments.

Amplitude and phase of an eigen-ray are given by Eqs 2.21 and 2.22 respectively. In the expression for the ray spreading factor S (Eq. 2.20), the range derivative $dr/d\theta_S$ is to be

estimated. This is obtained by determining the change δr in the total horizontal range of the eigen-ray for an infinitesimally small change in the projection angle $\delta\theta_S$ and taking the ratio of δr to $\delta\theta_S$. From a number of trial computations using different magnitudes of $\delta\theta_S$, it is found that a value of $\delta\theta_S$ of the order of 10^{-8} degrees gives stable results for a wide range of profile characteristics and source/receiver configurations. In the transmission loss computations presented here, a value of 10^{-8} is used for $\delta\theta_S$.

Volume absorption coefficient α_w in sea water is calculated using the Francois-Garrison equation (Appendix 1). Sea surface and sea bottom reflection coefficients are calculated using the Marsh-Schulkin-Kneale equation (Eq. 3.6) and Eq. 3.13 respectively. The number of surface and bottom reflections N_S and N_b as required by the ray amplitude equation (Eq. 2.21) are obtained directly from the eigen-ray identifier.

4.3. IMPLEMENTATION OF THE PROPAGATION MODEL

The propagation model is implemented on a personal computer. The model consists of two modules of computer program. The first module determines eigen-ray structures for specified source/receiver configurations. The output consists of eigen-ray identifiers and angles. The source code is written in a compiler BASIC which provides flexibility in using the character variables (Section 4.2.2), interactive program debugging facilities, and graphics support.

The second module uses the eigen-ray structures for further computations. Spreading loss of the rays and attenuation due to sea surface scattering, volume absorption in sea water, and sea bottom reflection are computed in this module. The outputs include the transmission loss and received time series of a monochromatic pulse transmission.

4.4. MODEL PERFORMANCE EVALUATION

In order to ensure that an implemented model is reliable and error-free, its performance is to be evaluated. Other than by wrong concepts and formulae, errors may enter a model through programming mistakes. A model may be validated by comparison with existing models that are known to be accurate or by applying it to bench-mark problems for which accurate solutions are available. A model assessed for its performance provides the necessary confidence while applying it to propagation problems. This also brings-out the limitations so that one could be sufficiently cautious while using the model. In the present study, the model computations of transmission loss are compared with Tindle's published results (Tindle, 1983) and also with results from a normal mode model of the lossy Pekeris channel (Vijayakumar, 1989). Time series simulations using the present model are compared with those in Tindle and Bold (1981).

4.4.1. Transmission loss computations
4.4.1.1. Environmental parameters

$$h_{rms} = 0 \qquad \text{SURFACE}$$

S *
(6 m)

* R
(7 m)

$D = 50$ m

$C_1 = 1508$ m s^{-1}

$\rho_1 = 1022$ kg m^{-3}

$\alpha_w = 0$

BOTTOM

$C_2 = 1605$ m s^{-1} $\quad \rho_2 = 1277.5$ kg m^{-3} $\quad \alpha_s$(given in the text)
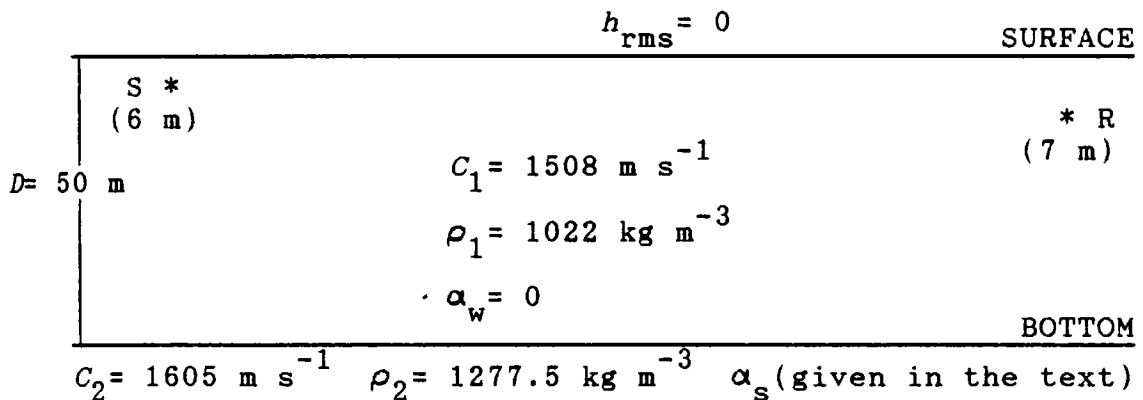
Fig. 4.5. Environmental parameters used for transmission loss computations.

Fig. 4.5 shows the environmental parameters used in the transmission loss computations. These inputs agree with those

81

in Tindle (1983). Following Tindle, computations are done for
two frequencies of 140 and 50 Hz. In the figure, water depth D
is 50 m. The source S and receiver R are at depths of 6 and 7
m respectively. Only those rays for which the bottom grazing
angles are less than the critical ($20.02°$) are considered in
the ray computations. Similarly, the normal mode model
includes only the discrete modes. Hence we restrict the
computations to ranges sufficiently away from the source (say
10 times the water depth, or 500 m) where mode theory results
might be considered valid.

Transmission loss (TL) is computed for two values of
compressional wave attenuation coefficient α_s in the sediment,
0.113 and 0.5 dB m^{-1} kHz^{-1}. The former value corresponds to an
attenuation of 0.013 neper m^{-1} kHz^{-1} used by Tindle. The
results show the effect of bottom attenuation on the
occurrence of beam displacement caustics and hence on the
computed acoustic field. The computations are done at a close
range interval of 10 m upto a range of 3 km and the results
are presented as curves of normalised pressure (given by
$10^{-TL/20}$) versus range in order to facilitate comparison with
Tindle's results.

4.4.1.2. Transmission at 140 Hz

There are three propagating modes at this frequency. The
wave length λ is ≈ 10.77 m so that $D \approx 4.6\lambda$. Acoustic pressure
versus range computed using the present model and the normal
mode model for an α_s of 0.113 dB m^{-1} kHz^{-1} are shown in Fig.
4.6. The results correspond to those in Fig. 3 of Tindle
(1983) which is reproduced in Fig. 4.7 for convenience in
making comparisons. From Fig. 4.6 it is seen that the ray
theory model satisfactorily simulates prominent features of
the acoustic field as predicted by normal mode theory.
Comparing with Fig. 4.7, the conspicuous peaks in the ray
theory results of Fig. 4.6 are seen to occur near to the
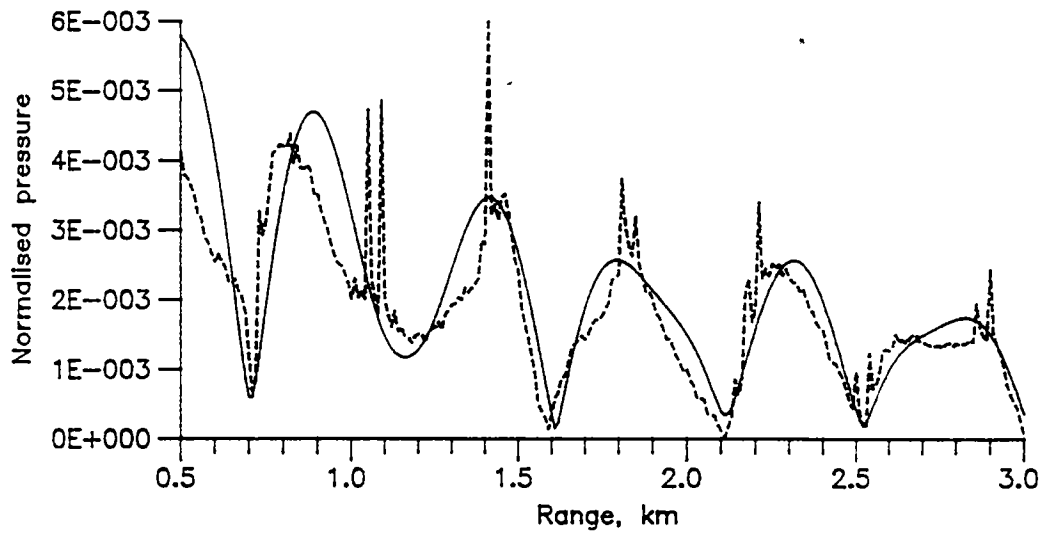locations of beam displacement caustics.

Fig. 4.6. Normalised acoustic pressure versus range at 140 Hz for a sediment attenuation coefficient of 0.113 dB m^{-1} kHz^{-1}.
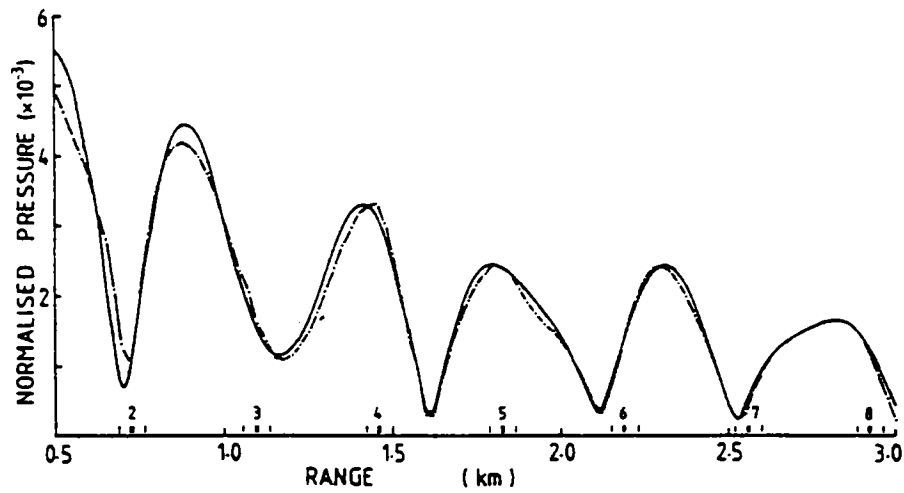(————Normal mode theory – – – –Modified ray theory)

Fig. 4.7. Same as Fig. 4.6, but reproduced from Fig. 3. of Tindle (1983). The bars show the locations of the caustics for rays with the number of bottom bounces indicated.
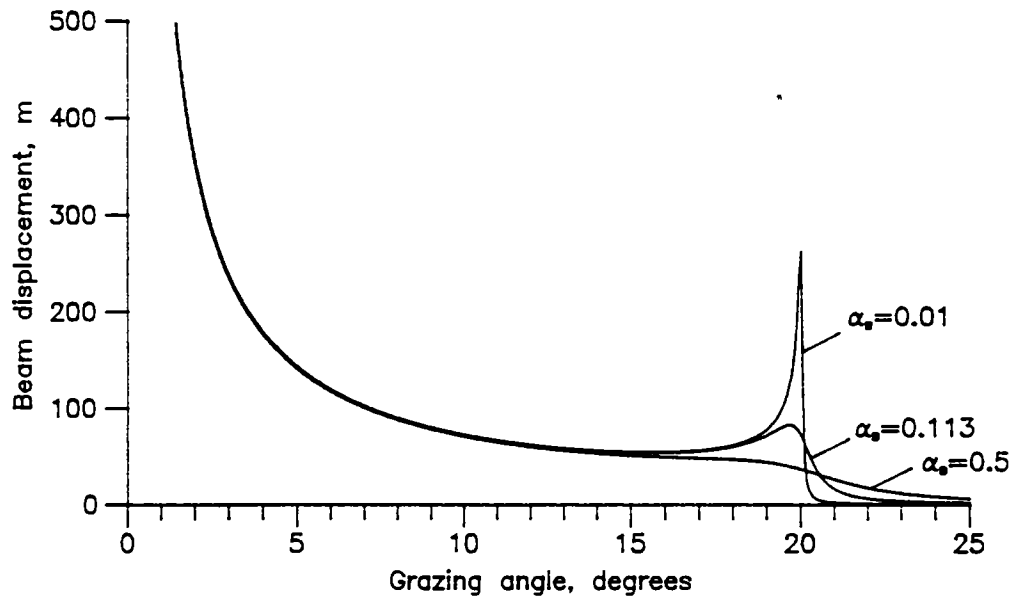
Fig. 4.8. Beam displacement versus grazing angle for three sediment attenuation coefficients. Frequency: 140 Hz.
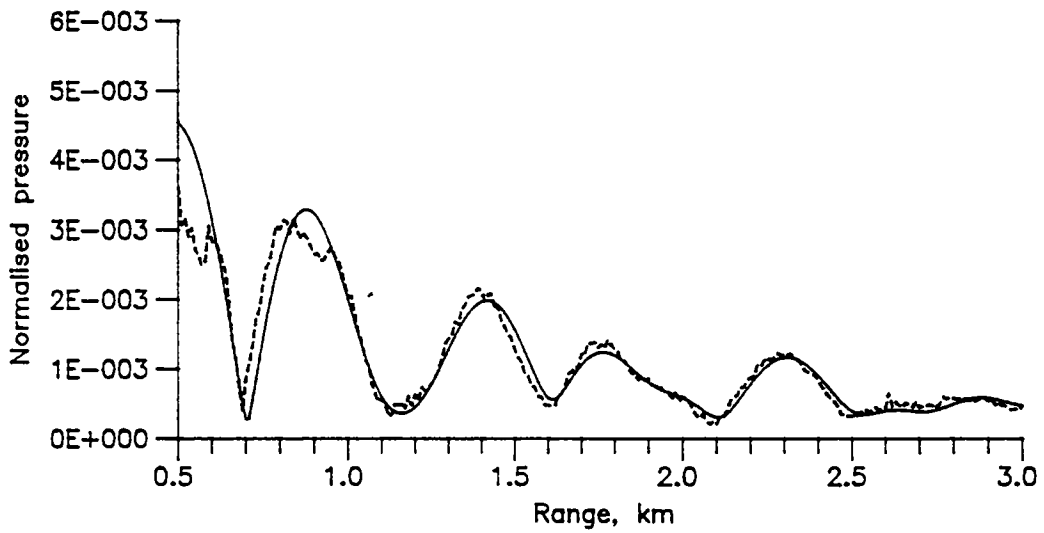

Fig. 4.9. Normalised acoustic pressure versus range at 140 Hz for a sediment attenuation coefficient of 0.5 dB m^{-1} kHz^{-1}.
(————Normal mode theory ------Modified ray theory)

Beam displacement caustics form due to the existence of a minimum in the beam displacement (Δ_h) versus grazing angle (θ) curve (Tindle, 1983). This minimum and hence the caustics gradually disappear as the compressional wave attenuation in the sediment is increased (Siegmann et al., 1987). Acoustic field at and near caustics should be treated separately using Airy functions in order to remove unrealistic anomalies produced by conventional ray theory (Tindle, 1983). The ray theory curves in Tindle's results are corrected for caustics, whereas the present results are uncorrected. That a minimum exists in the Δ_h versus θ curve at this frequency for an α_s of 0.113 is clear from Fig. 4.8, where beam displacement is plotted against grazing angle for a frequency of 140 Hz. Such a minimum is no longer present for α_s=0.5 (Fig. 4.8). Therefore we expect better agreement with mode theory for this value of α_s. This is verified true in Fig. 4.9 where the model computations are done for α_s=0.5 dB m^{-1} kHz^{-1}. Thus the major disagreements of the present results with mode theory in Fig. 4.6 is due to the neglect of caustic corrections.

4.4.1.3. Transmission at 50 Hz

The above computations are repeated for 50 Hz frequency. There is only one propagating mode at this frequency and the water depth is only 1.66 times the acoustic wave length. Fig. 4.10 presents the results of the computations, which may be compared with Fig. 8 of Tindle (1983) (reproduced here in Fig. 4.11). Sediment attenuation in this case is 0.113 dB m^{-1} kHz^{-1}. Normal mode theory predicts a smooth fall off in pressure with range as there is only one propagating mode. As seen from Figs 4.10 and 4.11, the ray approximation is poor at this frequency. Further deterioration of the present results (Fig. 4.10) is due to the neglect of caustics which are stronger at this frequency. This is understood from the more pronounced minimum in the Δ_h versus θ curve at this frequency than at 140 Hz (Fig. 4.12). However, the ray theory results converge better to those of mode theory for the higher

Fig. 4.10. Normalised acoustic pressure versus range at 50 Hz for a sediment attenuation coefficient of 0.113 dB m^{-1} kHz^{-1}.
(———— Normal mode theory ————— Modified ray theory)

Fig. 4.11. Same as Fig. 4.10, but reproduced from Fig. 8. of Tindle (1983).
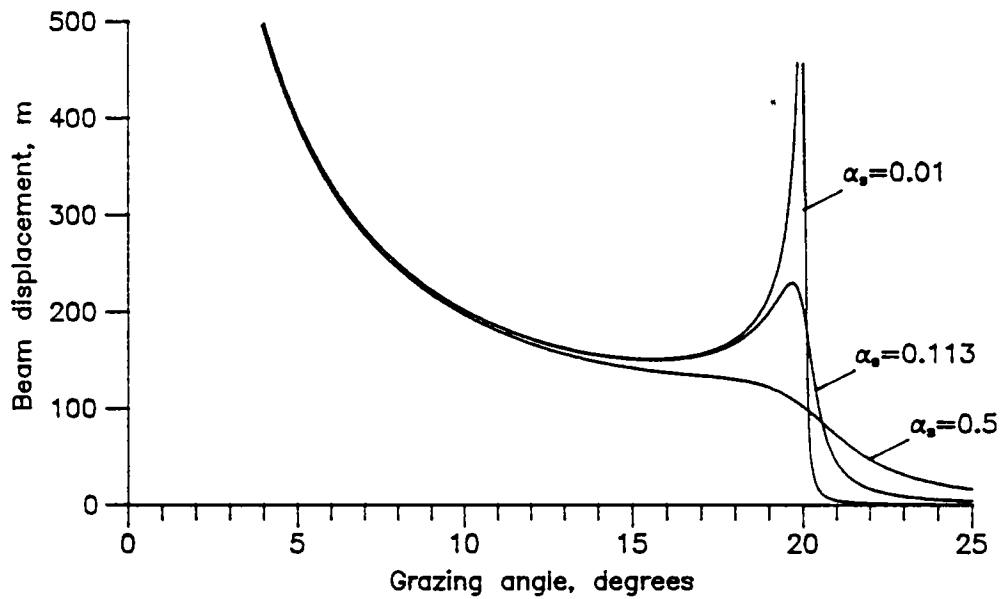
Fig. 4.12. Beam displacement versus grazing angle for three sediment attenuation coefficients. Frequency: 50 Hz.
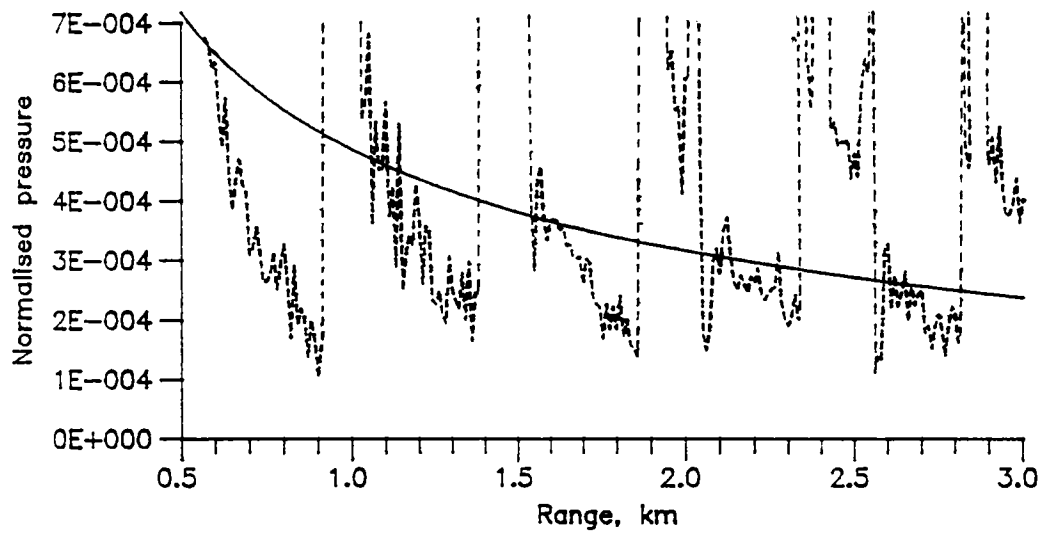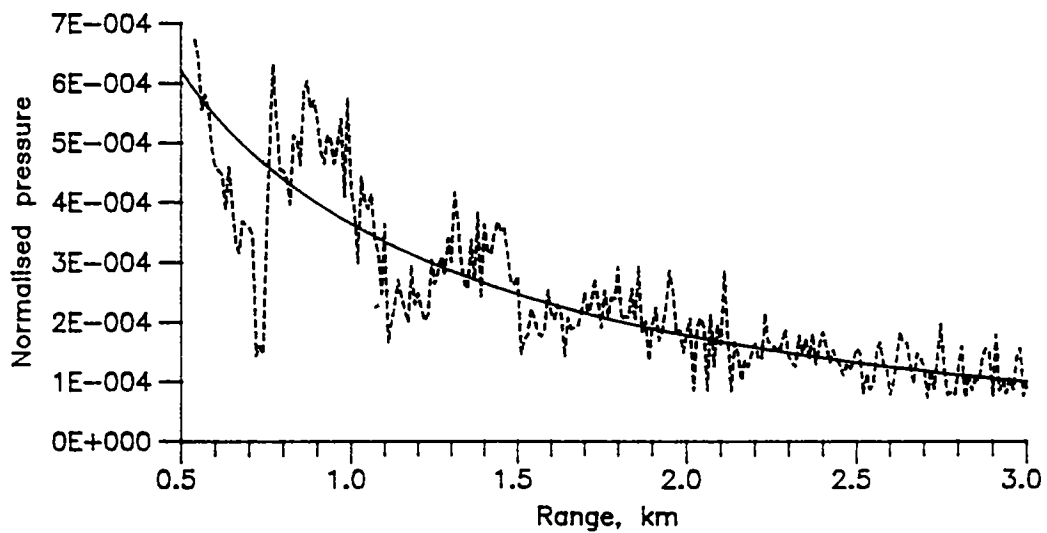

Fig. 4.13. Normalised acoustic pressure versus range at 50 Hz for a sediment attenuation coefficient of 0.5 dB m^{-1} kHz^{-1}.
(————Normal mode theory ------Modified ray theory)
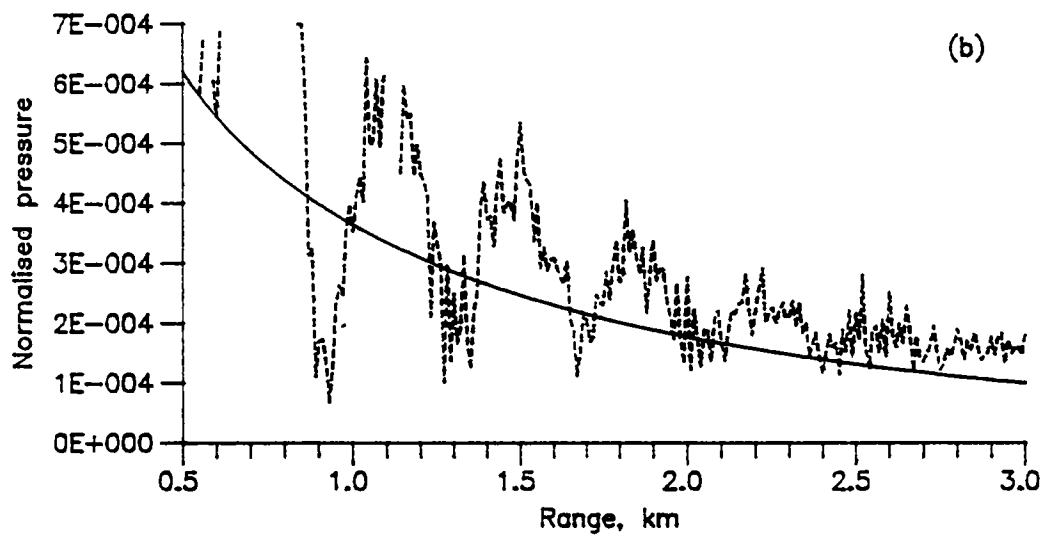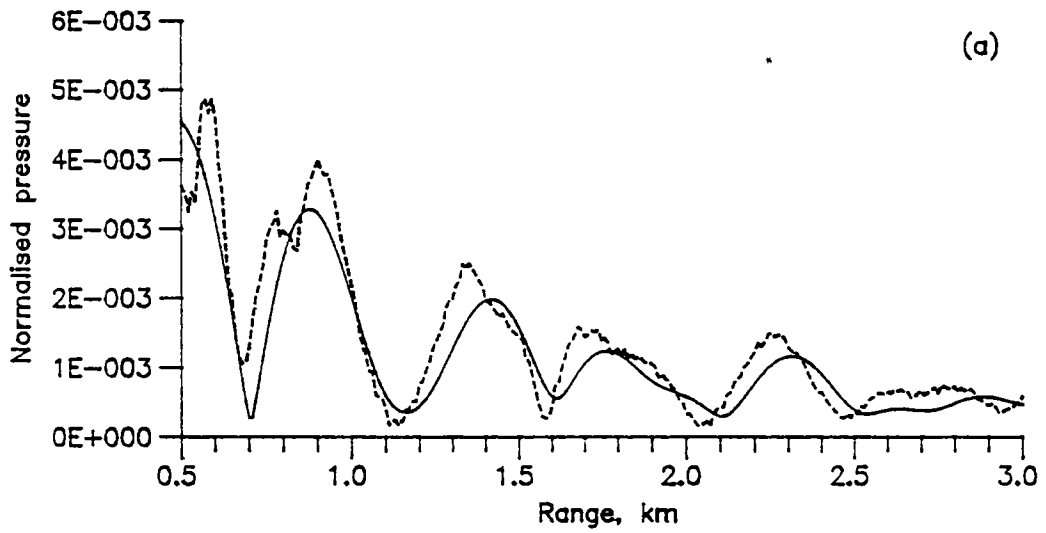
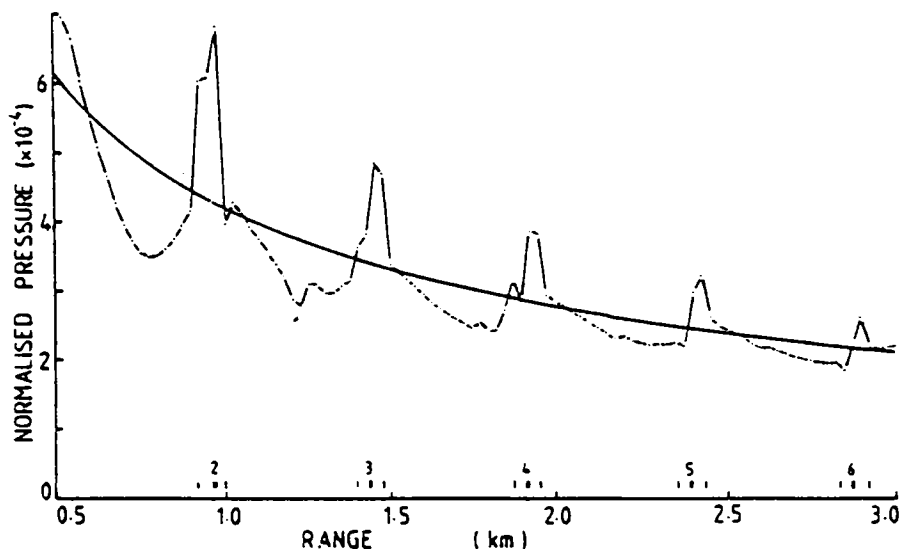Fig. 4.14. Normalised acoustic pressure versus range for (a) 140 Hz and (b) 50 Hz. Sediment attenuation coefficient is 0.5 dB m^{-1} kHz^{-1}. (——————Normal mode theory —————Conventional ray theory)

attenuation coefficient of 0.5 (Fig. 4.13), with the average levels showing good agreement.

4.4.1.4. Computations using conventional ray theory

Before concluding the discussion on transmission loss computation results, it might be interesting to examine the performance of conventional ray theory relative to modified ray theory. We consider the case with α_s=0.5 where there are no caustics to be dealt with. Conventional ray theory results (with Δ_h=0 and τ=0) are compared with normal mode results in Fig. 4.14(a) and (b) respectively for frequencies of 140 and 50 Hz. The difference from modified ray theory is immediately apparent especially for the case of 50 Hz, where conventional ray theory predicts relatively higher pressure levels compared to mode theory. According to theory, beam displacement decreases with increasing frequency so that this disagreement also decreases along with increasing frequency.

4.4.2. Time series simulations
4.4.2.1. Environmental parameters
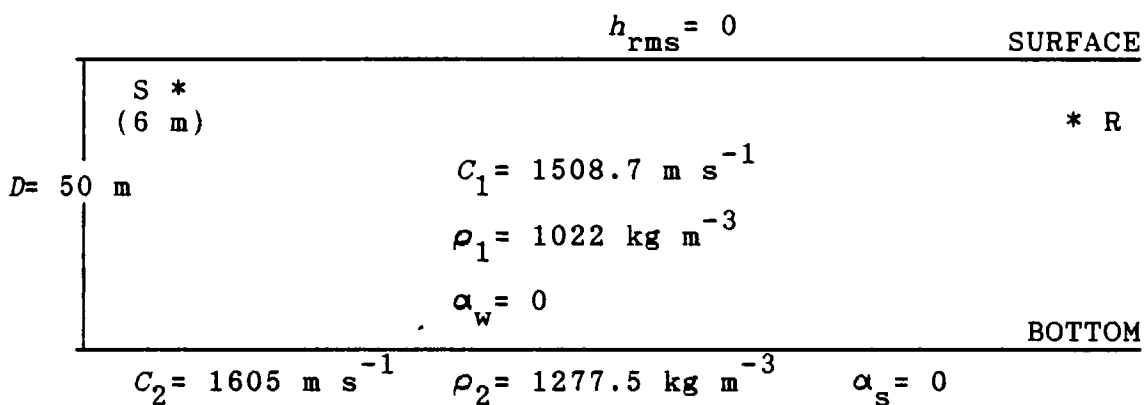
Fig. 4.15. Environmental parameters used for time series simulations

Fig. 4.15 gives the environmental parameters used in time-series simulation, and agree with those in Tindle and

84
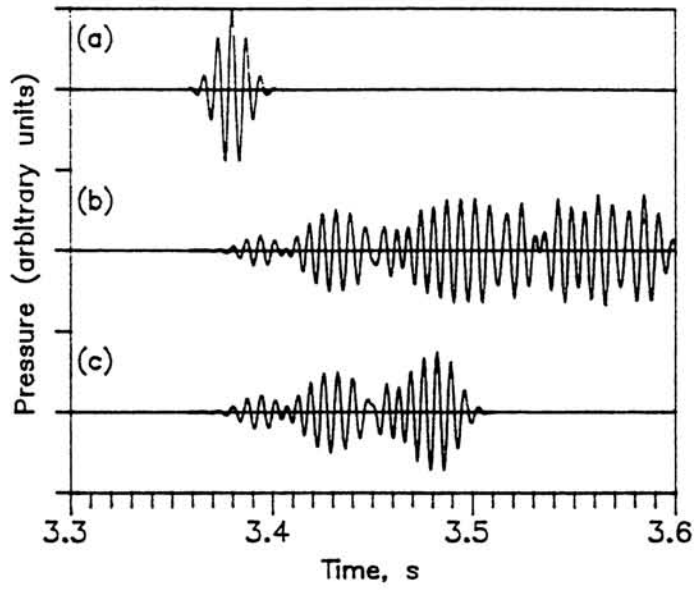
Fig. 4.16. Transmitted (a) and received (b)—(c) signals at 140 Hz. (a) transmitted pulse (b) conventional ray theory (c) modified ray theory
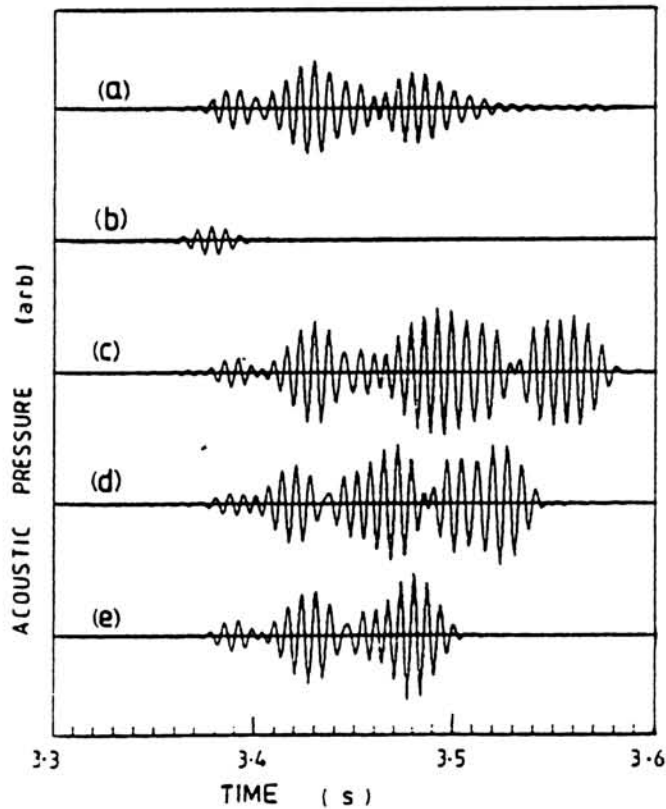
Fig. 4.17. Observed (a) and calculated (b)—(e) signals at 140 Hz. (b) Spherical spreading (c) no beam displacement (d) beam displacement but no time displacement (e) beam and time displacements included (reproduced from Fig. 2 of Tindle and Bold, 1981)
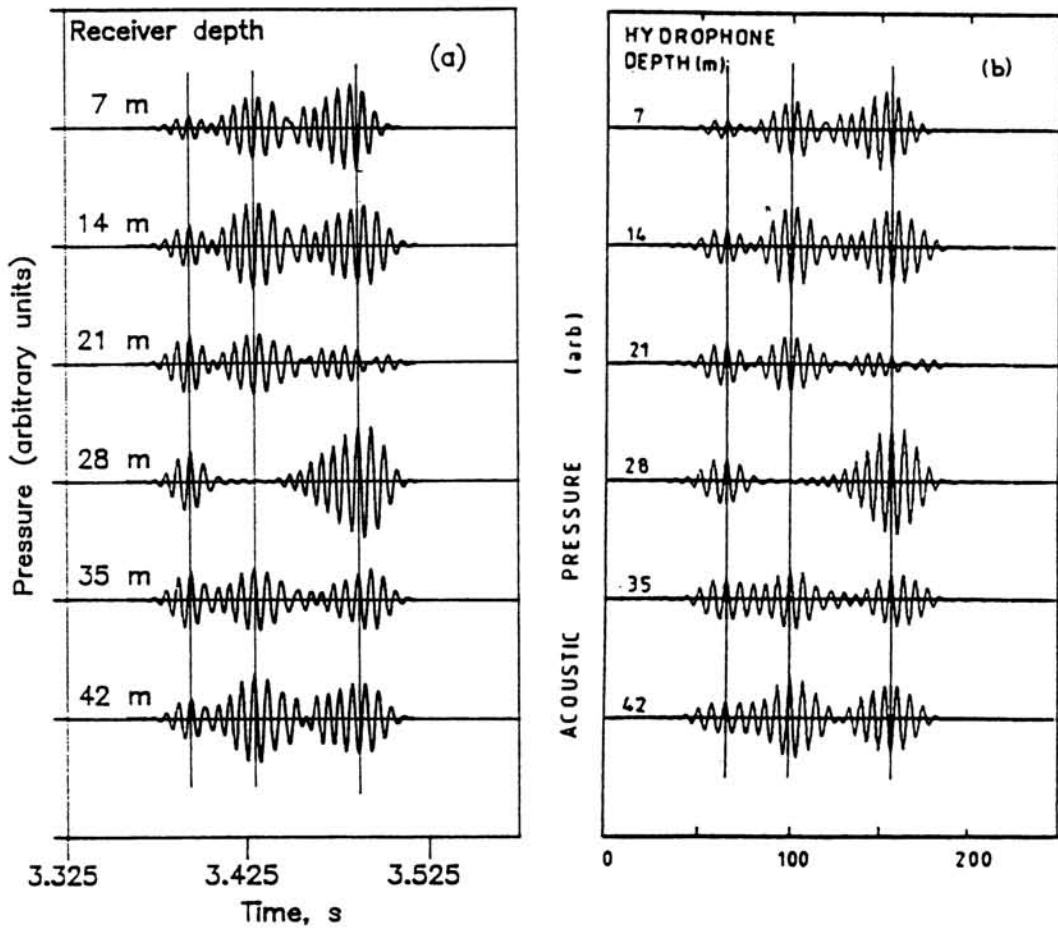
Fig. 4.18. Simulated wave forms at six receiver depths for pulses at 140 Hz. (a) Present results (b) Ray theory with beam displacement, reproduced from Fig. 4(a) of Tindle and Bold, 1981. The x-axis is time in ms.
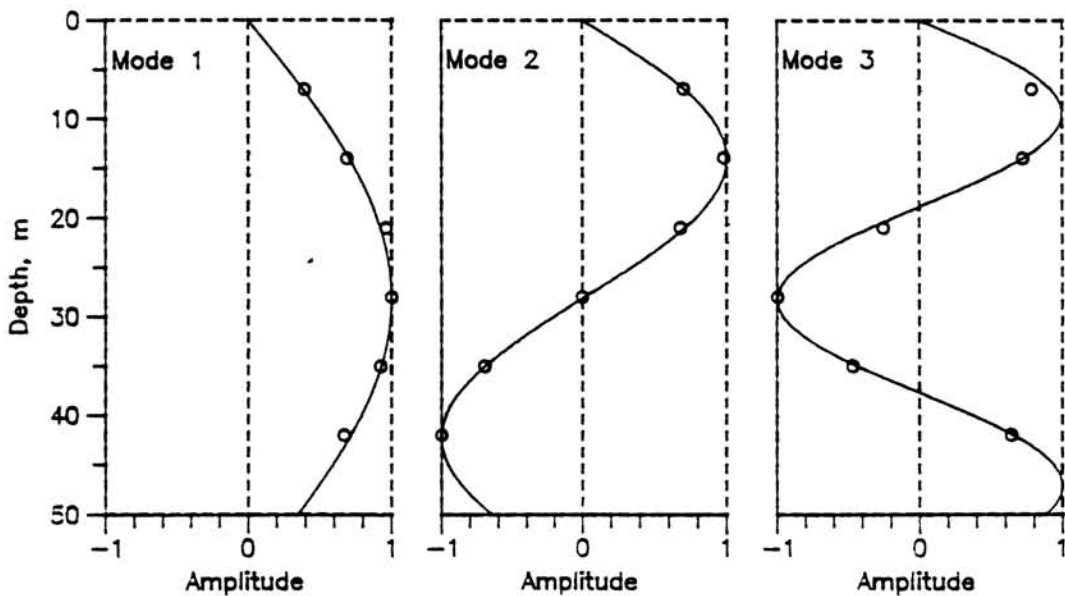
Fig. 4.19. Normalised mode amplitudes with depth for the three modes. ────── Computed using the normal mode model.   o Results from the modified ray theory model (as calculated from Fig. 4.18(a)).

Bold (1981). The source and the receiver are horizontally separated by a distance of 5.1 km. The results are compared with those in Tindle and Bold (1981).

4.4.2.2. Results of time series simulation

The transmitted pulse (Fig. 4.16(a)) is a 140 Hz cosine wave of four cycles with a Gaussian envelope. Figs 4.16(b) and (c) show the simulations of time series at a 7 m receiver using conventional and modified ray theory. These may be compared with corresponding results published by Tindle (Fig. 4.17). Tindle and Bold (1981) shows that their experimental result on the pulse transmission agrees well with modified ray theory where conventional ray theory fails. The second class of eigen-rays near the critical angle whose contributions are negligible are ignored in the modified ray theory simulations (Tindle, 1983). Good agreement is seen between the present simulation in Fig. 4.16(c) and Tindle's published result (Fig. 4.17(e)).

The three distinct arrivals in Fig. 4.16(c) correspond to the three propagating modes. Further results revealing this modal characteristic of the field are presented in Fig. 4.18. These simulations are for the same range of 5.1 km and frequency of 140 Hz. There are six receiver depths: 7, 14, 21, 28, 35 and 42 m. Results from computations using the present model are shown in Fig. 4.18(a) and similar results from Tindle and Bold (1981) are shown in Fig. 4.18(b). The three modes of propagation are clearly identifiable by their phase and amplitude behaviour with depth (Figs 4.18 and 4.19). These are indicated by three vertical lines in Fig. 4.18.

4.5. DISCUSSION

A shallow water sound propagation model based on modified ray theory was developed and presented in this chapter. It was

noted that corrections are to be applied for accurately representing the sound field at ray caustics, but this was not attempted in this study. In order to evaluate the model performance, model outputs were compared with those from a normal mode model of an isospeed channel and results from published literature. However, the ray theory model can handle an arbitrary sound speed profile in the water column so that propagation in more realistic environments might be modelled.

In the sound field computations, we saw that performance of the model is good in the absence of beam displacement caustics (Fig. 4.9). Even at a low frequency at which there was only one propagating mode, average level of the field showed good agreement with the mode theory results (Fig. 4.13). This is a relevant result, because, as discussed in detail in the next chapter (Section 5.2), it is necessary to apply some sort of averaging to transmission loss results from deterministic modelling before a meaningful comparison can be done with band- or time-averaged results from at-sea measurements of the sound field. Then the larger fluctuations in the coherent field are smoothed out and the results more or less represent realistic experimental measurements.

It was also seen that major features of the field are modelled satisfactorily even in the presence of relatively strong caustics, except in the immediate vicinity of the caustics (Fig. 4.6) and at very low frequencies (Fig. 4.10). Magnitudes of compressional attenuation in common sediment types overlying the continental shelves (mostly sandy sediments) are often high enough (Clay and Medwin, 1977:p-260; Hamilton, 1980) to suppress the presence of strong beam displacement caustics in the ray theory model, if attenuation is included in the calculation of beam displacement. Also, except at frequencies lower than a few hundred hertz, beam displacement is negligibly small and may be ignored in practical computations of the sound field; this is equally applicable to low-loss sea bottoms also. A probable source of

caustic formation in shallow waters is large sound speed gradients that might occur in the water column, for example in the presence of a strong thermocline. In such cases, accurate modelling of the sound field (in the thermocline region) requires corrections to be applied at and near the caustics.

The model was also used for simulations of monochromatic pulse transmission. Comparison of the simulation results (Fig. 4.16) with corresponding results of Tindle (Tindle and Bold, 1981) show that the received signal characteristics are simulated accurately. Modal structure of the field as predicted by the normal mode theory, with three propagating modes, is also reproduced fairly accurately by the ray theory model (Figs 4.18 and 4.19). These results indicate that the basic computations of eigen-ray amplitudes, phases, and travel times done in the model are fairly accurate.

Chapter 5

TRANSMISSION LOSS MODELLING IN COASTAL SEAS
-APPLICATION OF THE RAY THEORY MODEL

Sound propagation experiments at sea play an important
role in the development and validation of propagation models.
Details of experimental data collection and analysis
procedures for transmission loss estimation at sea are
discussed by Vijayakumar (1989). In this chapter, first the
experimental procedure is briefly outlined. Then we present
justifications behind comparison between band-averaged
transmission loss estimates and single frequency results from
deterministic modelling. This is followed by details of two
shallow water transmission loss experiments conducted on the
western continental shelf of India. Finally the experimental
results are compared with model computations and the results
are discussed.

5.1. SOUND PROPAGATION EXPERIMENTS AT SEA AND THE ESTIMATION OF TRANSMISSION LOSS

A sound propagation experiment essentially consists of a
sound source and a receiver (hydrophone). The source (single
frequency or broad-band) is usually carried on board a ship.
The receiver may be deployed from a ship or attached to a
surface/sub-surface buoy. Very often arrays of hydrophones
deployed in vertical or horizontal configurations are used in
place of a single hydrophone, thus enabling spatial sampling
of the sound field.

5.1.1. Underwater explosions as sound sources

Underwater explosions using "high explosives" (usually
TNT) are the most commonly employed sound sources in

transmission loss experiments. They act as omni-directional broad-band sound sources with high source levels. In spite of a few draw-backs such as those arising from non-repeatability of the signals, explosives find wide usage as underwater sound sources owing to their relative advantages over other types of sources. A good deal of research has been carried out on various aspects of these sound sources (Arons et al., 1948; Cole, 1948; Arons, 1954; Weston, 1960b; Christian, 1964; Gaspin and Shuler, 1971; Wakeley, 1978; Gaspin et al., 1979; Chapman, 1985,1988)

Fig. 5.1. shows a typical pressure-time waveform of an underwater explosion. In the figure the shock wave, with an
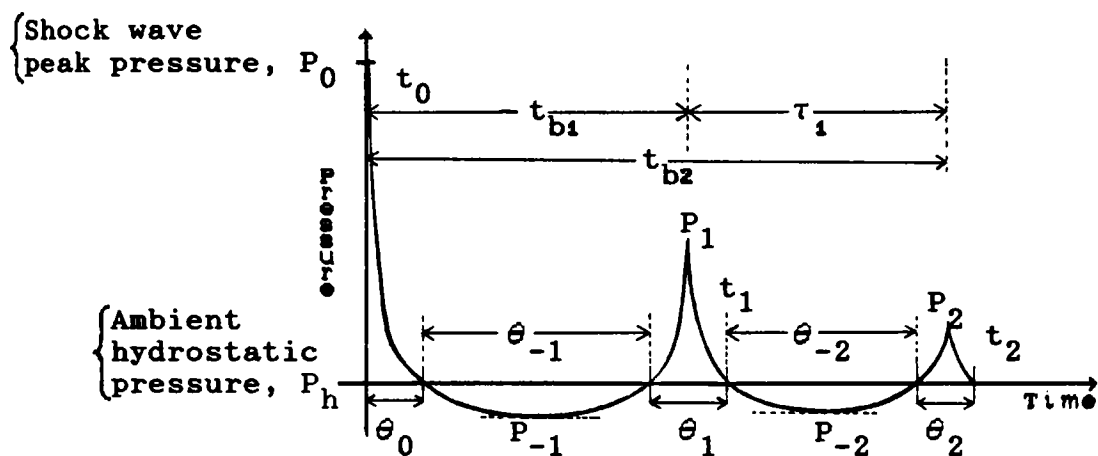
P_i = Peak pressures of ith bubble pulse (i= 1,2,...)

P_{-i} = Minimum pressure during i^{th} negative phase (i= 1,2,...)

t_0, θ_0 = Time constant and phase duration of the shock wave

t_{bi} = i^{th} bubble pulse period

τ_i = Time interval between the ith and $(i+1)^{th}$ bubble pulses

t_i = Time constant for the ith bubble pulse (i= 1,2,...)

θ_i = Phase duration of the ith bubble pulse (i= 1,2,...)

θ_{-i} = Phase duration of the ith negative pulse (i= 1,2,...)

Fig. 5.1. Schematic representation of a typical underwater explosive pressure-time signature (after Vijayakumar and Ajaikumar, 1990b)
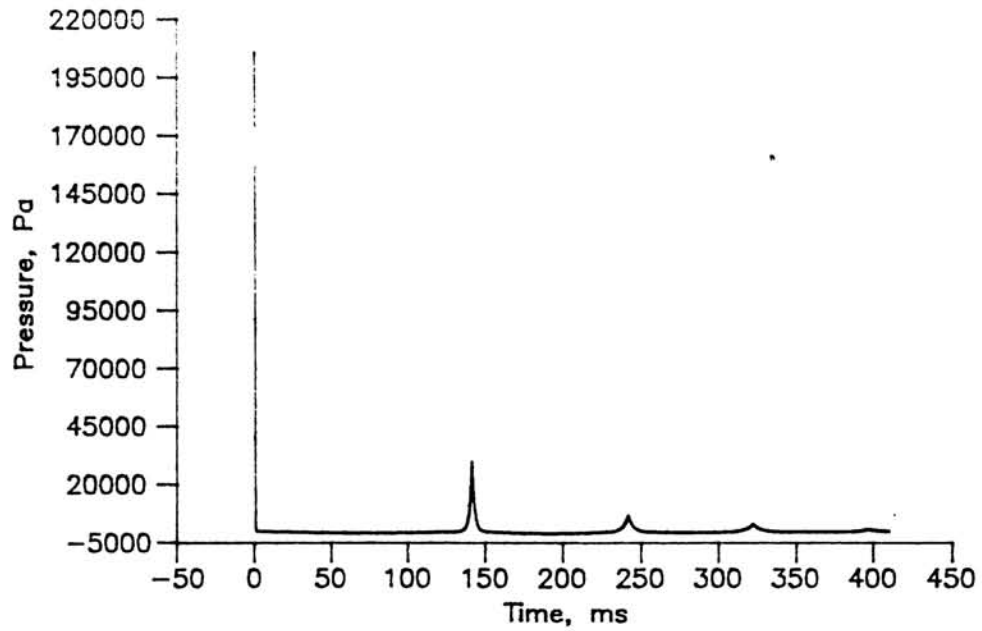
Fig. 5.2. Pressure—time waveform of an explosion of a 1 lb TNT charge at a depth of 8.5 m, as would be observed at a range of 100 m (computed following Wakeley, 1978).
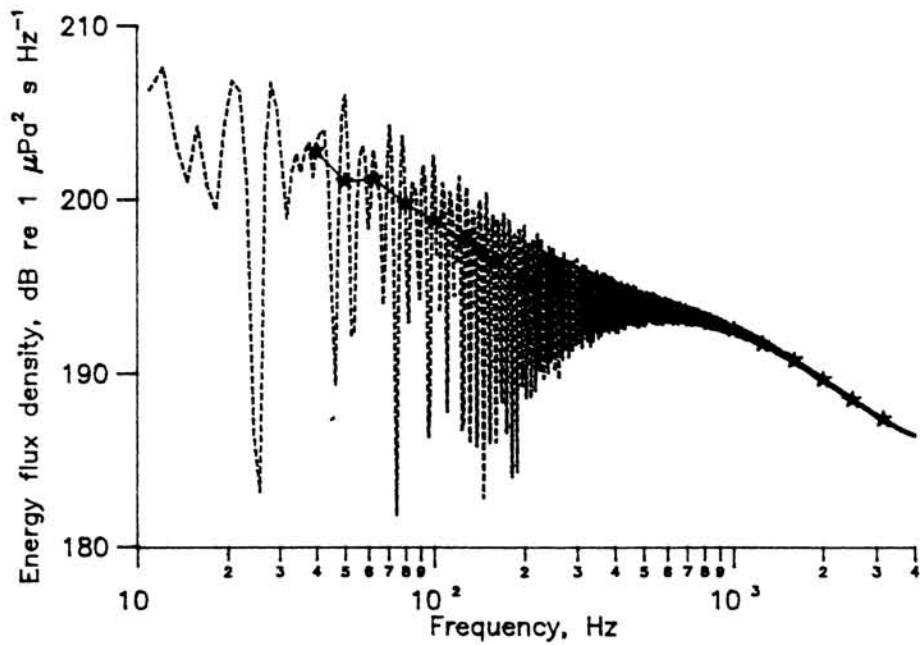
Fig. 5.3. Energy flux density for the signal shown in Fig. 5.2. (*) Band—averaged levels at third—octave central frequencies.

almost instantaneous rise in pressure followed by a sharp, exponential decay of very small time constant, is characteristic of a detonating explosive like TNT. The bubble pulses are generated by damped radial oscillations of the gas bubble resulting from the explosion, with simultaneous rising towards the sea surface. There is a well-established relation between the bubble pulse period and the depth of explosion which could be utilised for indirect estimation of the depth of explosion.

Accurate source levels of the explosive signals are essential for the estimation of transmission loss from propagation experiments. Experimental determination of source level spectra for the more common shallow explosions is difficult due to multipath interference. In such cases, a more reliable and convenient method is the frequency analysis of a pressure-time signature model of the explosion (Gaspin and Shuler, 1971; Wakeley, 1978). As an example, the pressure-time signature, as would be observed at a distance of 200 m, of a 1 lb (453.4 g) TNT explosion at a depth of 9 m is shown in Fig. 5.2. Corresponding source level spectrum of the signal and third-octave band-averaged levels are given in Fig. 5.3.

5.1.2. Propagation experiment and data analysis

Transmission loss experiments as referred to in this study are conducted as follows. Two ships are involved- a shooting ship for deployment of the explosives and a receiving ship carrying the recording equipment (Fig. 5.4). The recording equipment essentially consists of a vertical hydrophone array deployed from the ship, signal conditioners, and an instrumentation tape recorder.

At the start of the experiment the shooting ship opens out from a close range, detonating explosives at pre-decided distances from the receiving ship. Track of the shooting ship is selected so as to ensure a relatively constant water depth
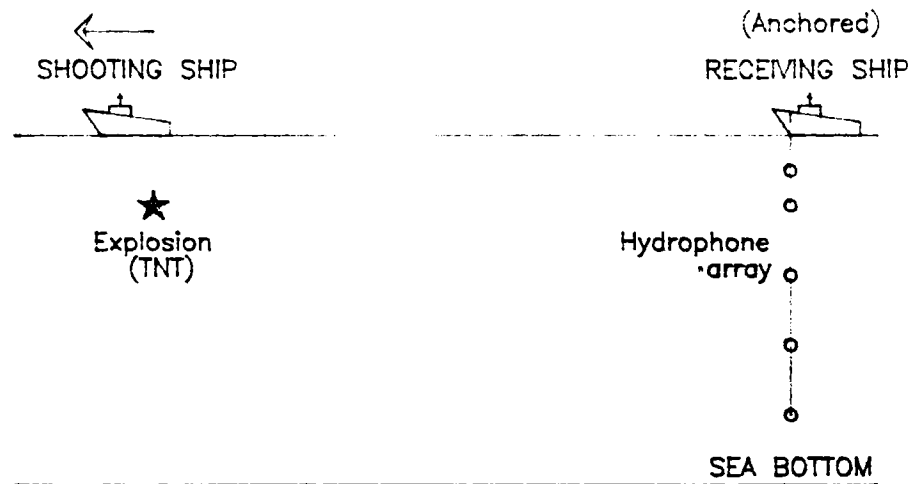
Fig. 5.4. The two—ship experiment.

over the propagation path. Throughout the experiment, distance between the ships is monitored at regular intervals using radar. Relevant environmental data is also collected, including temperature and salinity profiles, sea bottom samples, sea state (surface wave height), and echo soundings.

Signals as received by the receiving array are conditioned and recorded on the tape recorder. The recorded signals are analysed by playing back them to a spectrum analyser. The procedure of analysis involving corrections for noise, amplifier gains, and hydrophone sensitivities, before transmission loss estimates are obtained, is discussed by Vijayakumar (1989). Final output of the analysis, as used here, are transmission loss values as a function of receiver depth and range for standard 1/3 octave bands of frequency.

5.2. DETERMINISTIC MODELLING VERSUS EXPERIMENTAL DATA

Jensen (1981) addresses problems associated with deterministic modelling, particularly in the context of model/data comparisons, where the data are averaged over

91

third-octave bands. A deterministic model, such as the one developed in the previous chapter, allows only for completely regular and well-defined propagation paths through the ocean. Hence it gives only a simplified solution to the problem of propagation modelling.

Due to temporal fluctuations and spatial ' variations of the environment, deterministic modelling is not directly applicable to the oceans. Coherent transmission loss obtained from the model is a true deterministic representation of the acoustic field. When this transmission loss is plotted against range or frequency, the curve shows excursions from a mean curve of the same order of magnitude due to multipath interference. Only the mean curve represents a stable answer to propagation in a given environment where any slight changes in the frequency, source/receiver geometry, or the environmental inputs could lead to drastic changes in computed propagation loss at any given point in space (Jensen, 1981). One way to smooth out the fluctuations in the coherent field is to use an averaging with a fixed-width sliding range-window (Jensen, 1981, 1988; Dosso and Chapman, 1987; Chapman and Ward, 1990), or to use an incoherent (assuming a uniformly distributed random phase) addition of the modes/arrivals, which gives the incoherent transmission loss. In range-averaging, width of the range-window is so selected that peaks due to multipath interference get smoothed out.

Experimental transmission loss estimates also involve averaging within the corresponding third-octave bands. Within such a band the coherent transmission loss has rapid fluctuations, but the incoherent loss represents a mean curve for the coherent loss. Jensen (1981) shows that a band-averaged result is close to the incoherent result at the centre frequency of the band, and that a meaningful comparison can generally be done between band-averaged experimental data and model outputs at the centre frequencies when using the incoherent addition.
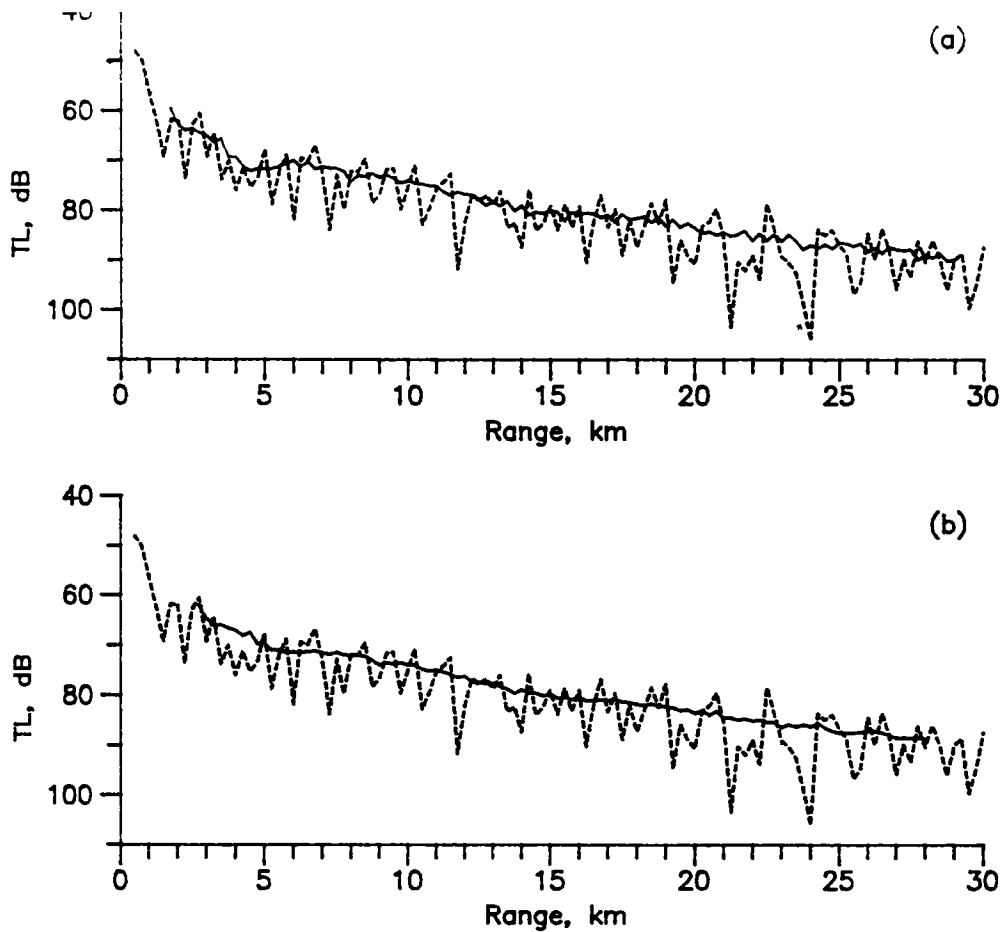
Fig. 5.5. The dashed curves represent coherent transmission loss computed at a range interval of 250 m for a receiver depth of 55 m and a frequency of 3150 Hz. Other inputs are as in Fig. 5.9. The full line is obtained after applying (a) 2 km (b) 4 km sliding range—window averaging.

As an example illustrating the effect of range-averaging on transmission loss, Fig. 5.5 shows the results of computations for a typical case, where the environmental parameters are as in Fig. 5.9. Frequency is 3150 Hz and the receiver depth is 55 m. Transmission loss is computed at a range interval of 250 m. It is seen that range-averaging using a 2 km sliding range-window satisfactorily smooths out fluctuations in the coherent field. Increasing the window size to 4 km has not significantly altered the final result.

Effects of a larger range interval and a smaller range-window were also examined. Increasing the range interval

to 500 m (keeping the same window width of 2 km) resulted in occasional departures of the order of 2-3 dB from the corresponding curve shown here. There were departures of the same order of magnitude or more when a smaller (1 km) window width was employed for averaging. A range interval of 250 m and a window width of 2 km are satisfactory for our present requirements. Though a closer range interval could have resulted in a smoother average curve, this was not attempted because fluctuations in the present results are well within tolerable limits and uncertainties in the model inputs could cause deviations more significant than these fluctuations.
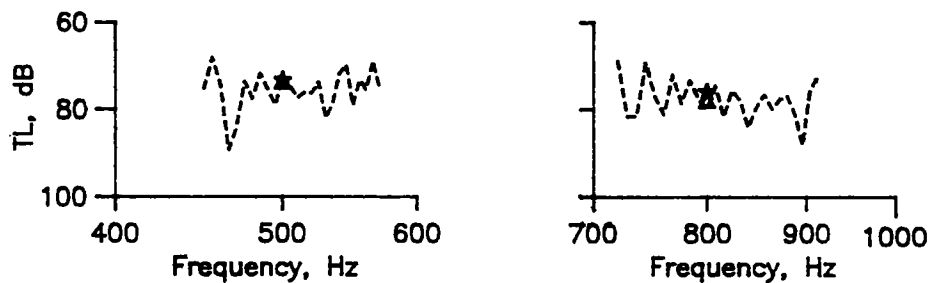
Fig. 5.6. Comparison of (★)band— and (△)range—averaged transmission losses. The dashed curves represent coherent transmission loss. Receiver depth: 55 m, Range: 22.25 km. Other inputs are as in Fig. 5.9.

Fig. 5.6 is a comparison between range-averaged and band-averaged transmission loss. The band-averaging is done over 25 data points in the respective third-octave bands. The range-averaged result is for the centre frequency of the band. We see that both the results are the same for all practical purposes. In the transmission loss versus range results to be presented in this chapter, a range interval of 250 m is used and averaging is done by applying a 2 km sliding range-window. Similarly for obtaining the frequency response of the channel, range-averaged transmission loss taken over a 2 km range-window (centred at the receiver range) are used.

The next section presents details of two shallow water sound propagation experiments, transmission loss data from

which are compared with model computations. One of these experiments was conducted off Kochi and the other off Bombay.

5.3. EXPERIMENTAL DETAILS AND THE ENVIRONMENTAL DATA

5.3.1. The experiment off Kochi

An experiment for transmission loss estimation was conducted off Kochi on 16 May 1988. The location was $9°48.2'$ N, $75°44.8'$ E where the receiving ship *RV Gaveshani* of the National Institute of Oceanography (NIO), Goa remained anchored during the experiment. The water depth was 70 m. A vertical array of three hydrophones was deployed from the receiving ship, with individual hydrophones at depths of 5, 30, and 55 m. The shooting ship (IN Ship) opened out deploying 1 lb TNT charges and following the 70 m depth contour. Most of the explosions were at depths of 7-8 m.

Location	Depth (m)	Composition (%)			Wet density (kg m^{-3})	Sound speed (m s^{-1})
		Sand	Silt	Clay		
$9°44.5'$ N $75°44.5'$ E	†78	85.65	13.04	1.30	--	--
$10°56.5'$ N $75°46.5'$ E	†79	82.18	13.36	4.44	--	--
$9°50.1'$ N $75°45.2'$ E	‡67	87.00	7.00	6.00	1960	*1830

†Siddiquie and Almeida (1985)   ‡ Murty *et al.* (1984)
*laboratory measurement at 1 MHz

Table 5.1. Characteristics of sediment collected at locations near to the experimental site off Kochi.

The sound speed profile was derived from bathythermograph data collected on board the receiving ship. The profile and a
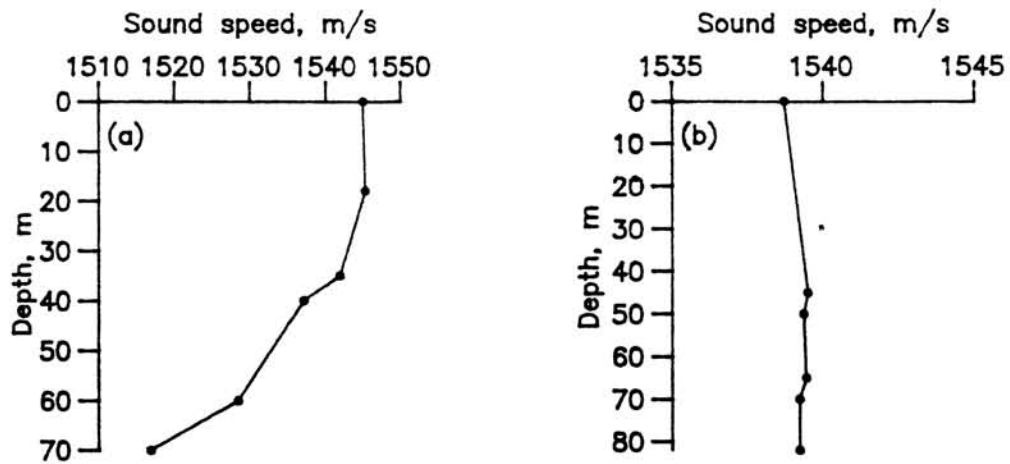
Fig. 5.7. Sound speed profiles at the two experimental locations. (a) off Kochi (b) off Bombay
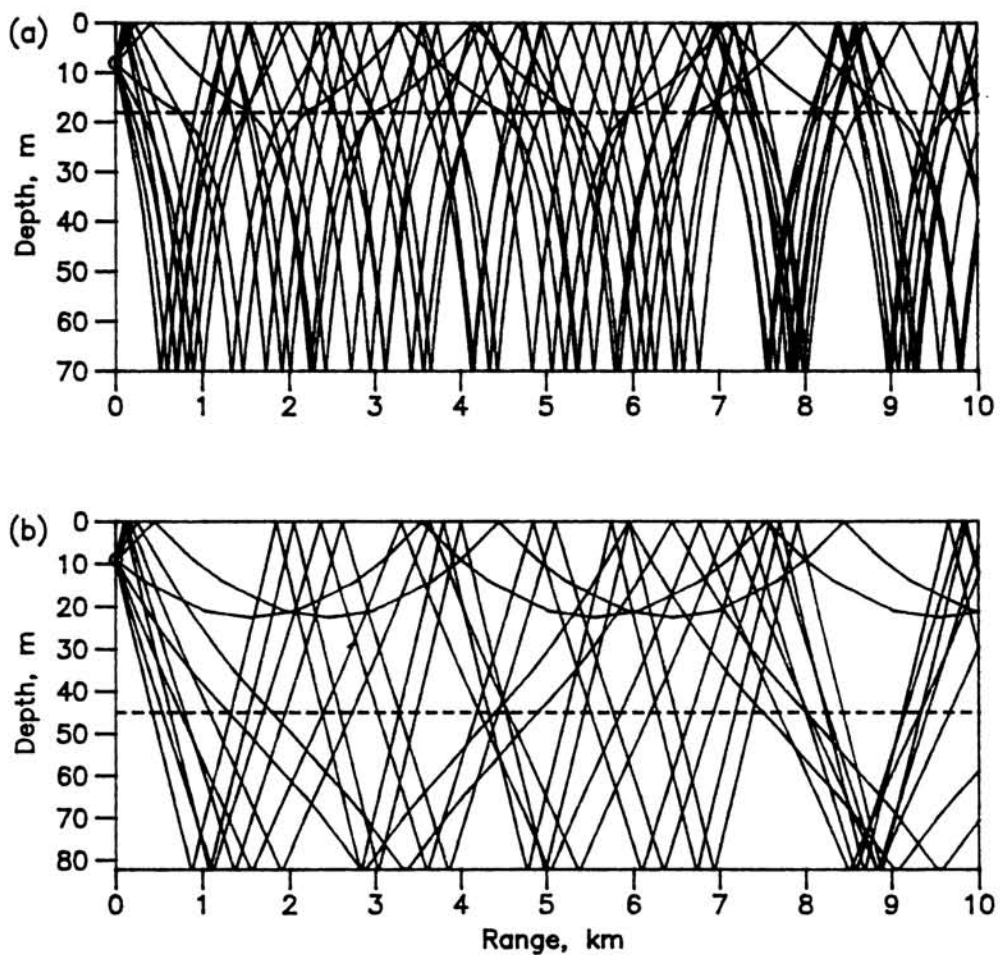
Fig. 5.8. Ray diagrams for the two experimental locations, (a) off Kochi (b) off Bombay. Rays are drawn for a beam width of 10° and at an interval of 1°. The dashed line is the lower boundary of the surface duct.

ray diagram for a source depth of 8 m are shown in Fig. 5.7(a) and 5.8(a) respectively. It is seen that a relatively strong downward refraction condition prevailed. The presence of a surface duct of 18 m thickness is also indicated, with a sound speed gradient of 0.0167 s^{-1}. The sea state was 3.

Sea bottom along the propagation track is sandy with more than 80% sand content (Siddiquie and Almeida, 1985; Table 5.1). For a sediment sample collected at a nearby location, Murty et al. (1984) reported sand content of the same order. An rms bottom roughness of 0.03 m for the area was also estimated from echo type correlations.

5.3.2. The experiment off Bombay

The second experiment to be considered here was conducted off Bombay ($18°49.75'$ N, $71°35.75'$ E) on 18 January 1986. The station depth was 82 m and the sea state was 1. A vertical hydrophone array with individual hydrophones at 15, 30, 45, 60, and 75 m was deployed from the receiving ship RV Gaveshani anchored at the above location. The shooting ship (IN Ship) detonated 1.25 lb TNT charges at different ranges from the receiving ship, while following a constant-depth track. The explosions were at a depth of about 9 m. The sound speed profile and a corresponding ray diagram for a 9 m source are shown in Fig. 5.7(b) and 5.8(b) respectively. There was a 45 m surface duct with a sound speed gradient of 0.0173 s^{-1}.

Murty and Pradeepkumar (1986) discuss geological and geo-acoustical properties of the continental shelf off Bombay. Sediments of the middle shelf (40-90 m depth) are dominated by calcareous sands. The sediment sample collected at the experimental location was medium sand for which density and sound speed are given as 1900 kg m^{-3} and 1850 m s^{-1} respectively. The middle shelf is also dominated by sharp pinnacles of the order of 2-4 m height. A continuous seismic profiler (CSP) survey was conducted along a track towards

96

shallower waters and beginning at the experimental location. From this survey they infer the presence of three layers of sand with thicknesses of 25, 20, and 10 m upto a distance of 23 km, with a weak reflector in the first layer gradually merging with the second layer. From correlation of the CSP data with core sample data, the layer is indicated to be sandy.

5.4. COMPARISONS WITH MODEL COMPUTATIONS OF TRANSMISSION LOSS

Justifications behind comparisons between band-averaged experimental data and deterministic model outputs were presented in Section 5.2. The previous section (Section 5.3) presented details of the two transmission loss experiments, data from which are compared with computations using the propagation model. Before proceeding to the comparisons, certain relevant points regarding the experimental data and the model results are brought out which could be of help in analysing and interpreting the comparisons.

5.4.1. General considerations
5.4.1.1. Experimental transmission loss data

Vertical arrays of hydrophones were used as receivers in both the experiments. For each of the ranges at which the charges were detonated, a single explosion was selected and analysed for all the receivers in the array and for the whole third-octave bands for which data is available. Though transmission loss data for the third-octave centre frequencies in the 40-3150 Hz range are presented here, only the data for frequencies > 100 Hz are considered reliable due to suspected interference from the platform (ship) noise (Vijayakumar and Salam, 1987). No data is available for higher central frequencies. It is also noted that most of the data points are about 4 km (2 nautical mile) or more distance apart, and the distances are obtained by radar ranging.

5.4.1.2. Modelling the sea bottom effects

Earlier discussions in Chapters 1 and 3 stressed the decisive role played by sea bottom on shallow water sound propagation. Both magnitude and frequency dependence of the sediment compressional attenuation coefficient can significantly influence transmission loss modelling results. For example, Beebe et al., (1982) used the Biot-Stoll sediment model for low frequency (25 to 800 Hz) transmission loss prediction in three shallow water locations with varying sediment types. They obtained good agreement between measured and predicted transmission loss values for 25, 80, and 250 Hz. Shear wave effects in the bottom were not considered in their study. Though it is now accepted in principle that the attenuation in porous sediments varies non-linearly with frequency, at least in a limited low-frequency band, experimental evidences in this regard for real ocean bottom sediments are still controversial (Kibblewhite, 1989).

Mitchell and Focke (1983) investigated the role of sea bottom attenuation profile in shallow water propagation. They showed that constraints placed by a propagation model in describing the environment directly affect the results and conclusions of analyses performed on propagation measurements. Re-analysing a few published results from literature, they demonstrated that propagation measurements interpreted in terms of a non-linear frequency dependence of attenuation can also be interpreted in terms of a linear dependence, if the attenuation is considered to vary with depth.

However, in one of their experimental studies on inverse methods, Zhou et al. (1987b) note that "for the low frequency range, a non-linear frequency dependence of the acoustic attenuation in the upper sedimentary layer is required to explain many aspects of shallow water sound propagation, including the non-occurrence or lowering of the optimum

98

frequency for acoustic propagation in shallow water (Zhou *et al.*, 1987a) and the increase of sea bottom reflection loss with increasing frequency (Zhou, 1986) at small grazing angles". Before arriving at this opinion they also considered a linear frequency dependence model with a negative attenuation profile which could possibly· explain the experimental observations, as demonstrated by Mitchell and Focke (1983). It was found that the negative gradient in attenuation required by this model was much too strong to be acceptable for the mixed sand and silt sediments, in the light of the then available data or models.

In Section 3.3.3 it was pointed out that shear wave effects could not be ignored while modelling propagation over a sea bottom with consolidated sediments or a thin sediment cover over a hard substrate. There have also been works reported on shallow water propagation modelling where high values of shear speeds in sediments were required to match observations with model results (Ferla *et al.*, 1980; Jensen and Kuperman, 1983). The corresponding propagation models assumed the compressional attenuation to be constant with depth. Mitchell and Focke (1983) observe that such interpretations are not convincing because the shear speeds are greater than any measured in natural sediments (e.g., Hamilton, 1980). They show that an attenuation profile with a positive gradient and realistic shear wave velocities could also explain the same experimental observations.

5.4.1.3. Computations using the present model

In our computations we assume a linear frequency dependence for the sediment compressional attenuation. This is reasonable for the frequency range and the sandy sediments under consideration (e.g., Kibblewhite, 1989). Compressional wave attenuation for surface sands varies between about 0.25 and 0.6 dB m^{-1} kHz^{-1} (Hamilton, 1980). As there are no attenuation measurements or estimates for both the

experimental sites, the values given by Hamilton are used as guide-lines.

In Chapter 3 we examined the effects of shear waves on bottom reflection coefficient and beam displacement (Section 3.3.4.4). It was shown that the effect of shear waves on reflection coefficient is significant only at higher grazing angles. The effect on phase change and beam displacement are not negligible at small grazing angles. A shear speed of 472 m s^{-1} was used for the sample computation which, however, is on the higher side as far as fine sand is concerned (Hamilton, 1980; also Section 5.4.1.2). No experimental data are available regarding shear properties of sediments at the experimental sites, so again we depend on Hamilton for a reasonable estimate- of the order of 100-200 m s^{-1} for sandy sediments in the depth range of 0-10 m (Hamilton, 1980). From shallow water transmission loss computations using the present model and including shear wave speeds of this order of magnitude, it was observed (not presented here) that the coherent transmission loss pattern shifts in the range (distance from the source) in the presence of shear waves, but the range-averaged transmission loss (with which we compare the experimental data) is not affected noticeably. This observation is justified considering low grazing angles of propagation dominant in shallow waters. At low grazing angles, phase of the reflection coefficient is more affected than its magnitude, as noted in Section 3.3.4.4. Hence we ignore the shear wave effects, if any, in the transmission loss computations to be presented here.

It would be helpful to have an idea on the effective thickness of the sea bottom that interacts with the sound energy. The bottom interaction is frequency dependent and the depth of penetration increases with decreasing frequency. To obtain an estimate of the effective depth ΔD of sea bottom interaction, we use the relation (Lo et al., 1983; Zhou et al., 1987)

$$\Delta D = \frac{\rho_2 \, c_1}{2\pi \, f\rho_1} \sqrt{1 - (c_1/c_2)^2} \qquad\qquad (5.1)$$

With typical values of $\rho_1 = 1022$ kg m^{-3} and $c_1 = 1540$ m s^{-1} for the water column and $\rho_2 = 1900$ kg m^{-3}, $c_2 = 1850$ m s^{-1} for a homogeneous sea bottom, ΔD is about 8 m for $f =$ 100 Hz and about 25 cm for $f =$ 3150 Hz. Thus the observed transmission loss characteristics presented here are influenced by only the first few metres (<10 m) of the sea bottom.

During both the experiments, sound speed profiles were collected only at the location of the receiver array. In the model computations it is assumed that the same profile prevailed throughout the duration of the experiment and along the propagation track. Sediment data along the propagation tracks were not collected. Hence information from earlier measurements at nearby locations and data collected at the receiver location are assumed applicable. Surface wave height measurements were not taken during both the experiments. The rms roughness heights used in the model computations are based on the corresponding observations of the sea state.

The next two sections present the model/data comparisons. As no estimates of sediment compressional attenuation are available, in the model computations we try to tune the attenuation coefficient so as to get satisfactory agreement of the model outputs with the experimental transmission loss results.

The comparisons are shown in the form of three types of graphs, using standard methods of presentation. In the first type, transmission loss is plotted against distance for a given depth and frequency. The second type shows behaviour of transmission loss with frequency as observed at selected ranges and at a given receiver depth. The third type of graph (used here only for the off Kochi location) shows variation of transmission loss with distance and receiver depth for a given

101

frequency. In all these graphs, the model results are range-averaged transmission loss obtained as explained in Section 5.2, and the experimental data are band-averaged results for the corresponding third-octave bands. The above three types of comparisons are sufficient to establish efficacy of the model in predicting transmission loss characteristics of an environment. However from the nature of the experimental data used here, it is clear that comparisons using the second type of graph (frequency response of the channel), provide a better indication of model performance than the transmission loss versus range comparisons.

5.4.2. Comparison for the location off Kochi

$h_{rms} = 0.25$ m   SURFACE

S *
(8 m)
                    $C(z) = $ [Fig. 5.7(a)]
$D = 70$ m   R * (30 m)

                    $\rho_1 = 1022$ kg m^{-3}

                                                    R * (55 m)
                    α_w
                                                    BOTTOM

$C_2 = 1850$ m s^{-1} $\rho_2 = 1900$ kg m^{-3} $\alpha_s = 0.0002$ dB m^{-1} Hz^{-1}
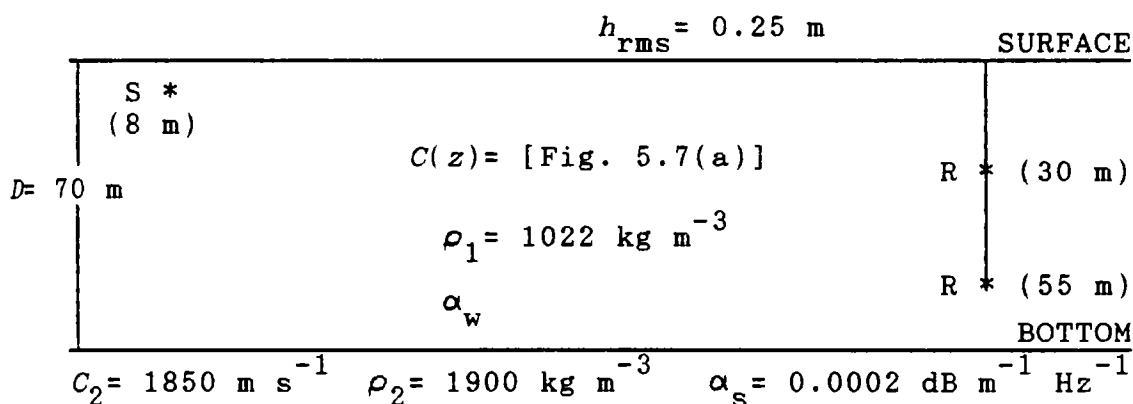
Fig. 5.9. Environmental parameters used for transmission loss computations. Location: off Kochi.

For transmission loss computations we select the two receiver depths of 30 and 55 m that conform to the assumption of typical shallow water propagation conditions, with only SRBR rays present. The sound speed profile is as shown in Fig. 5.7(a). A source depth of 8 m is used. Other environmental parameters are as in Fig. 5.9. An rms roughness height of 0.25 m is used corresponding to sea state 3.

Fig. 5.10 shows the comparison of transmission loss against range for five selected frequencies, and Fig. 5.11 is
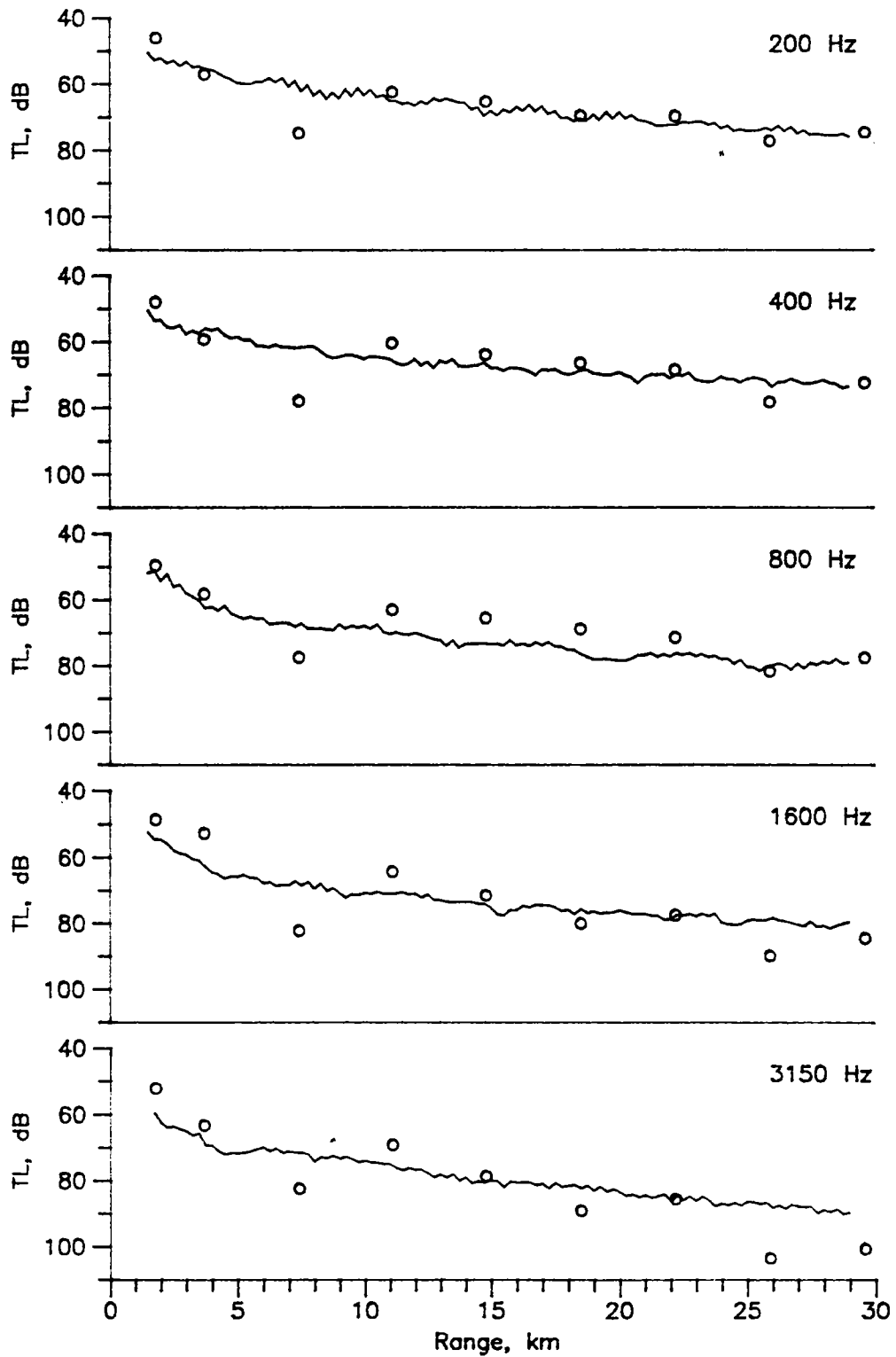
Fig. 5.10. Ray theory computations of transmission loss versus experimental data collected off Kochi for different frequencies. Receiver depth: 55 m. —— Ray theory. o Experimental data.
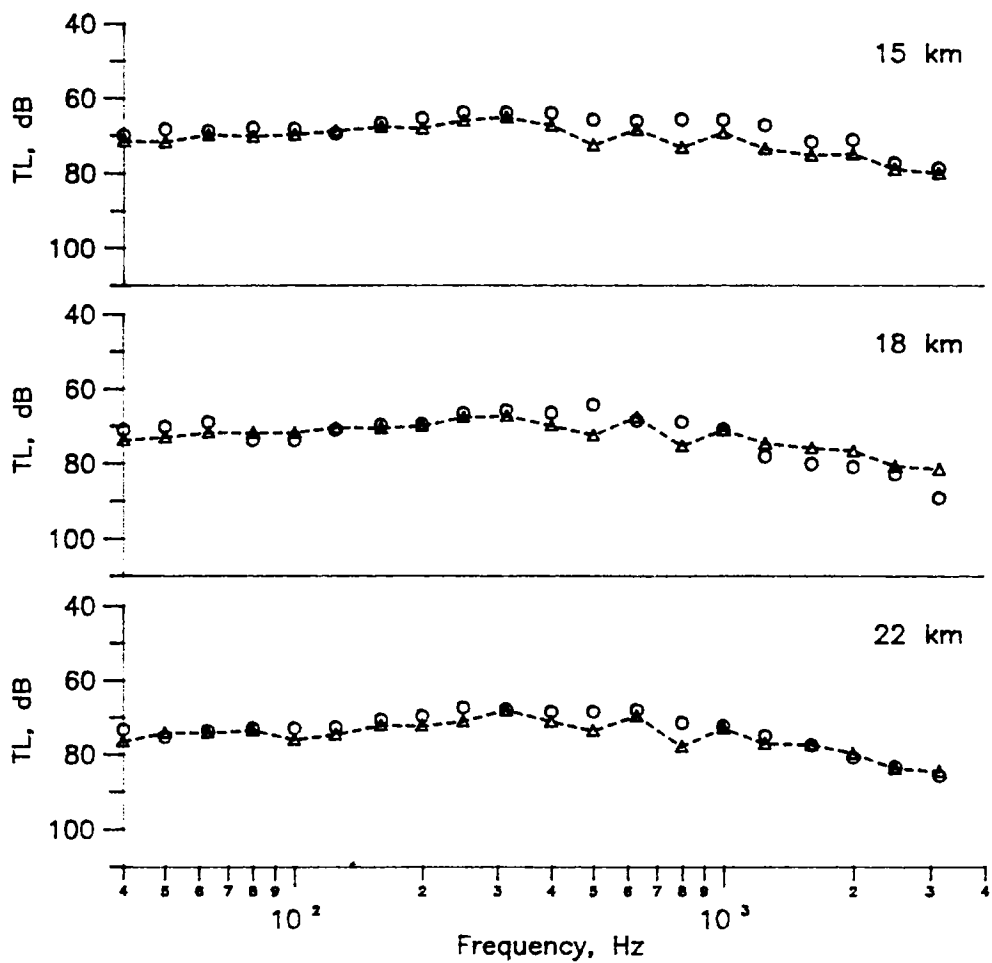
Fig. 5.11. Frequency response of the experimental location off Kochi for three ranges of 15,18, and 22 km. Receiver depth: 55 m. ---△--- Ray theory. ○ Experiment.
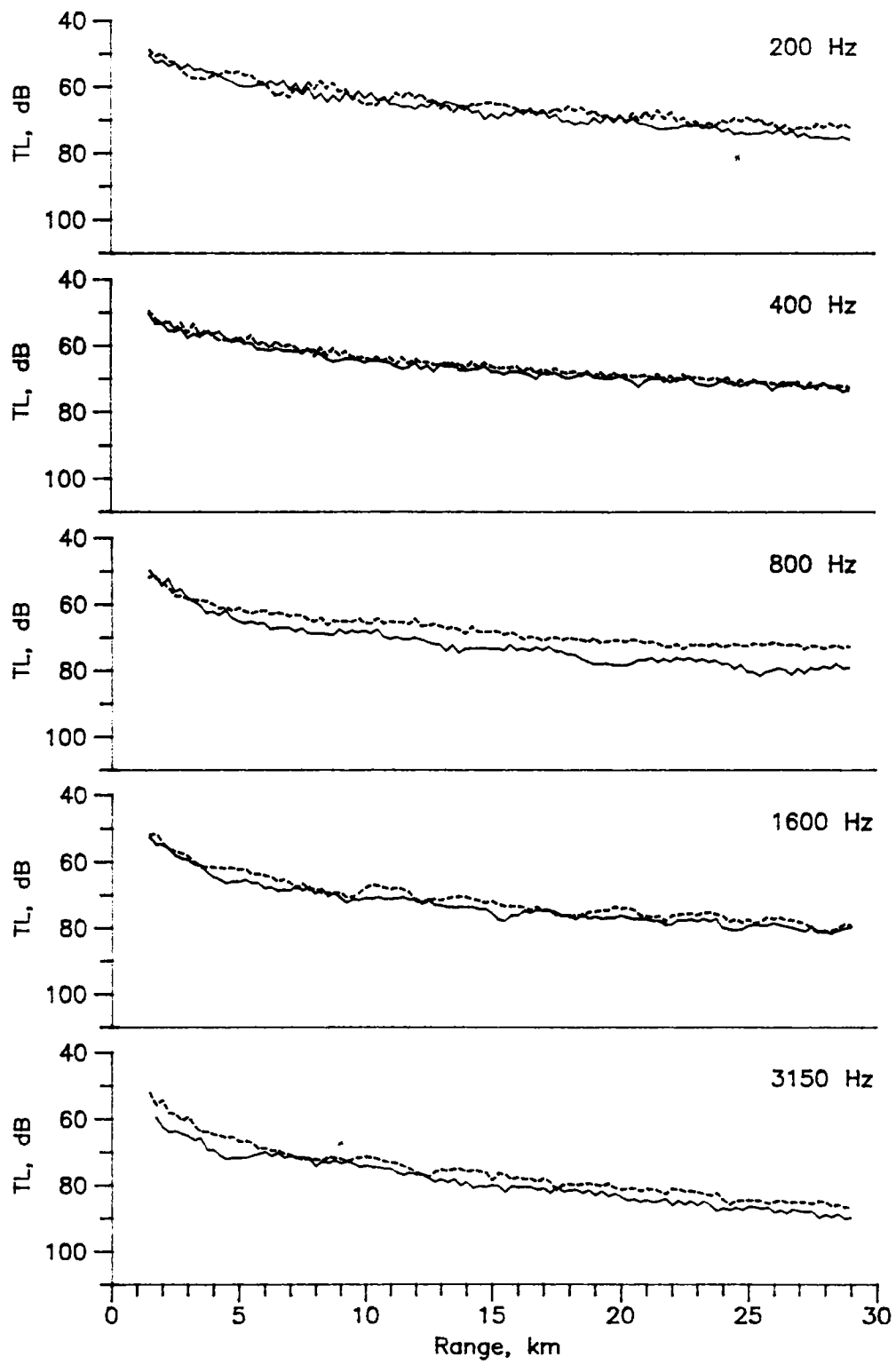
Fig. 5.12. Computed transmission loss (range-averaged) for two receiver depths (------30 m and ———55 m) and for different frequencies. Location: off Kochi.
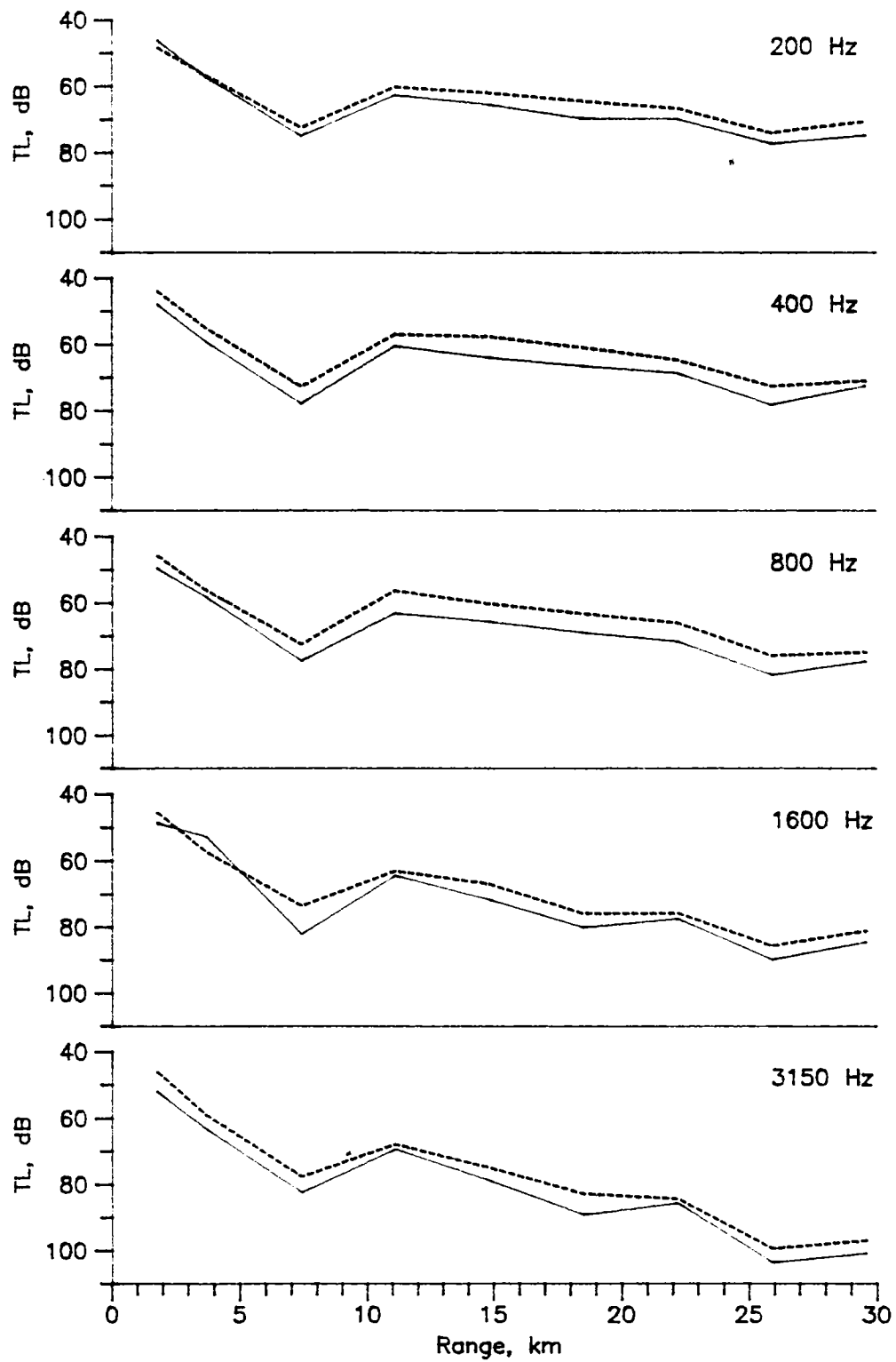
Fig. 5.13. Experimental transmission loss for two receiver depths
(-----30 m and ——55 m) and for different frequencies.
Location: off Kochi.

the comparison of experimental and theoretical frequency response of the channel at three distances from the source. In both the figures the receiver depth is 55 m.

Variation of transmission loss with range and receiver depth for five frequencies is shown in Figs 5.12 and 5.13. The two receiver depths are 30 and 55 m. Fig. 5.12 present the theoretical results and Fig. 5.13 show the experimental data.

5.4.3. Comparison for the location off Bombay

$$h_{rms}= 0.1 \text{ m} \qquad \text{SURFACE}$$

```
S *
(9 m)
                    C(z)= [Fig. 5.7(b)]
D= 82 m
                    ρ₁= 1022 kg m⁻³                    R * (45 m)

                    αw
                                                        BOTTOM
```

$C(z)=$ [Fig. 5.7(b)]

$\rho_1 = 1022$ kg m^{-3}

α_w

$$C_2 = 1850 \text{ m s}^{-1} \quad \rho_2 = 1900 \text{ kg m}^{-3} \quad \alpha_s = \begin{cases} 0.0006 \\ 0.006 \end{cases} \text{ dB m}^{-1} \text{ Hz}^{-1}$$
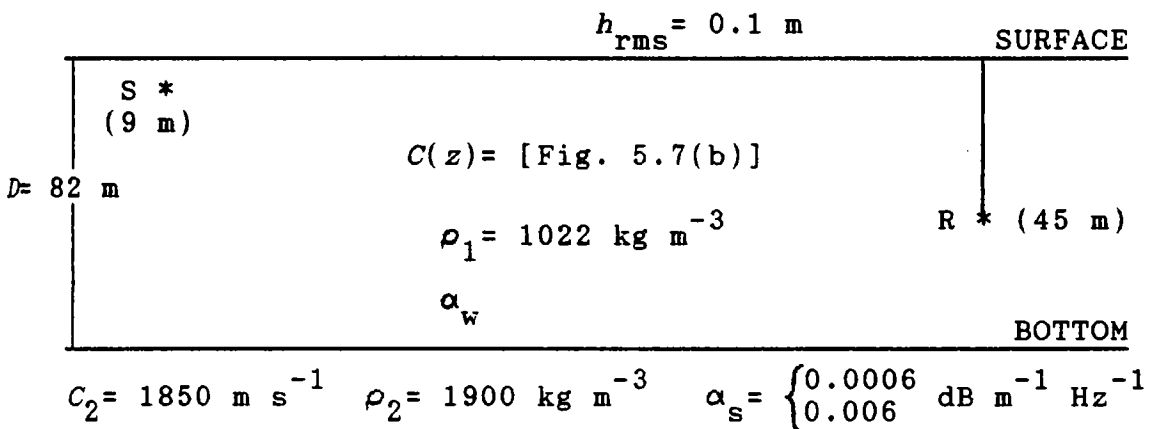
Fig. 5.14. Environmental parameters used for transmission loss computations. Location: off Bombay.

Environmental parameters used in the model computations are shown in Fig. 5.14. An rms roughness height of 0.1 m is used, corresponding to the sea state number of 1. Only one receiver depth (45 m) is considered, which is at the lower boundary of the surface duct and located approximately mid-depth in the water column.

Figs 5.15 to 5.18 show comparison of the experimental results with the model computations. Fig. 5.15 shows variation of the experimental transmission loss with range for a frequency of 200 Hz. Fig. 5.16 compares experimental and theoretical transmission loss at 500 Hz as a function of range. The theoretical results are for two values of sediment
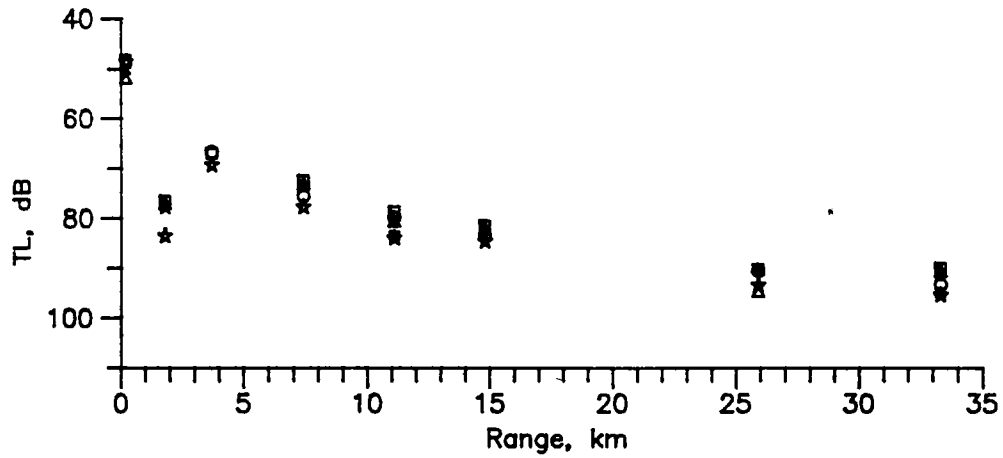
Fig. 5.15. Experimental transmission loss at 200 Hz frequency for the location off Bombay. The symbols are for receiver depths of (o)15, (□)30, (▲)45, (★)60, and (×)75 m.
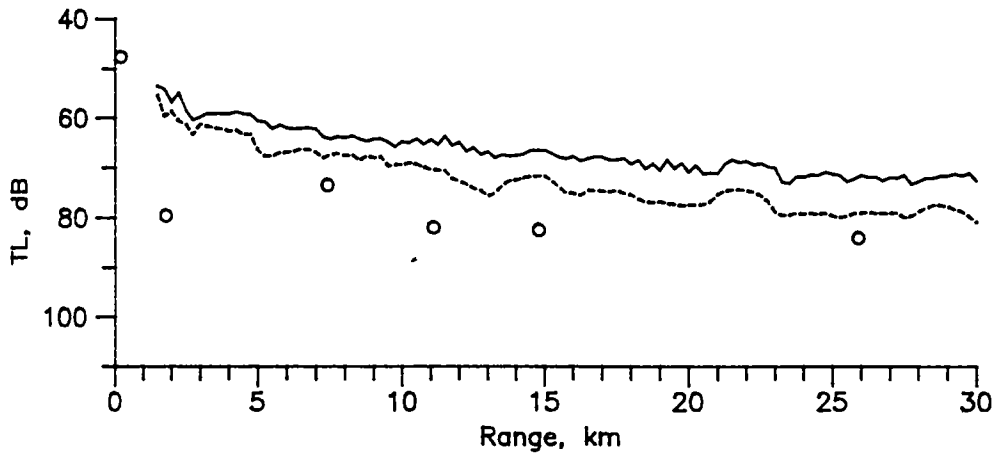
Fig. 5.16. Transmission loss versus range for 500 Hz frequency for the location off Bombay. The circles represent experimental data. The full line is for a sediment attenuation coefficient of 0.0006 dB m^{-1} Hz^{-1} and the dashed curve is for an attenuation coefficient of 0.006. Receiver depth: 45 m.
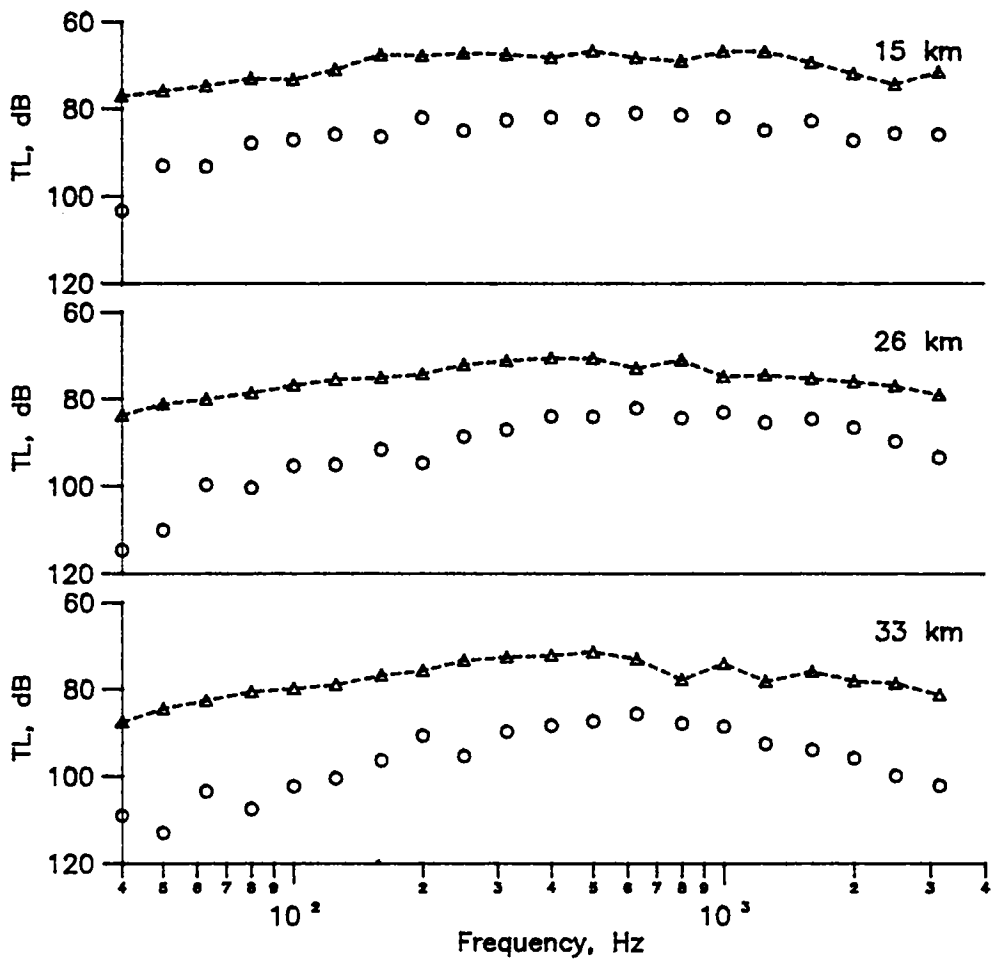
Fig. 5.17. Experimental and theoretical frequency response for the location off Bombay. Receiver depth: 45 m. The ranges are 15,26 and 33 km. ----▲--- Ray theory (compressional wave attenuation in sediment: 0.0006 dB m^{-1} Hz^{-1}).   o   Experiment.
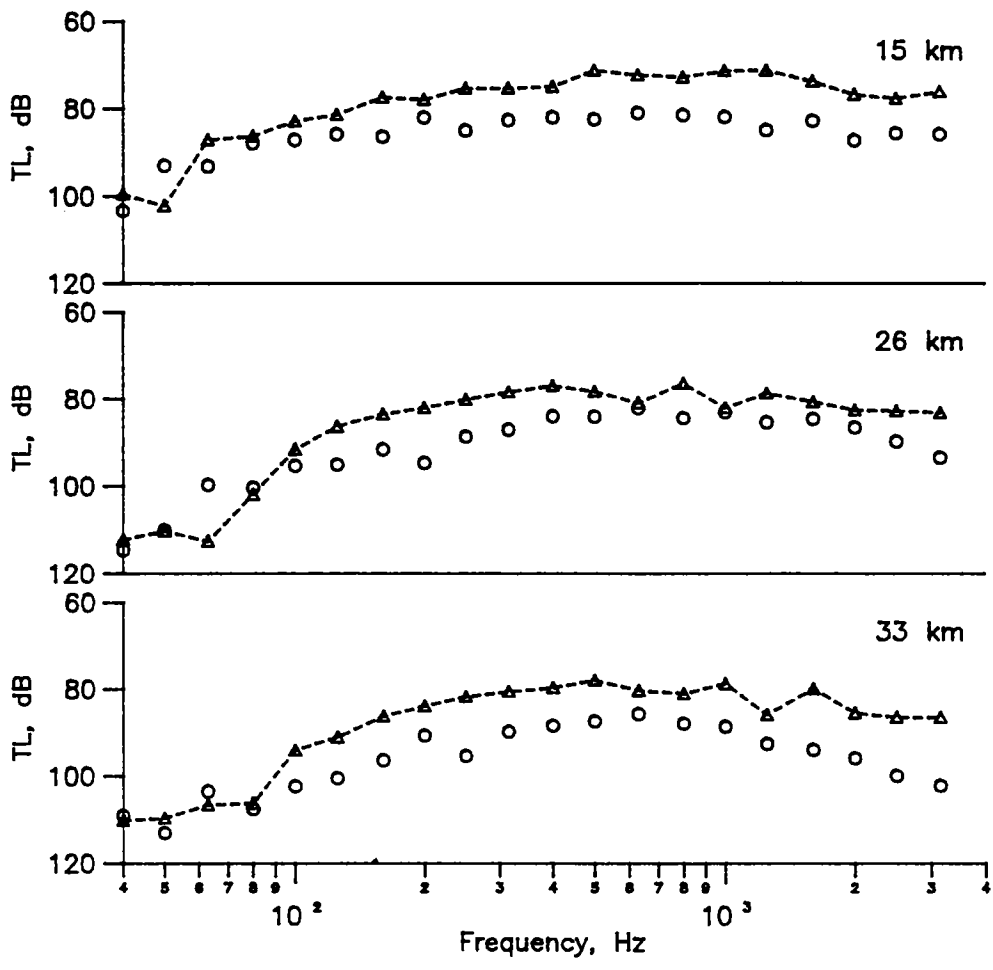
Fig. 5.18. Experimental and theoretical frequency response for the location off Bombay. Receiver depth: 45 m. The ranges are 15,26 and 33 km. ----▲--- Ray theory (compressional wave attenuation in sediment is 10 times that in Fig. 5.17).   o Experiment.

attenuation coefficient, viz., 0.0006 and 0.006 dB m^{-1} Hz^{-1}. Figs 5.17 and 5.18 compare experimental and theoretical frequency response for three distances from the source. In Fig. 5.17 the sediment attenuation is 0.0006 dB m^{-1} Hz^{-1} whereas it is 0.006 in the case of Fig. 5.18.

5.5. DISCUSSION

In general, there is good agreement of the off Kochi data with the model computations, whereas the results are not as satisfactory for the off Bombay data.

Figs 5.10 and 5.11 show variation of transmission loss with range and frequency respectively for the experimental location off Kochi. It is seen that the model is able to satisfactorily reproduce trends in the experimental data out to the maximum range of 30 km. It may be recalled that the experimental data is derived from independent single explosions for each range (Section 5.4.1.1) and that repeatability of explosive signals is generally poor. When we consider these facts and simplicity of the assumed environmental model, the agreement between theory and the experiment could be considered very good. Sediment attenuation was tuned and fixed at the value of 0.0002 dB m^{-1} kHz^{-1} before obtaining these results.

Further confirmation on efficacy of the model in predicting the transmission loss characteristics is obtained from a comparison between Figs 5.12 and 5.13. The model predicts lower transmission loss for the shallower receiver located approximately mid-depth in the channel. The experimental results also show consistently lower loss at the shallower receiver. The order of magnitude by which the losses differ between the two receivers also show good agreement.

104

Next we consider the experiment off Bombay. From the respective sound speed profiles one might infer that propagation condition was more favourable at the location off Bombay than that off Kochi (Figs 5.7 and 5.8). However, it is seen that experimental transmission loss values off Bombay are relatively high compared to those off Kochi. For example, the loss is nearly 20 dB higher at 15 km range for a frequency of 500 Hz (Figs 5.11 and 5.17). The difference is still higher at low frequencies and high losses are observed even at shorter ranges (Fig. 5.15). Losses of similar order of magnitude are observed for all the five receiver depths except in the high frequency limit where the shallow receivers show trapping by the surface duct. Compared to the off Kochi experiment, the frequency response for the location is more sharp with a well-defined optimum frequency band centred near 600 Hz.

Model computations with reasonable inputs of $h_{rms}=0.1$ m and $\alpha_s=0.0006$ dB m^{-1} Hz^{-1} (for sand) do not compare well with the experimental data (Figs 5.16 and 5.17). However, the results are encouraging since the general behaviour of transmission loss with range and frequency are acceptably modelled except for good numerical agreement. With an estimated h_{rms} of the order of 0.1 m (corresponding to the sea state number of 1), sea surface scattering alone is not sufficient to account for the observed high-frequency transmission loss. Sea bottom undulations along the propagation track (Section 5.3.2) could probably account for this loss in terms of additional scattering. However, there is no data available on bottom roughness along the propagation track. Assumption of an average roughness may not solve the problem as there could be range-variation in the roughness.

Range and/or depth dependence of the shelf geology and the presence of additional attenuation mechanisms could be the causes of increased loss at lower frequencies. For example, the shelf is relatively more variable in sediment composition and distribution compared to off Kochi and presence of gas in

the sediment is reported at some locations in the area (Murty and Pradeepkumar, 1986). There are no evidences of a shallow basement for the area or strong layering in the first few metres of the sea bottom. Neglect of shear wave generation in the sediment does not seem to be a serious omission as the high losses are not restricted to low frequencies. An arbitrarily chosen sediment attenuation coefficient of 0.006 dB m^{-1} Hz^{-1} has been somewhat successful in representing the observed low-frequency roll-off in the frequency response curve (Fig. 5.18). It is recognized that this value of the attenuation coefficient is relatively high, being ten times the upper limit of compressional attenuation normally quoted for surface sands. Our aim here is only to demonstrate the effect of a higher equivalent sea bottom attenuation, consisting of the normal compressional attenuation and the attenuation due to other mechanisms, presently of unconfirmed origin, which has not been explicitly accounted for. Probably the depth dependence of compressional speed and attenuation are to be ascertained before firm conclusions are arrived at using the results from the present model, where the sea bottom is modelled as a homogeneous sediment half-space.

Chapter 6

SUMMARY AND CONCLUSIONS

A ray theoretical model of shallow water sound propagation with practical applications has been developed and implemented. Performance of the model is evaluated by comparisons with a normal mode propagation model and also with published results from the literature. Capabilities of the model are demonstrated and limitations are discussed. The model is applied to transmission loss modelling at two coastal stations off the west coast of India and the results are discussed.

The ray theoretical approach was chosen on account of its simplicity and also the ease it offers for practical implementation on a computer without bringing-in complex mathematics. The environment is modelled as a range-independent water column with an arbitrary sound speed profile and overlying a homogeneous sea bottom. The ray computations are based on the linear segmentation approximation of the sound speed profile (Section 2.2.3). Effects of three important sound attenuation mechanisms, viz., absorption in sea water, scattering at the sea surface, and reflection at the sea bottom have been incorporated into the model in order to obtain realistic outputs. Methods employed for ray tracing, transmission loss computation, and time series simulation are presented. Potential of modified ray theory as an alternative to normal mode theory for practical computations in shallow waters is discussed.

Theoretical and empirical models for the estimation of sea surface coupled losses are presented and the respective predictions of loss are compared (Section 3.2). Distinctions between these two types of models are brought out and it is

demonstrated that use of sea state numbers for characterizing the sea surface roughness introduces considerable uncertainty in the estimated loss. The closed-form solutions for scattering loss (Marsh *et al.*, 1961; Brekhovskikh and Lysanov, 1982) agree with Kuo's model (Kuo, 1988) at small grazing angles. Kuo's model is considered to be more accurate and applicable to a wider range of environmental conditions. Compared to the closed-form solutions, this model predicts high scattering loss at larger grazing angles and wave heights. In the propagation model presented here, scattering loss is computed using the Marsh *et al.* model.

The sea bottom is modelled as a homogeneous, visco-elastic, semi-infinite half-space. Effect of shear waves in the bottom on modified ray theory is examined by deriving equations for beam displacement and by a sample computation in the case of very fine sand (Appendix 3 and Section 3.3.4.4). The following effects are observed. Bottom reflection loss increases in the presence of shear waves and this is more significant at larger grazing angles. There is a significant increase in the phase shift at grazing angles less than the critical (θ_c). The beam displacement (Δ_h) is less at low grazing angles.

One significant achievement in this study is the development and implementation of an efficient algorithm for eigen-ray finding in a range-independent environment with an arbitrary sound speed profile (Section 4.2). Compared to other available implementations, the present algorithm can be extended to model propagation in range-dependent environments.

Performance of the propagation model is assessed by comparison with a normal mode model and also with results available from published literature. Comparisons of the computed sound field show that the results are in good agreement with normal mode theory in the absence of beam displacement caustics (Section 4.4.1). Major features of the

field are modelled satisfactorily even in the presence of relatively strong caustics, except in their near vicinity and at very low frequencies. It is also noted that compressional attenuation in common sediments overlying the continental shelves (mostly sandy sediments) are sufficiently high to suppress the formation of strong beam displacement caustics in ray theory modelling, if attenuation is included in the calculation of beam displacement.

At sufficiently low frequencies where there is only one propagating mode, the model fails in accurately reproducing the field behaviour versus range. This is not an unexpected result, but even in this case the average pressure levels agree with mode theory, provided that strong caustics are not present. This result is relevant because, in most practical problems requiring transmission loss modelling, it is the average rather than the coherent field that is of interest. Thus, in the model versus experimental data presented in this study (Chapter 5), the model results are averaged values obtained by employing a fixed-width range-window averaging.

The model is also used for simulation of monochromatic pulse transmission (Section 4.4.2). Time-series simulations using the present model are shown to be in good agreement with similar results from published literature. Modal structure of the sound field is also modelled satisfactorily. These results confirm that the model is fairly accurate in its basic computations of eigen-ray amplitudes, phases, and travel times.

Experimental methods for at-sea transmission loss estimation are outlined in Chapter 5 (Section 5.1). Details of two such experiments on the western continental shelf of India are presented and corresponding transmission loss estimates are compared with computations using the present model. These comparisons, between band-averaged experimental data and single-frequency results from the deterministic model, are

justified based on several arguments and example computations (Section 5.2). Relevant points regarding the model/data comparisons are discussed (Section 5.4.1). The comparisons between experimental and theoretical frequency responses are better indicators of the model performance than those showing variation of transmission loss with range. Effect of shear waves on the range-averaged (incoherent) shallow-water transmission loss is seen to be negligible for the case of a homogeneous sediment bottom.

Compressional attenuation in the sediment is a critical model input with significant control over the computed transmission loss. As estimates or measurements of the attenuation coefficient for both the experimental locations are not available, results from literature are used as guide-lines in this regard. For both the locations we tried to tune the sediment attenuation coefficient in order to get better agreement between the experimental data and model results. We were successful in this regard for the data off Kochi, where an attenuation of 0.0002 dB m^{-1} Hz^{-1} in the sediment was found to be satisfactory for explaining the experimentally observed transmission loss characteristics (Section 5.4.2).

Experimental transmission loss values are relatively high for the location off Bombay. No realistic amount of sediment attenuation (as per the literature) could model this high loss (Section 5.4.3). However, trends in the experimental data are acceptably modelled. Sea bottom in the middle shelf region off Bombay is relatively rough. Also, the shelf is more variable in the sediment types and their distribution compared to that off Kochi (Section 5.3.2). Bottom shear wave effects, if any, alone is not sufficient to explain the observed losses as the high losses are not limited to low frequencies. Further, there are no evidences of a shallow basement for the area. Hence the high losses are attributed to range and/or depth variability of the bottom, both in roughness and composition. It is shown

110

that a high value of (equivalent) compressional attenuation in the sediment (of presently unconfirmed origin) could satisfactorily model the observed low-frequency roll-off in the frequency response of the channel. Range/depth dependence of sediment properties are not taken into account in the present model. Therefore more studies are 'required to be carried out before firm conclusions might be arrived at regarding exact causes for the high losses.

As pointed out in the above paragraph, one of the limitations of the present model is its inability to take into account depth dependence of sediment characteristics. This can be rectified by incorporating a more sophisticated model of the sea bottom in place of the present homogeneous half-space model. Another limitation is that certain wave theory effects like frequency response of a surface duct or diffraction phenomena are not accounted for. Thus, interpretation of low-frequency modelling requires caution in certain cases- for example, if the source and receiver are within a surface duct and the frequency is near to or below the duct cut-off frequency. This is a limitation imposed by the basic ray theoretical approach where the frequency dependent modal cut-off for the duct is not reflected. Obviously, this limitation vanishes at sufficiently high frequencies. And as demonstrated by the results in Chapter 5, the model provides useful results for other source/receiver configurations where SRBR rays are dominant. Caustic corrections were not attempted in the present study. Hence another condition that may lead to anomalous results is the occurrence of refraction caustics, for example in the presence of a strong thermocline, though the average results may be satisfactory for many practical applications.

Regarding modelling of more complex environments, it is easier to incorporate certain amount of range-dependence into the present model, for example, in the form of variable sediment characteristics. With appropriate modifications in

the eigen-ray finding algorithm, range-variations in the bottom slope or sound speed profile can be taken care of. This is not a difficult task in the present case as the algorithm has been formulated in a more general way, rather than exclusively for a range-independent environment.

Simple deterministic modelling of sound propagation as presented here necessarily involves several simplifying assumptions regarding the environment. But we do have vast areas of the shallow sea where such approximations are valid, and where a simple model might be applied with success as demonstrated in this study.

FRANCOIS-GARRISON EQUATION FOR SOUND ABSORPTION IN SEA WATER
(Francois and Garrison, 1982b)

$$\begin{array}{ccccc} \text{Total} \\ \text{Absorption} \end{array} = \begin{array}{c} \text{Boric acid} \\ \text{contribution} \end{array} + \begin{array}{c} \text{Magnesium sulphate} \\ \text{contribution} \end{array} + \begin{array}{c} \text{Pure water} \\ \text{contribution} \end{array}$$

$$\alpha_w = \frac{A_1 P_1 f_1 f^2}{f^2 + f_1^2} + \frac{A_2 P_2 f_2 f^2}{f^2 + f_2^2} + A_3 P_3 f^2$$

for frequency f in kHz, α is in dB km^{-1}.

Boric acid contribution

$$A_1 = \frac{8.86}{C} \times 10^{(0.78 pH - 5)} \qquad\qquad \text{dB km}^{-1} \text{ kHz}^{-1}$$

$$P_1 = 1$$

$$f_1 = 2.8 \ (S/35)^{0.5} \ 10^{(4 - 1245/\theta)} \qquad\qquad \text{kHz}$$

where C is the sound speed in m s^{-1}, given approximately by
$C = 1412 + 3.21 T + 1.19 S + 0.0167 D$,
T is the temperature ($^\circ$C), $\theta = 273 + T$, S is the salinity (ppt),
pH is the pH value of the sea water, and D is the depth (m).

Magnesium sulphate contribution

$$A_2 = 21.44 \frac{S}{C} (1 + 0.025 T) \qquad\qquad \text{dB km}^{-1} \text{ kHz}^{-1}$$

$$P_2 = 1 - 1.37 \times 10^{-4} \ D + 6.2 \times 10^{-9} \ D^2$$

$$f_2 = \frac{8.17 \times 10^{(8 - 1990/\theta)}}{1 + 0.0018(S - 35)} \qquad\qquad \text{kHz}$$

Pure water contribution

For $T \leq 20^\circ$C,

$$A_3 = 4.937 \times 10^{-4} - 2.59 \times 10^{-5} \ T + 9.11 \times 10^{-7} \ T^2$$
$$- 1.50 \times 10^{-8} \ T^3 \qquad\qquad \text{dB km}^{-1} \text{ kHz}^{-1}$$

For $T > 20^\circ$C,

$$A_3 = 3.964 \times 10^{-4} - 1.146 \times 10^{-5} \ T + 1.45 \times 10^{-7} \ T^2$$
$$- 6.5 \times 10^{-10} \ T^3 \qquad\qquad \text{dB km}^{-1} \text{ kHz}^{-1}$$

$$P_3 = 1 - 3.83 \times 10^{-5} \ D + 4.9 \times 10^{-10} \ D^2$$

Appendix 2

CHARACTERIZATION OF THE SEA SURFACE ROUGHNESS

A commonly used statistical parameter in describing the sea surface spectrum is the *significant wave height* ($H_{1/3}$). It is defined as the average of the heights (crest-to-trough) of the one-third highest waves in a sequence of waves observed at a point (Sverdrup and Munk, 1947). Two other parameters of interest are the *average trough-to-crest wave height* (H_{av}) and the *rms displacement* (h_{rms}) about the mean sea surface. h_{rms} is synonymous with the term *rms roughness height* used in literature on sea surface scattering (Urick, 1982).

The term *fully developed sea* or *fully arisen sea* is used to describe the sea whose wave spectrum contains components of all frequencies ($0 \leq f < \infty$), each with the maximum energy of which it is capable, under a given wind speed. In other words, in a fully developed sea, an equilibrium exists between the transfer of energy from the steady wind to the sea and the dissipation of wave energy through wave breaking and turbulence. This happens when there is no limitation on the fetch (the area over which the wind blows) and duration of the wind. The frequency spectrum for wind waves in a fully developed sea can be completely described in terms of the wind speed. Such a spectrum was proposed by Neumann and Pierson (1957). Pierson and Moskowitz (1964) proposed a more update spectrum. Using the relationship $\omega^2 = gk$ (where ω= angular frequency, k= wave number and g= acceleration due to gravity) for deep water waves, the frequency spectrum can be converted into a wave number spectrum and a relation between wave height and the wind speed can be arrived at.

Some useful inter-relations among different wave height parameters for a Neumann-Pierson (NP) spectrum are given below (Eller, 1985; Kuo, 1988):

$$H_{1/3} = 1.60 \ H_{av}$$
$$H_{1/3} = 4.02 \ h_{rms}$$
$$H_{av} = 2.503 \ h_{rms}$$
$$H_{av} = 0.625 \ H_{1/3}$$
$$h_{rms} = 0.25 \ H_{1/3}$$
$$h_{rms} = 0.399 \ H_{av}$$

(1)

According to Schulkin and Shaffer (1964), if NP spectrum is employed, the relation between H_{av} and the wind speed w measured at a height of 10 m above the sea surface can be written as

$$H_{av} = 2.6 \times 10^{-3} \ w^{2.5} \text{ ft, where } w \text{ is in knots.} \tag{2}$$

Using the conversion factors 1 knot= 0.51 m s^{-1} and 1 ft= 0.3048 m, this can be rewritten as

$$H_{av} = 4.266 \times 10^{-3} \ w^{2.5} \text{ m, where } w \text{ is in m s}^{-1}. \tag{3}$$

Kuo (1988) gives the relation

$$h_{rms} = 1.77 \times 10^{-3} \ w^{2.5} \text{ m, where } w \text{ is in m s}^{-1}. \tag{4}$$

Using the conversion factor $H_{av} = 2.503 \ h_{rms}$,

$$H_{av} = 4.430 \times 10^{-3} \ w^{2.5} \text{ m} \tag{5}$$

or $H_{av} = 2.763 \times 10^{-3} \ w^{2.5}$ ft, where w is in knots (6)

The wave spectrum at any given observation point is a composite picture of waves locally generated by the prevailing wind and those coming from adjacent disturbances, if any, which may have different directions and amplitudes. The expressions given above are valid for a sea fully arisen under the influence of local phenomena alone. On many occasions the sea surface is not fully developed or the spectrum is

Sea surface Description	Sea state	Wind speed		$H_{1/3}$ m (ft)	
		Beau-fort scale	Range m s^{-1} (knots)	For 12h wind	Fully arisen sea
Mirror-like	0	0	<0.5 (< 1)		
Ripples		1	0.5- 1.7 (1- 3)		
Small wavelets	1	2	1.8- 3.3 (4- 6)	<0.3 (<1)	<0.3 (<1)
Large wavelets, Scattered white-caps	2	3	3.4- 5.4 (7-10)	0.3- 0.61 (1- 2)	0.3 - 0.61 (1 - 2)
Small waves, frequent white-caps	3	4	5.5- 8.4 (11-16)	0.61- 1.5 (2 - 5)	0.61- 1.8 (2 - 6)
Moderate waves, many whitecaps	4	5	8.5-11.1 (17-21)	1.50- 2.4 (5 - 8)	1.80- 3.0 (6 - 10)
Large waves, whitecaps every-where, spray	5	6	11.2-14.1 (22-27)	2.4 - 3.7 (8 - 12)	3.0 - 5.2 (10 - 17)
Heaped-up sea, blown spray, streaks	6	7	14.2-17.2 (28-33)	3.7 - 5.2 (12 - 17)	5.2 - 7.9 (17 - 26)
Moderately high, long waves, spindrift	7	8	17.3-20.8 (34-40)	5.2 - 7.3 (17 - 24)	7.9 -11.9 (26 - 39)

Table 1. Approximate relation between scales of wind speed, wave height, and sea state (*after* Wenz, 1962)

influenced by far-away disturbances. Either direct measurements of wave characteristics or suitable hindcasting/forecasting techniques are required for a satisfactory representation of the wave spectrum.

A commonly employed method of . sea surface characterization is the visual estimation of the *sea state* (Table 1). Sea state is a number corresponding to a range of visually estimated average wave heights (approximately equal to $H_{1/3}$). Visual estimation of sea state is used when direct wave recording is not possible or available. There are no fractional sea states defined; and another difficulty with this type of description is that even experienced observers on board ship sometimes differ in sea state estimates by one or two numbers. Ideally, one should know the surface wave spectrum for a complete description of the sea state.

Appendix 3

DERIVATION OF THE EXPRESSIONS FOR COMPUTING BEAM DISPLACEMENT ON REFLECTION FROM A LOSSY SEA BOTTOM THAT CAN SUSTAIN SHEAR

Eller and Gershfeld (1985) gives an expression for the complex reflection coefficient R for plane waves between two homogeneous fluid media, when the lower medium is lossy and can support shear:

$$Re^{i\psi} = \frac{P + i(1-S)Q}{P - i(1+S)Q} \tag{1}$$

where

$$P = (\rho_2/\rho_1)\sin\theta \left[1 - 2(\beta_2/C_1)^2 \cos^2\theta\right]^2 \tag{2}$$

$$Q = \left[\cos^2\theta - (C_1/C_2)^2\right]^{1/2} \tag{3}$$

and

$$S = 4(\rho_2/\rho_1)(\beta_2/C_1)^3 \sin\theta \cos^2\theta \left[1 - (\beta_2/C_1)^2 \cos^2\theta\right]^{1/2} \tag{4}$$
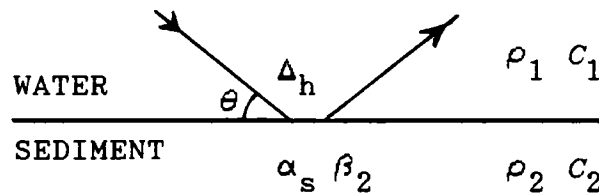
Fig. 1. Diagram showing the geometry of reflection at a semi-infinite, lossy sediment half-space. The symbols are explained below.

The geometry of reflection including beam displacement is shown in Fig. 1.

θ = grazing angle of incidence

ρ_1, ρ_2 = water and sediment densities

C_1, C_2 = water and sediment sound speeds

α_s = compressional wave attenuation coefficient

β_2 = shear wave speed

Δ_h = beam displacement

118

Sound speed in the lower medium is treated as a complex number such that plane wave absorption coefficient is proportional to frequency f. Thus, C_2 is replaced as indicated in the expression

$$1/C_2 \longrightarrow (1/C_2) - i\left[\frac{0.1151}{2\pi}\right]\alpha_s \qquad . \qquad (5)$$

where α_s is the absorption coefficient in dB m^{-1} Hz^{-1}. With this generalization of C_2, the quantity Q in Eq. 3 becomes complex.

Beam displacement Δ_h is given by

$$\Delta_h = \frac{\partial \psi}{\partial k} \text{ where } k = (\omega/C_1) \cos\theta \qquad (6)$$

In the above equation

$$\frac{\partial \psi}{\partial k} = \frac{\partial \psi}{\partial \theta} \frac{\partial \theta}{\partial k}$$

$$= \frac{\partial \psi}{\partial \theta}\left[\frac{-\lambda}{2\pi \sin\theta}\right], \text{ because } \frac{\partial k}{\partial \theta} = -\left[\frac{2\pi \sin\theta}{\lambda}\right] \qquad (7)$$

Therefore,

$$\Delta_h = \frac{\partial \psi}{\partial \theta}\left[\frac{\lambda}{2\pi \sin\theta}\right] \qquad (8)$$

Expressions for ψ and $\partial\psi/\partial\theta$

Phase change on reflection $\psi = \tan^{-1}\left[\text{Im}(\text{Eq. 1})/\text{Re}(\text{Eq. 1})\right]$ (9) where Im and Re represent the real and imaginary parts.

Let $Q = Q_1 + iQ_2$ in Eq. 1. Then,

$$R = \frac{P + i(1-S)(Q_1 + iQ_2)}{P - i(1+S)(Q_1 + iQ_2)} = \frac{P + iQ_1 - iQ_1 S - Q_2 + SQ_2}{P - iQ_1 - iQ_1 S + Q_2 + SQ_2}$$

$$= \frac{A + iQ_1(1-S)}{B - iQ_1(1+S)}, \text{ where } A = (P + SQ_2 - Q_2) \text{ and } B = (P + SQ_2 + Q_2)$$

Thus

$$R= \left[\frac{AB-Q_1^{\,2}(1-S^2)}{B^2+Q_1^{\,2}(1+S)^2} \right] + i \left[\frac{Q_1\left[B(1-S)+A(1+S)\right]}{B^2+Q_1^{\,2}(1+S)^2} \right] \qquad (10)$$

The phase change on reflection ψ is given by

$$\psi= \tan^{-1} \left[\frac{Q_1\left[B(1-S)+A(1+S)\right]}{AB-Q_1^{\,2}(1-S^2)} \right]$$

$$\psi= \tan^{-1} \left[\frac{2PQ_1}{(P+SQ_2)^2-Q_2^{\,2}-Q_1^{\,2}(1-S^2)} \right] \qquad (11)$$

$$\partial\psi/\partial\theta = \left[\frac{1}{1+u^2} \right] \partial u/\partial\theta \qquad (12)$$

where $u= \left[\dfrac{2PQ_1}{(P+SQ_2)^2-Q_2^{\,2}-Q_1^{\,2}(1-S^2)} \right]$

Let $aNr= 2PQ_1$ and $aDr= (P+SQ_2)^2-Q_2^{\,2}-Q_1^{\,2}(1-S^2)$ so that $u= aNr/aDr$. Then,

$$\partial u/\partial\theta = \frac{\partial}{\partial\theta}(aNr/aDr)= \frac{aDr\,\frac{\partial}{\partial\theta}(aNr) - aNr\,\frac{\partial}{\partial\theta}(aDr)}{aDr^2} \qquad (13)$$

where

$$\frac{\partial}{\partial\theta}(aNr)= \frac{\partial}{\partial\theta}(2PQ_1)= 2\left[P\frac{\partial}{\partial\theta}(Q_1)+ Q_1\frac{\partial}{\partial\theta}(P) \right] \qquad (14)$$

and

$$\frac{\partial}{\partial\theta}(aDr)= \frac{\partial}{\partial\theta}\left[(P+SQ_2)^2-Q_2^{\,2}-Q_1^{\,2}(1-S^2) \right]$$

$$= 2\left[P+SQ_2 \right]\left[\frac{\partial}{\partial\theta}(P)+ S\frac{\partial}{\partial\theta}(Q_2)+ Q_2\frac{\partial}{\partial\theta}(S) \right]- \left[2Q_2\frac{\partial}{\partial\theta}(Q_2) \right]-$$

$$\left[Q_1^{\,2}(-2S\frac{\partial}{\partial\theta}(S)+ (1-S^2)2Q_1\frac{\partial}{\partial\theta}(Q_1) \right] \qquad (15)$$

Eq. 13 can be evaluated knowing $\frac{\partial}{\partial\theta}(P),\frac{\partial}{\partial\theta}(S),\frac{\partial}{\partial\theta}(Q_1)$ and $\frac{\partial}{\partial\theta}(Q_2)$.

Expression for $\frac{\partial}{\partial\theta}(P)$

$$\frac{\partial}{\partial\theta}(P) = \frac{\partial}{\partial\theta}\left\{ \frac{\rho_2}{\rho_1}\sin\theta \left[1-2\left(\frac{\beta_2}{C_1}\right)^2\cos^2\theta\right]^2 \right\}$$

$$= \frac{\rho_2}{\rho_1}\left\{ 8\left(\frac{\beta_2}{C_1}\right)^2\left[1-2\left(\frac{\beta_2}{C_1}\right)^2\cos^2\theta\right]\sin^2\theta\cos\theta + \right.$$

$$\left. \left[1-2\left(\frac{\beta_2}{C_1}\right)^2\cos^2\theta\right]^2\cos\theta \right\} \qquad (16)$$

Expression for $\frac{\partial}{\partial\theta}(S)$

$$\frac{\partial}{\partial\theta}(S) = \frac{\partial}{\partial\theta}\left\{ 4\frac{\rho_2}{\rho_1}\left(\frac{\beta_2}{C_1}\right)\sin\theta\cos^2\theta\left[1-\left(\frac{\beta_2}{C_1}\right)^2\cos^2\theta\right]^{1/2} \right\}$$

$$= 4\frac{\rho_2}{\rho_1}\left(\frac{\beta_2}{C_1}\right)^3\left\{ \left(\frac{\beta_2}{C_1}\right)^2\left[1-\left(\frac{\beta_2}{C_1}\right)^2\cos^2\theta\right]^{-1/2}\sin^2\theta\cos^3\theta + \right.$$

$$\left. \left[1-\left(\frac{\beta_2}{C_1}\right)^2\cos^2\theta\right]^{1/2}\left[\cos^3\theta - 2\sin^2\theta\cos\theta\right] \right\} \qquad (17)$$

Expressions for Q_1 and Q_2

$$Q = \left\{\cos^2\theta - (C_1/C_2)^2\right\}^{1/2} = Q_1 + iQ_2$$

With $1/C_2 \longrightarrow (1/C_2) - i\alpha$ where α is in neper m^{-1},

$$Q = \left\{\cos^2\theta - C_1^2\left[(1/C_2)-i\alpha\right]^2\right\}^{1/2}$$

$$= \left\{ \left[\cos^2\theta - (C_1/C_2)^2 + C_1^2\alpha^2\right] + i\left[2\alpha C_1^2/C_2\right] \right\}^{1/2}$$

$$= \left[r\,e^{i\phi}\right]^{1/2} = r^{1/2}\left[\cos\frac{\phi}{2} + i\sin\frac{\phi}{2}\right]$$

$$= r^{1/2}\cos \frac{\phi}{2} + i \ r^{1/2}\sin \frac{\phi}{2} \tag{18}$$

where

$$r= \sqrt{\left[\cos^2 \theta - (C_1/C_2)^2 + C_1^2\alpha^2\right]^2 + \left[2\alpha C_1^2/C_2\right]^2} \tag{19}$$

$$\phi= \tan^{-1}\left\{\frac{2\alpha C_1^2/C_2}{\cos^2 \theta - (C_1/C_2)^2 + C_1^2\alpha^2}\right\} \tag{20}$$

Hence $Q_1= \left[r^{1/2}\cos \frac{\phi}{2}\right]$ and $Q_2= \left[r^{1/2}\sin \frac{\phi}{2}\right]$ can be evaluated.

Expressions for $\frac{\partial}{\partial \theta}(Q_1)$ and $\frac{\partial}{\partial \theta}(Q_2)$

$$\frac{\partial}{\partial \theta}(Q_1)= r^{1/2} \frac{\partial}{\partial \theta}\left[\cos \frac{\phi}{2}\right] + \cos \frac{\phi}{2} \frac{\partial}{\partial \theta}\left[r^{1/2}\right] \tag{21}$$

where

$$\frac{\partial}{\partial \theta}\left[\cos \frac{\phi}{2}\right]= -\sin \left[\frac{1}{2} \tan^{-1}\left\{\frac{2\alpha C_1^2/C_2}{\cos^2 \theta - (C_1/C_2)^2 + C_1^2\alpha^2}\right\}\right]$$
$$\frac{1}{2}\left\{\frac{1}{1+\tan^2 \phi}\right\} \left\{\frac{-2\alpha C_1^2/C_2 \cdot 2\cos \theta \cdot (-\sin \theta)}{\left[\cos^2 \theta - (C_1/C_2)^2 + C_1^2\alpha^2\right]^2}\right\} \tag{22}$$

and

$$\frac{\partial}{\partial \theta}\left[r^{1/2}\right]= \frac{\partial}{\partial \theta}\left[\left[\cos^2 \theta - (C_1/C_2)^2 + C_1^2\alpha^2\right]^2 + \left[2\alpha C_1^2/C_2\right]^2\right]^{1/4}$$

$$= \frac{1}{4}\left[\left[\cos^2 \theta - (C_1/C_2)^2 + C_1^2\alpha^2\right]^2 + \left[2\alpha C_1^2/C_2\right]^2\right]^{-3/4}$$

$$\frac{\partial}{\partial \theta}\left[\left[\cos^2 \theta - (C_1/C_2)^2 + C_1^2\alpha^2\right]^2 + \left[2\alpha C_1^2/C_2\right]^2\right]$$

$$= \frac{1}{4}\left[\left[\cos^2 \theta - (C_1/C_2)^2 + C_1^2\alpha^2\right]^2 + \left[2\alpha C_1^2/C_2\right]^2\right]^{-3/4}$$

$$\left[4\cos^3 \theta (-\sin \theta) + 2\left(C_1^2\alpha^2 - (C_1/C_2)^2\right) 2\cos \theta (-\sin \theta)\right] \tag{23}$$

122

$$\frac{\partial}{\partial \theta}(Q_2) = r^{1/2} \frac{\partial}{\partial \theta}\left[\sin \frac{\phi}{2}\right] + \sin \frac{\phi}{2} \frac{\partial}{\partial \theta}\left[r^{1/2}\right] \tag{24}$$

where

$$\frac{\partial}{\partial \theta}\left[\sin \frac{\phi}{2}\right] = \cos\left[\frac{1}{2}\tan^{-1}\left\{\frac{2\alpha C_1^2/C_2}{\cos^2\theta - (C_1/C_2)^2 + C_1^2\alpha^2}\right\}\right]$$
$$\frac{1}{2}\left\{\frac{1}{1+\tan^2\phi}\right\}\left\{\frac{-2\alpha C_1^2/C_2 \cdot 2\cos\theta \cdot (-\sin\theta)}{\left[\cos^2\theta - (C_1/C_2)^2 + C_1^2\alpha^2\right]^2}\right\} \tag{25}$$

BIBLIOGRAPHY

Akal, T. (1980) Sea floor effects on shallow water acoustic propagation. In *Bottom-interacting ocean acoustics*, W.A. Kuperman and F.B. Jensen (Ed.), Plenum, New York

Anand, G.V. and K.V. Avudainayagam (1989) Modified three dimensional ray theory of acoustic propagation in a wedge-shaped ocean. J. Acoust. Soc. Ind., XVII, 230

Anand, G.V. and P. Balasubramanian (1983) *Modified ray theory of underwater acoustic propagation in isovelocity ocean with a sloping bottom. Part-I: Downslope propagation.* STICS Report 22, Indian Institute of Science, Bangalore

Arons, A.B. (1954) Underwater explosion shock wave parameters at large distances from the charge. J. Acoust. Soc. Am., 26, 343

Arons, A.B., J.P. Slifko, and A. Carter (1948) Secondary pressure pulses due to gas globe oscillations in underwater explosions. J. Acoust. Soc. Am., 20, 271

Baker, W.F. (1975) New formula for calculating acoustic propagation loss in a surface duct in the sea. J. Acoust. Soc. Am., 57, 1198

Balasubramanian, P. (1989) A ray theoretical sound propagation model for a range-independent ocean with arbitrary sound speed profile. J. Acoust. Soc. Ind., XVII, 211

Balasubramanian, P. and M.M. Muni (1990a) A transmission loss model based on the exact effective depth of a Pekeris ocean waveguide including shear wave effects. J. Acoust. Soc. Ind., XVIII, 88

Balasubramanian, P. and M.M. Muni (1990b) A note on "The effective depth of a Pekeris ocean waveguide, including shearwave effects" [Chapman et al., J. Acoust. Soc. Am., 85, 648-653 (1989)]. J. Acoust. Soc. Am., 88, 564

Balasubramanian, P. and K.G. Radhakrishnan (1989) *Implementation of a range dependent transmission loss model based on parabolic equation method*. Departmental report No. RR-13/89, Naval Physical and Oceanographic Laboratory, Kochi

Balasubramanian, P. and K.G. Radhakrishnan (1990) PE:IFD model versus off Cochin experimental data. J. Acoust. Soc. Ind., XVIII, 78

Bannister, R.W., D.G. Browning, and R.N. Denham (1974) The effect of seamounts on SOFAR channel propagation. J. Acoust. Soc. Am., 55, 417

Bannister, R.W., R.N. Denham, K.M. Guthrie, and D.G. Browning (1977) Project TASMAN TWO: Low-frequency propagation measurements in the South Tasman Sea. J. Acoust. Soc. Am., 62, 847

Barnard, G.R. and R.L. Deavenport (1978) Propagation of sound in underwater surface channels with rough boundaries. J. Acoust. Soc. Am., 63, 709

Bartberger, C.L. (1978) *PLRAY- A ray propagation loss program*. Nav. Air. Dev. Ctr., Rept. No. NADC-77296-30

Baxter, L., R. Brockhurst, and E.E. Hays (1964) Some deep-water sound-transmission paths south of Cyprus. J. Acoust. Soc. Am., 2124

Baxter, L. and M.H. Orr (1982) Fluctuations in sound transmission through internal waves associated with the

thermocline: A computer model for acoustic transmission through sound velocity fields calculated from thermistor chain, CTD, XBT, and acoustic backscattering. _J. Acoust. Soc. Am._, _71_, 61

Beebe, J.H. and C.W. Holland (1986) Shallow water propagation effects over a complex, high velocity bottom. _J. Acoust. Soc. Am._, _80_, 244

Beebe, J.H., S.T. McDaniel, and L.A. Rubano (1982) Shallow-water transmission loss prediction using the Biot sediment model. _J. Acoust. Soc. Am._, _71_, 1417

Biot, M.A. (1956a) Theory of propagation of elastic waves in a fluid-saturated porous solid. I. Low-frequency range. _J. Acoust. Soc. Am._, _28_, 168

Biot, M.A. (1956b) Theory of propagation of elastic waves in a fluid-saturated porous solid. II. Higher-frequency range. _J. Acoust. Soc. Am._, _28_, 179

Bjorno, L. (1977) Finite-amplitude wave propagation through water-saturated marine sediments. _Acustica_, _38_, 195

Blatstein, I.M. (1971) Calculations of underwater explosion pulses at caustics. _J. Acoust. Soc. Am._, _49_, 1568

Blatstein, I.M. (1972) Comparison of ray theory and modified ray theory near a convergence zone caustic. _J. Acoust. Soc. Am._, _52_, 1060

Brekhovskikh, L.M. (1960) _Waves in layered media_. Academic Press, New York

Brekhovskikh, L.M. (1980) _Waves in layered media_. 2nd Edition, Academic Press, New York

Brekhovskikh, L.M. and Y. Lysanov (1982) *Fundamentals of ocean acoustics*. Springer-Verlag, Berlin

Bryan, G.M., M. Truchan and J.I. Ewing (1963) Long range SOFAR studies in the South Atlantic Ocean. <u>J. Acoust. Soc. Am.</u>, <u>35</u>, 273

Bucker, H.P. (1964) Normal-mode sound propagation in shallow water. <u>J. Acoust. Soc. Am.</u>, <u>36</u>, 251

Bucker, H.P. (1970) Sound propagation in a channel with lossy boundaries. <u>J. Acoust. Soc. Am.</u>, <u>48</u>, 1187

Bucker, H.P. (1980) Wave propagation in a duct with boundary scattering (with application to a surface duct). <u>J. Acoust. Soc. Am.</u>, <u>68</u>, 1768

Bucker, H.P. and H.E. Morris (1965) Normal-mode intensity calculations for a constant depth shallow water channel. <u>J. Acoust. Soc. Am.</u>, <u>38</u>, 1010

Bucker, H.P. and H.E. Morris (1967) Epstein normal-mode model of a surface duct. <u>J. Acoust. Soc. Am.</u>, <u>41</u>, 1475

Chapman, N.R. (1985) Measurement of the waveform parameters of shallow explosive charges. <u>J. Acoust. Soc. Am.</u>, <u>78</u>, 672

Chapman, N.R. (1988) Source levels of shallow explosive charges. <u>J. Acoust. Soc. Am.</u>, <u>84</u>, 697

Chapman, N.R., R.W. Bannister, and R.K.H. Falconer (1990) The effect of an elastic basement in the interpretation of bottom loss data. <u>J. Acoust. Soc. Am.</u>, <u>87</u>, 2044

Chapman, N.R. and P.D. Ward (1990) The normal-mode theory of air-to-water sound transmission in the ocean. <u>J. Acoust. Soc. Am.</u>, <u>87</u>, 601

Chen, C.T. and F.J. Millero (1977) Speed of sound in sea water at high pressures. _J. Acoust. Soc. Am._, _62_, 1129

Christian, E.A. (1964) Shock-wave energy-spectrum scaling. _J. Acoust. Soc. Am._, _36_, 2418

Clay, C.S. and H. Medwin (1977) _Acoustical oceanography: Principles and applications._ Wiley-Interscience, New York

Cohen, J.S. and B.F. Cole (1977) Shallow water propagation under downward refraction conditions. _J. Acoust. Soc. Am._, _61_, 213

Cohen, J.S. and L.J. Einstein (1970) _Continuous gradient ray tracing system (CONGRATS) II_, U.S. Naval Underwater Systems Center Rep. 1069

Cole, R.H. (1948) _Underwater explosions._ Princeton U.P., Princeton, NJ

Cornyn, J.J. (1973a) _GRASS: A digital computer ray-tracing and transmission loss prediction system. Volume I- Overall description._ U.S. Naval Research Lab., Rept. 7621

Cornyn, J.J. (1973a) _GRASS: A digital computer ray-tracing and transmission loss prediction system. Volume II- User's manual._ U.S. Naval Research Lab., Rept. 7642

Del Grosso, V.A. (1974) New equation for the speed of sound in natural waters (with comparisons to other equations). _J. Acoust. Soc. Am._, _56_, 1084

Del Grosso, V.A. and C.W. Mader (1972) Speed of sound in sea water samples. _J. Acoust. Soc. Am._, _52_, 961

Denham, R.N. (1966) Intensity-decay laws for sound propagation

in shallow water of variable depth. J. Acoust. Soc. Am., 39, 1170

DiNapoli, F.R. (1971) *Fast field program for multilayered media.* Naval Underwater Systems Center, Rept. No. 4103

Dosso, S.E. and N.R. Chapman (1987) Measurement and modeling of downslope acoustic propagation loss over a continental slope. J. Acoust. Soc. Am., 81, 258

Ebbeson, G.R. and R.G. Turner (1983) Sound propagation over Dickins Seamount in the Northeast Pacific Ocean. J. Acoust. Soc. Am., 73, 143

Eby, R.K., A.O. Williams, Jr., R.P. Ryan, and P. Tamarkin (1960) Study of acoustic propagation in a two-layered model. J. Acoust. Soc. Am., 32, 88

Eckart, C. (1953) The scattering of sound from the sea surface. J. Acoust. Soc. Am., 25, 566

Eller, A.I. (1985) Implementation of rough surface scattering loss in sonar performance models. Oceans '85: Ocean Engg. and the Environment, Conference Record Vol. 1, 494. San Diego, California

Eller, A.I. (1986) *Implementation of rough surface loss in sonar performance models.* NORDA Rev., 31

Eller, A.I. and D.A. Gershfeld (1985) Low-frequency acoustic response of shallow water ducts. J. Acoust. Soc. Am., 78, 622

Ellis, D.D. and D.M.F. Chapman (1985) A simple shallow water propagation model including shear wave effects. J. Acoust. Soc. Am., 78, 1087

Emery, W.J., T.J. Reid, J.A. DeSanto, R.N. Baer, and J.P. Dugan (1979) Mesoscale variations in the deep sound channel and effects on low-frequency and propagation. *J. Acoust. Soc. Am.*, 66, 831

Evans, R.B. (1983) A coupled mode solution for acoustic propagation in a waveguide with stepwise depth variations of a penetrable bottom. *J. Acoust. Soc. Am.*, 74, 188

Evans, R.B. (1986) *COUPLE: a user's manual.* Rep. TN-332, Nav. Ocean Res. and Dev. Activity, NSTL Station, MS

Ewing, M. and J.L. Worzel (1948) Long-range sound transmission. *Geol. Soc. Am. Mem.*, 27, New York

Fenner, D.F. and P.J. Bucca (1972a) Sound velocity structure of the northwest Indian Ocean. *J. Mar. Biol. Ass. Ind.*, 14, 61

Fenner, D.F. and P.J. Bucca (1972b) *The sound velocity structure of the North Indian Ocean.* Tech. Rep. No. TR-231, U.S. Naval Oceanogr. Off., Washington, D.C

Ferla, M.C., G. Dreini, F.B. Jensen, and W.A. Kuperman (1980) Broad-band model/data comparisons for acoustic propagation in coastal waters. In *Bottom-interacting ocean acoustics*, W.A. Kuperman and F.B. Jensen (Ed.), Plenum, New York

Fisher, F.H. and V.P. Simmons (1977) Sound absorption in sea water. *J. Acoust. Soc. Am.*, 62, 558

Fofonoff, N.P. and R.C. Millard, Jr. (1984) Algorithms for computation of fundamental properties of sea water. *UNESCO Technical papers in marine science*, 44, 46 (Paris)

Fortuin, L. (1970) Survey of literature on reflection and scattering of sound waves at the sea surface. *J. Acoust.*

Soc. Am., _47_, 1209

Francois, R.E. and G.R. Garrison (1982a) Sound absorption based on ocean measurements. Part I: Pure water and magnesium sulfate contributions. _J. Acoust. Soc. Am._, _72_, 896

Francois, R.E. and G.R. Garrison (1982b) Sound absorption based on ocean measurements. Part II: Boric acid contribution and equation for total absorption. _J. Acoust. Soc. Am._, _72_, 1879

Frisk, G.V., J.A. Doutt, and E.E. Hays (1986) Geoacoustic models for the Icelandic Basin. _J. Acoust. Soc. Am._, _80_, 591

Frisk, G.V., J.F. Lynch, and S.D. Rajan (1989) Determination of compressional wave speed profiles using modal inverse techniques in a range-dependent environment in Nantucket Sound. _J. Acoust. Soc. Am._, _86_, 1928

Gaspin, J.B., J.A. Goertner, and I.M. Blatstein (1979) The determination of acoustic source levels for shallow under-water explosions. _J. Acoust. Soc. Am._, _66_, 1453

Gaspin, J.B. and V.K. Shuler, (1971) _Source levels of shallow underwater explosions._ Naval Ord. Lab. Rep. NOLTR 71-160, AD 734381

Gershfeld, D.A. and A.I. Eller (1985) Geometric considerations in determining the optimum frequency of acoustic propagation in a shallow water waveguide. _J. Acoust. Soc. Am._, _78_, 632

Greenspan, M. and C.E. Tschiegg (1957) Sing-around ultrasonic velocimeter for liquids. _Rev. Sci. Instrum._, _28_, 897. Also, _J. Acoust. Soc. Am._, _31_, 1038 (1959)

Guthrie, K.M. (1974) The connection between normal modes and

rays in underwater acoustics. J. Sound Vib., 32, 289

Guthrie, K.M. and C.T. Tindle (1976) Ray effects in the normal mode approach to underwater acoustics. J. Sound Vib., 47, 403

.

Hale, F.E. (1961) Long-range sound propagation in the deep ocean. J. Acoust. Soc. Am., 33, 456

Hamilton, E.L. (1972) Compressional wave attenuation in marine sediments. Geophysics, 37, 620

Hamilton, E.L. (1974a) Prediction of deep-sea sediment properties: State of the art. In *Deep-sea sediments, Physical and mechanical properties*, A.L. Inderbitzen (Ed.), Plenum, New York

Hamilton, E.L. (1974b) Geoacoustic models of the sea floor. In *Physics of sound in marine sediments*, L. Hampton (Ed.), Plenum, New York

Hamilton, E.L. (1976) Sound attenuation as a function of depth in the sea floor. J. Acoust. Soc. Am., 59, 528

Hamilton, E.L. (1980) Geo-acoustic modeling of the sea floor. J. Acoust. Soc. Am., 68, 1313

Henrick, R.F. and H.S. Burkom (1983) The effect of range dependence on acoustic propagation in a convergence zone environment. J. Acoust. Soc. Am., 73, 173

Hughes, S.J., D.D. Ellis, D.M.F. Chapman, and P.R. Staal (1990) Low-frequency acoustic propagation loss in shallow water over hard-rock seabeds covered by a thin layer of elastic-solid sediment. J. Acoust. Soc. Am., 88, 283

Ingenito, F. (1973) Measurements of mode attenuation coeffi-

cients in shallow water. *J. Acoust. Soc. Am.*, *53*, 858

Ingenito, F., R.H. Ferris, W.A. Kuperman, and S.N. Wolf (1978)
Shallow water acoustics summary report (First phase). NRL
Report 8179, U.S. Naval Research Laboratory, Washington,
D.C.

Ingenito, F. and S.N. Wolf (1976) Acoustic propagation in
shallow water overlying a consolidated bottom. *J. Acoust.
Soc. Am.*, *60*, 611

Jensen, F.B. (1981) Sound propagation in shallow water: A
detailed description of the acoustic field close to the
surface and bottom. *J. Acoust. Soc. Am.*, *70*, 1397

Jensen, F.B. (1988) Wave theory modeling: A convenient
approach to cw and pulse propagation modeling in low freq-
uency acoustics. *IEEE J. Oceanic Engg.*, *13*, 186

Jensen, F.B. and M.C. Ferla (1979) *SNAP: The SACLANTCEN
normal-mode acoustic propagation model.* SACLANT ASW Research
Centre Memorandum SM-121, SACLANT ASW Research Centre, Italy

Jensen, F.B. and M.C. Ferla (1990) Numerical solutions of
range-dependent benchmark problems in ocean acoustics. *J.
Acoust. Soc. Am.*, *87*, 1499

Jensen, F.B. and W.A. Kuperman (1982) *Consistency tests of
acoustic propagation models.* SACLANTCEN Memorandum SM-157.
SACLANT ASW Research Centre, Italy

Jensen, F.B. and W.A. Kuperman (1983) Optimum frequency of
propagation in shallow water environments. *J. Acoust. Soc.
Am.*, *73*, 813

Jensen, F.B. and M.G. Martinelli (1985) *The SACLANTCEN
parabolic equation model (PAREQ).* SACLANT Undersea Research

Centre, Italy

Karthikeyan, C. (1981) *Sound transmission loss in shallow sea*. Departmental report No. RR-15/81, Naval Physical and Oceanographic Laboratory, Kochi

Karthikeyan, C. (1985) *Studies on sound transmission in shallow sea*. Master's Thesis, Indian Institute of Science, Bangalore, August 1985

Karthikeyan, C. (1986a) *A normal mode transmission loss program*. Departmental report No. RR-1/86, Naval Physical and Oceanographic Laboratory, Kochi

Karthikeyan, C. (1986b) *A shallow water sound transmission loss model*. Departmental report No. RR-4/86, Naval Physical and Oceanographic Laboratory, Kochi

Kibblewhite, A.C. (1989) Attenuation of sound in marine sediments: A review with emphasis on new low-frequency data. J. Acoust. Soc. Am., 86, 716

Kibblewhite, A.C. and R.N. Denham (1965) Experiment on propagation in surface sound channels. J. Acoust. Soc. Am., 38, 63

Kibblewhite, A.C. and R.N. Denham (1967) Long-range sound propagation in the South Tasman Sea. J. Acoust. Soc. Am., 41, 401

Kinsler, L.E. and A.R. Frey (1962) *Fundamentals of Acoustics*. 2nd Edition, Wiley Eastern Limited, New Delhi

Kornhauser, E.T. and W.P. Raney (1955) Attenuation in shallow-water propagation due to an absorbing bottom. J. Acoust. Soc. Am., 27, 689

Krol, H.R. (1973) Intensity calculations along a single ray. *J. Acoust. Soc. Am.*, 53, 864

Kuo, E.Y.T. (1964) Wave scattering and transmission at irregular surfaces. *J. Acoust. Soc. Am.*, 36, 2135

Kuo, E.Y.T. (1988) Sea surface scattering and propagation loss: Review, Update, and New Predictions. *IEEE J. Oceanic Engg.*, 13, 229

Kuperman, W.A. and F. Ingenito (1977) Attenuation of the coherent component of sound propagating in shallow water with rough boundaries. *J. Acoust. Soc. Am.*, 61, 1178

Kutschale, H.W. (1973) *Rapid computation by wave theory of propagation loss in the Arctic Ocean.* Rept. CU-8-73, Columbia University, NY

Lawrence, M.M. (1985) Ray theory modeling applied to low frequency acoustic interaction with horizontally stratified ocean bottoms. *J. Acoust. Soc. Am.*, 78, 649

Lee, D. and G. Botseas (1982) *IFD: An implicit finite-difference computer model for solving the parabolic equation.* Naval Underwater Systems Center, Rep. TR-6659, New London, CT

Leroy, C.C. (1968) Formulas for the calculation of underwater pressure in acoustics. *J. Acoust. Soc. Am.*, 44, 651

Leroy, C.C. (1969) Development of simple equations for accurate and more realistic calculation of the speed of sound in sea water. *J. Acoust. Soc. Am.*, 46, 216

Levenson, C. and R.A. Doblar (1976) Long-range acoustic propagation through the Gulf Stream. *J. Acoust. Soc. Am.*, 59, 1134

Lo, E.C., J.X. Zhou, and E.C. Shang (1983) Normal mode filtering in shallow water. <u>J. Acoust. Soc. Am.,</u> <u>74,</u> 1833

Ludwig, D. (1966) Uniform asymptotic expansions at a caustic. <u>Commun. Pure Appl. Math.,</u> <u>19,</u> 215

Lurton, X. (1992) The range-averaged intensity model: A tool for underwater acoustic field analysis. <u>IEEE J. Oceanic Engg.,</u> <u>17,</u> 138

Mackenzie, K.V. (1960) Reflection of sound from coastal bottoms. <u>J. Acoust. Soc. Am.,</u> <u>32,</u> 221

Mackenzie, K.V. (1961) Long-range shallow water transmission. <u>J. Acoust. Soc. Am.,</u> <u>33,</u> 1505

Mackenzie, K.V. (1981) Nine-term equation for sound speed in the oceans. <u>J. Acoust. Soc. Am.,</u> <u>70,</u> 807

Marsh, H.W. (1961) Exact solution of wave scattering by irregular surfaces. <u>J. Acoust. Soc. Am.,</u> <u>33,</u> 330

Marsh, H.W. and M. Schulkin (1967) *Report on the status of Project AMOS. (Acoustic, Meteorological and Oceanographic Survey)* (1 Jan. 1953 to 31 Dec. 1954), USL Rep. No. 255A, USN Underwater Sound Lab., New London

Marsh, H.W., M. Schulkin, and S.G. Kneale (1961) Scattering of underwater sound by the sea surface. <u>J. Acoust. Soc. Am.,</u> <u>33,</u> 334

Medwin, H. (1975) Speed of sound in water: A simple equation for realistic parameters. <u>J. Acoust. Soc. Am.,</u> <u>58,</u> 1318

Medwin, H. and R.P. Spaulding, Jr. (1980) The seamount as a diffracting body. In *Bottom-interacting ocean acoustics,*

W.A. Kuperman and F.B. Jensen (Ed.), Plenum, New York

Mellberg, L.E., O.M. Johannessen, D.N. Connors, G. Botseas, and D.G. Browning (1991) Acoustic propagation in the western Greenland Sea frontal zone. *J. Acoust. Soc. Am.,* 89, 2144

Milder, D.M. (1969) Ray and wave invariants for SOFAR channel propagation. *J. Acoust. Soc. Am.,* 46, 1259

Miller, J.F. and F. Ingenito (1975) *Normal mode FORTRAN programs for calculating sound propagation in the ocean.* U.S. Naval Research Lab., Memo. Rept. 3071

Miller, J.F. and S.N. Wolf (1980) *Modal acoustic transmission loss (MOATL): A transmission loss computer program using a normal-mode model of the acoustic field in the ocean.* U.S. Naval Research Lab., Rep. 8429

Moler, C.B. and L.P. Solomon (1970) Use of splines and numerical integration in geometrical acoustics. *J. Acoust. Soc. Am.,* 48, 739

Munk, W. and C. Wunsch (1979) Ocean acoustic tomography: a scheme for large scale monitoring. *Deep-Sea Res.,* 26A, 123

Murphy, E.L. (1974) Improvements of the ray-mode analogy for estimating the frequency of minimum attenuation for modes in shallow water. *Proc. SACLANTCEN Conf., Sound Propagation in Shallow Water, Vol II*

Murphy, E.L. (1977) Ray displacements and time delays in the ray-mode analogy. *J. Acoust. Soc. Am., (Suppl. 1),* 61, S11

Murphy, E.L. and J.A. Davis (1974) Modified ray theory for bounded media. *J. Acoust. Soc. Am.,* 56, 1747

Murthy, P.G.K. and G.R.K. Murthy (1986) A case study on the

137

influence of internal waves on sound propagation in the sea. *J. Sound Vib.,* *108,* 447

Murty, G.R.K. and M.M. Muni (1987) A study of some physical properties of sediments of the backwaters and the adjoining continental shelf off Cochin, India. *Marine Geology,* *76,* 121

Murty, G.R.K. and M.M. Muni (1988) Statistical characteristics of seafloor topographic features of the Arabian Sea and Bay of Bengal. *J. Acoust. Soc. Ind.,* XVI, 306

Murty, K.R.G.K., G.R.K. Murty, and M.M. Muni (1984) *Marine geoacoustcal studies on the continental shelf off Cochin.* Departmental report No. RR-8/84, Naval Physical and Oceanographic Laboratory, Kochi

Murty, K.R.G.K., G.R.K. Murty, and M.M. Muni (1986) Acoustic aspects of sea floor and the bottom sediments of the continental shelf off Cochin. *J. Acoust. Soc. Ind.,* XIV, 21

Murty, G.R.K. and T. Pradeepkumar (1986) *Geoacoustic modelling of the continental shelf off Bombay.* Departmental Report No. RR-7/86, Naval Physical and Oceanographic Laboratory, Kochi

Murty, G.R.K. and T. Pradeepkumar (1987) Acoustic reflectivity characteristics of sediments of the continental shelf off Visakhapatnam. *Proceedings of the Acoustical Society of India,* 1987

Murty, G.R.K. and T. Pradeepkumar (1988) Influence of variable bottom sediment characteristics on shallow water sound propagation. *J. Acoust. Soc. Ind.,* XVI, 316

Murty, G.R.K. and T. Pradeepkumar (1989) Biot-Stoll sediment model- An experimental assessment for predicting compressional sound speed in sediments. *J. Acoust. Soc.*

Ind., XVII, 222

Murty, G.R.K. and T. Pradeepkumar (1990) On the applicability of sound speed models to marine sediments of the continental shelf off Cochin: An experimental assessment. J. Acoust. Soc. Ind., XVIII, 92

Murty, T.V.R., Y.K. Somayajulu, and J.S. Sastry (1990) Computations of some acoustic ray parameters in the Bay of Bengal. Ind. J. Mar. Sci., 19, 235

Neumann, G. and W.J. Pierson, Jr. (1957) A detailed comparison of theoretical wave spectra and wave forecasting methods. Deut. Hydrogr. Z., 10, 73, 134

Newman, A.V. and F. Ingenito (1972) A normal mode computer program for calculating sound propagation in shallow water with an arbitrary velocity profile. NRL Memorandum Rpt. 2381, U.S. Naval Research Laboratory, Washington, D.C.

Nobes, D.C. (1989) A test of a simple model of the acoustic velocity in marine sediments. J. Acoust. Soc. Am., 86, 290

Northrop, J. (1970) Underwater sound propagation across the Hawaiian arch. J. Acoust. Soc. Am., 48, 417

Novarini, J.C. and D.R.O. Bruno (1982) Effects of the sub-surface bubble layer on sound propagation. J. Acoust. Soc. Am., 72, 510

Nutile, D.A. and A.N. Guthrie (1979) Acoustic shadowing by seamounts. J. Acoust. Soc. Am., 66, 1813

Officer, C.B. (1958) Introduction to the theory of sound transmission with application to the ocean. McGraw-Hill Book Company, New York

Pedersen, M.A. (1961) Acoustic intensity anomalies introduced by constant velocity gradients. _J. Acoust. Soc. Am._, 33, 465

Pedersen, M.A. (1962) Comparison of experimental and theoretical image interference in deep water acoustics. _J. Acoust. Soc. Am._, 34, 1197

Pedersen, M.A. (1968) Ray theory applied to a wide class of velocity functions. _J. Acoust. Soc. Am._, 43, 619

Pedersen, M.A. and D.F. Gordon (1967) Comparison of curvilinear and linear profile approximation in the calculation of underwater sound intensities by ray theory. _J. Acoust. Soc. Am._, 41, 419

Pekeris, C.L. (1948) Theory of propagation of explosive sound in shallow water. _Geol. Soc. Am. Mem._, 27, New York

Pierce, A. (1965) Extension of the method of normal modes to sound propagation in an almost-stratified medium. _J. Acoust. Soc. Am._, 37, 19

Pierson, W.J., Jr., and L. Moskowitz (1964) A proposed spectral form for fully developed seas based on the similarity theory of S.A. Kitaigorodskii. _J. Geophys. Res._, 69, 5181

Plumpton, N.G. and C.T. Tindle (1989) Saddle point analysis of the reflected acoustic field. _J. Acoust. Soc. Am._, 85, 1115

Pradeepkumar, T.P. and Mathew, B. (1988) The deep sound channel in the Indian Ocean. _J. Acoust. Soc. Ind._, XVI, 1

Rao, T.C.S. (1975) Method for plotting sound ray paths in the potential layer from bathythermograms. _Ind. J. Mar. Sci._, 4, 103

Rao, M.G.S. and K.V. Sundararamam (1974) Sound velocity structure in the upper 500 m of Arabian Sea during September-December 1962. Ind. J. Mar. Sci., 3, 5

Ryder, R.D. and A.O. Williams, Jr. (1973) Normal-mode propagation in water layers having linear gradients of sound speed. J. Acoust. Soc. Am., 53, 899

Sachs, D. and A. Silbiger (1971) The focussing of harmonic sound and transient pulses in stratified media. J. Acoust. Soc. Am., 49, 824

Schmidt, H. (1988) *SAFARI: Seismo-acoustic fast field algorithm for range-independent environments*. Rep. SR-113, SACLANT Undersea Research Centre, Italy

Schulkin, M. (1968) Surface-coupled losses in surface sound channels. J. Acoust. Soc. Am., 44, 1152

Schulkin, M. and H. Marsh, (1962) Absorption of sound in sea water. J. Acoust. Soc. Am., 34, 864

Schulkin, M. and H. Marsh (1978) Low frequency sound absorption in the ocean. J. Acoust. Soc. Am., 63, 43

Schulkin, M. and R. Shaffer (1964) Backscattering of sound from the sea surface. J. Acoust. Soc. Am., 36, 1699

Siddiquie, H.N. and F. Almeida (1985) *Surficial geology of the continental shelf off Cochin (for the Naval Physical and Oceanographic Laboratory, Cochin)*. National Institute of Oceanography, Dona Paula, Goa, India

Siegman, W.L., M.J. Jacobson, and L.D. Law (1987) Effects of bottom attenuation on acoustic propagation with a modified ray theory. J. Acoust. Soc. Am., 81, 1741

Somayajulu, Y.K., L.V.G. Rao, and V.V.R. Varadachari (1980) Small scale features of sound velocity structure in the northern Arabian Sea during February-May 1974. Ind. J. Mar. Sci., 9, 141

Spiesberger, J.L. and K. Metzger (1991) New estimates of sound speed in water. J. Acoust. Soc. Am., 89, 1697

Spofford, C.W. (1974) The FACT Model. Volume 1, Acoust. Environ. Support Detachment, Office of Naval Research, Maury Ctr. Rept. 109

Stewart, K.R. (1965) Ray acoustical model of the ocean using a depth/sound speed profile with a continuous first derivative. J. Acoust. Soc. Am., 38, 339

Stoll, R.D. (1974) Acoustic waves in saturated sediments. In Physics of sound in marine sediments, L. Hampton (Ed.), Plenum, New York

Stoll, R.D. (1977) Acoustic waves in ocean sediments. Geophysics, 42, 715

Stoll, R.D. (1978) Experimental studies of attenuation in sediments. J. Acoust. Soc. Am., 64, 5143(A)

Stoll, R.D. (1985) Marine sediment acoustics. J. Acoust. Soc. Am., 77, 1789

Stoll, R.D. and G.M. Bryan (1970) Wave attenuation in saturated sediments. J. Acoust. Soc. Am., 47, 1440

Stoll, R.D. and R.E. Houtz (1983) Attenuation measurement with sonobuoys. J. Acoust. Soc. Am., 73, 163

Sutton, H.G., H. Hemer, and J.E. Nafe (1957) Physical analysis of deep-sea sediments. Geophysics, 22, 779

Sverdrup, H.U. and W. Munk (1947) *Wind, Sea, and Swell: Theory of relations for forecasting.* U.S. Navy H.O. Pub. No. 601, (U.S. Navy Hydrographic Office, Washington, D.C)

Tappert, F.D. (1977) The parabolic approximation method. In *Wave Propagation and Underwater Acoustics*, J.B. Keller and J.S. Papadakis (Ed.), Springer-Verlag, Berlin

Thomson D.J. and N.R. Chapman (1983) A wide angle split-step algorithm for the parabolic equation. J. Acoust. Soc. Am., 74, 1848

Thorp, W.H. (1965) Deep-ocean sound attenuation in the sub and low kilocycle per second region. J. Acoust. Soc. Am., 38, 648

Tindle, C.T. (1979) The equivalence of bottom loss and mode attenuation per cycle in underwater acoustics. J. Acoust. Soc. Am., 66, 250

Tindle, C.T. (1983) Ray calculations with beam displacement. J. Acoust. Soc. Am., 73, 1581

Tindle, C.T. and G.E.J. Bold (1981) Improved ray calculations in shallow water. J. Acoust. Soc. Am., 70, 813

Tindle, C.T. and G.B. Deane (1985) Sound propagation over a sloping bottom using rays with beam displacement. J. Acoust. Soc. Am., 78, 1366

Tindle, C.T. and K.M. Guthrie (1974) Rays as interfering modes in underwater acoustics. J. Sound Vib., 34, 291

Tindle, C.T. and N.G. Plumpton (1988) Ray analysis near the critical angle. J. Acoust. Soc. Am., (Suppl. 1), 84, S174

143

Tindle, C.T. and D.E. Weston (1980) Connection of acoustic beam displacement, cycle distances, and attenuation for rays and normal modes. J. Acoust. Soc. Am., 67, 1614

Tindle, C.T., D.E. Weston, and S.G. Payne (1980) Cycle distances and attenuation in shallow water. J. Acoust. Soc. Am., 68, 1489

Tolstoy, I. (1958) Shallow water test of the theory of layered wave guides. J. Acoust. Soc. Am., 30, 348

Tolstoy, I. (1959) Modes, rays, and travel times. J. Geophys. Res., 64, 815

Tolstoy, I. (1960) Guided waves in fluid with continuously variable velocity overlying an elastic solid: Theory and experiment. J. Acoust. Soc. Am., 32, 81

Tolstoy, I. (1968) Phase changes and pulse deformation in acoustics. J. Acoust. Soc. Am., 44, 675

Tolstoy, I. and C.S. Clay (1966) Ocean Acoustics. Theory and experiment in underwater sound. McGraw-Hill Book Company, New York

Uretsky, J.L. (1963) Reflection of a plane sound wave from a sinusoidal surface. J. Acoust. Soc. Am., 35, 1293

Uretsky, J.L. (1965) .The scattering of plane waves from periodic surfaces. Ann. Phys. (N.Y.) 33, 400

Urick, R.J. (1963) Low-frequency sound attenuation in the deep ocean. J. Acoust. Soc. Am., 35, 1413

Urick, R.J. (1965) Caustics and convergence zones in deep-water sound transmission. J. Acoust. Soc. Am., 38, 348

Urick, R.J. (1966) Long range deep sea attenuation measurement. _J. Acoust. Soc. Am._, 34, 904

Urick, R.J. (1969) Intensity summation of modes and images in shallow water sound transmission. _J. Acoust. Soc. Am._, 46, 780

Urick, R.J. (1975) _Principles of underwater sound_, McGraw-Hill Book Company, New York

Urick, R.J. (1982) _Sound propagation in the sea._ Peninsula Publishing, California

Urick, R.J. (1983) _Principles of underwater sound_, 3rd Edition, McGraw-Hill Book Company, New York

Vijayakumar, O. (1989) _Experimental studies on sound propagation in shallow waters off the west coast of India._ Ph.D. Thesis, Indian Institute of Science, Bangalore, August 1989

Vijayakumar, O. and M.P. Ajaikumar (1989) _A normal mode analytical model for sound propagation in shallow waters and comparison with experimental data._ Departmental report No. RR-8/89, Naval Physical and Oceanographic Laboratory, Kochi

Vijayakumar, O. and M.P. Ajaikumar (1990a) Frequency dependence of sound propagation in shallow water. _J. Acoust. Soc. Ind._, XVII, 96

Vijayakumar, O. and M.P. Ajaikumar (1990b) A model for the estimation of source levels of shallow underwater explosions. _J. Acoust. Soc. Ind._, XVII, 100

Vijayakumar, O. and K.A.A. Salam (1987) _Shallow water sound propagation studies off Bombay._ Departmental report No. RR-4/87, Naval Physical and Oceanographic Laboratory, Kochi

Wakeley, J., Jr. (1978) Coherent ray tracing- measured and predicted shallow water frequency spectrum. *J. Acoust. Soc. Am.*, *63*, 1820

Weinberg, H. (1971) A continuous-gradient curve-fitting technique for acoustic-ray analysis. *J. Acoust.* Soc. Am., 50, 975

Weinberg, H. (1973) *Navy Interim Surface Ship Model (NISSM II)*. U.S. NUSC Technical Rep. 4527

Weinberg, H. (1975) Application of ray theory to acoustic propagation in horizontally stratified oceans. *J. Acoust. Soc. Am.*, *58*, 97

Weinberg, H. (1981a) Effective range derivative for acoustic propagation loss in a horizontally stratified ocean. *J. Acoust. Soc. Am.*, *70*, 1736

Weinberg, H. (1981b) *Generic Sonar Model*, U.S. Naval Undersea Systems Centre, TD 5971C

Wenz, G.M. (1962) Acoustic ambient noise in the ocean: Spectra and sources. *J. Acoust. Soc. Am.*, *34*, 1936

Weston, D.E. (1960a) A Moire fringe analog of sound propagation in shallow water. *J. Acoust. Soc. Am.*, *32*, 647

Weston, D.E. (1960b) Underwater explosions as acoustic sources. *Proc. Phys. Soc. London*, *76*, 233

Weston, D.E. (1963) Propagation of sound in shallow water. *Radio and Electronic Engineer*, *26*, 329

Weston, D.E. and C.T. Tindle (1979) Reflection loss and mode attenuation in a Pekeris model. *J. Acoust. Soc. Am.*, *66*, 872

Westwood, E.K. (1989a) Complex ray methods for acoustic interaction at a fluid-fluid interface. J. Acoust. Soc. Am., 85, 1872

Westwood, E.K. (1989b) Ray methods for flat and sloping shallow-water waveguides. J. Acoust. Soc. Am., 85, 1885

Westwood, E.K. (1990) Ray model solutions to the benchmark wedge problems. J. Acoust. Soc. Am., 87, 1539

Westwood, E.K. and C.T. Tindle (1987) Shallow water time series simulation using ray theory. J. Acoust. Soc. Am., 81, 1752

Westwood, E.K. and P.J. Vidamar (1987) Eigenray finding and time series simulation in a layered-bottom ocean. J. Acoust. Soc. Am., 81, 912

Wilson, W.D. (1960) Equation for the speed of sound in sea water. J. Acoust. Soc. Am., 32, 1357

Yarger, D.F. (1976) *The user's guide for the RAYMODE propagation loss program.* U.S. Naval Underwater Systems Center, Tech. Memo. 222-10-76

Yeager, E., F.H. Fisher, J. Miceli, and R. Bressel (1973) Origin of the low-frequency sound absorption in sea water. J. Acoust. Soc. Am., 53, 1705

Zhou, J.X. (1986) Inversion techniques for obtaining seabed low-frequency reflection loss at small grazing angles in shallow water. J. Acoust. Soc. Am., (Suppl. 1), 79, S68

Zhou, J.X., X.Z. Zhang, and P.H. Rogers (1987a) Effect of frequency dependence of sea-bottom attenuation on the optimum frequency for acoustic propagation in shallow water. J. Acoust. Soc. Am., 82, 287

Zhou, J.X., X.Z. Zhang, P.H. Rogers, and J. Jarzynski (1987b) Geoacoustic parameters in a stratified sea bottom from shallow-water acoustic propagation. J. Acoust. Soc. Am., 82, 2068

148